DISTRIBUTED CONTROL AND OPERATION OF DECARBONIZED AND INFORMATIZED LOW-VOLTAGE NETWORKS WITH MULTI-ENERGY RESOURCES

QIAN HU

PhD

The Hong Kong Polytechnic University

2021

The Hong Kong Polytechnic University

Department of Electrical Engineering

Distributed Control and Operation of Decarbonized and Informatized Low-Voltage Networks with Multi-Energy Resources

Qian Hu

A thesis submitted in partial fulfilment of the requirements for the degree of Doctor of Philosophy

June 2021

CERTIFICATE OF ORIGINALITY

I hereby declare that this thesis is my own work and that, to the best of my knowledge and belief, it reproduces no material previously published or written, nor material that has been accepted for the award of any other degree or diploma, except where due acknowledgement has been made in the text.

_____ _____ (Signed)

_____Qian Hu_____(Name of student)

Abstract

Driven by environmental concerns, low-voltage networks are undergoing a significant transformation of decarbonization with the growing integration of renewable energy resources. Meanwhile, the deployment of information and communication technology (ICT) empowers the informatization of low-voltage networks to support intelligent functionalities. However, despite benefits achieved under transformations of decarbonization and informatization, new challenges are posed which cannot be tackled efficiently and effectively by using centralized control and operational schemes. To address arising challenges, this thesis focuses on the reconstruction of control strategies and operational schemes for future decarbonized and informatized low-voltage networks.

The thesis firstly gives attention to ensure the stable and economic operation of the microgrid (MG). Due to the distributed nature of inverter-based distributed energy resources (DERs) in the MG, a distributed secondary control structure is favorable to enhance the performance and scalability of MGs. Pinning-based control techniques are adopted to develop a distributed secondary frequency and voltage control for islanded MGs to maintain stable operation under frequent power fluctuations. Moreover, the impact of the communication topology on the pinning-based secondary control is examined analytically. Then the communication network for the MG is designed to minimize the communication cost and achieve control convergence.

Furthermore, the islanded MG is divided into some nanogrids (NGs) for the sake of effective management for DERs. Based on the MG partition, the thesis then

investigates how NGs can be coordinated to participate in peer-to-peer trading and provide ancillary service provision in an islanded MG. A multi-market paradigm is designed to realize the trading of both energy and ancillary service among NGs and optimal offering strategies are developed to maximize the profit of producer NGs in three consecutive markets in different time phases. Moreover, a distributed real-time operation is enabled so that the frequency regulation service can be provided economically.

Resulted from intermittency of renewable energies, an increasing number of minor and temporary voltage violations will be experienced in a highly renewable penetrated distributed network. The thesis further develops a fully distributed voltage regulation scheme for dominantly resistive distribution networks, considering the financial incentives of the electric vehicle fleet (EVF). It includes an optimal planning stage for the planning of EVF charging/discharging and a distributed regulation stage for real-time voltage regulation. Based on the parallel-consensus control, the voltage can be collectively regulated through P and Q support from EVFs in a fully distributed and economical manner.

Extensive applications of ICT require exceptional awareness of cybersecurity-related issues in the distribution network. Last but not least, the thesis focuses on the eavesdropping attack to address the pressing demand for privacy preservation in distributed schemes. A privacy-preserving distributed energy management system (EMS) for distribution network is presented, fulfilling the core task to prevent information disclosure of each agent during the information exchange. Secure exchange protocols based on the homomorphic cryptosystem are developed so that

the leakage of agents' private information (price information, power usage data, and power utilization ratio) in iterative communications can be effectively prevented.

Publications Arising from the Thesis

1. **Q. Hu**, S. Q. Bu and V. Terzija, "A Distributed P and Q Provision Based Voltage Regulation Scheme by Incentivized EV Fleet Charging for Resistive Distribution Networks," *IEEE Transactions on Transportation Electrification*, 2021. Early access. (Chapter 4)
2. **Q. Hu,** Z. Q. Zhu, S. Q. Bu, K. W. Chan, F. X. Li, "A Multi-market Nanogrid P2P Energy and Ancillary Service Trading Paradigm: Mechanisms and Implementations," *Applied Energy,* vol. 293, p. 116938, Jul. 2021. (Chapter 3)
3. **Q. Hu**, S. Q. Bu, "Cost-Effective Communication Network Planning Considering Performance of Pinning Based Secondary Control in Microgrids," *International Journal of Electrical Power and Energy System,* 2021. (In press) (Chapter 2)
4. **Q. Hu,** S. Q. Bu, W. C. Su and V. Terzija, "A Homomorphically Encrypted Energy Management System for Active Distribution Network under Eavesdropping Attacks," *IEEE Transactions on Smart Grid.* (Under review) (Chapter 5)
5. **Q. Hu,** S. Q. Bu, "Distributed Control and Operations of Decarbonized and Informatized Low-voltage Networks: A Systematic Review of Opportunities and Challenges," *Renewable & Sustainable Energy Review.* (Ready for submission)
6. **Q. Hu**, S. Q. Bu, "Economic Frequency Regulation Based on Nanogrid Partition and Cost-Driven Droop Function: Enable A Scattered Microgird," *2020 International Conference on Smart Grids and Energy Systems (SGES),* Perth, Australia, 2020, pp. 320-325. (Chapter 2&3)
7. **Q. Hu**, S. Q. Bu, B. W. Zhou and P. Zhang, "A Fully Distributed Multi-Stage Voltage Regulation Strategy for Distribution Network Based on Intelligent Bus Terminal Technology," *Distributed Energy*, vol. 4, no. 6, 2019.
8. **Q. Hu**, S. Q. Bu, S. W. Xia and H. Cai, "A Novel Voltage Regulation Strategy for Secure Operation of High Renewable Penetrated Distribution Networks with Different R/X and Topologies," *2019 IEEE Innovative Smart Grid Technologies - Asia (ISGT Asia), Chengdu, China, 2019,* pp 3424-3229. (Chapter 4)
9. **Q. Hu**, H. Y. Li and S. Q. Bu, "The Prediction of Electric Vehicles Load Profiles

Considering Stochastic Charging and Discharging Behavior and Their Impact Assessment on a Real UK Distribution Network," *Energy Procedia*, Volume 158, 2019, Pages 6458-6465.

Acknowledgements

This thesis summarizes the research work I accomplished for Ph.D. program in the Department of Electrical and Electronic Engineering, Hong Kong Polytechnic University, from 2018 to 2021.

Foremost, I would like to express my sincerest gratitude to my supervisor, Dr. Siqi Bu, for trusting me to conduct this Ph.D. research and encouraging me to aim high and achieve more. His knowledge, guidance and support have contributed a lot to the outcomes of this thesis. I truly appreciate his patience and support in all uncertain situations that occurred during my Ph.D. journey.

I am very grateful to current and previous members of Dr. Bu's research group: Dr. Shiwei Xia, Mr. Jiaxin Wen, Dr. Jianqiang Luo, Dr. Qi Wang, Mr. Yong Hu, Ms Chaoyun Wang, Ms Jiangfeng Zhang. Mr. Ruoheng Wang, etc. It was a great experience to learn from you, discuss with you, and share happy memories for our group activities.

Lastly, my family always is my biggest motivation to reach goals and achieve good results. I would like to thank their love, care and support.

Table of Contents

List of Figures

List of Tables

List of Abbreviations

ADN	Active distribution network
BRP	Balancing responsible party
BMS	Battery management systems
CPS	Cyber-physical system
CRM	Capacity remuneration mechanism
DER	Distributed energy resource
DG	Distributed generation
DoS	Denial of service
EMS	Energy management system
ESS	Energy storage system
EVF	Electric vehicle fleet
ESS	Energy storage system
FDI	False data injection
ICT	Information and communication technology
IBT	Intelligent bus terminal
IoT	Internet of things
LMI	Linear matrix inequalities
MAS	Multi-agent system
MG	Microgrid
MP	Marginal price
MINLP	Mixed-integer nonlinear programming
MISDP	Mixed-integer semidefinite program
NG	Nanogrid
P2P	Peer-to-peer
PV	Photovoltaics
PAB	Pay-as-bid
PAO	Pay as the opportunity cost
PoC	Point of connection

PSC	Pinning synchronization control
RLC	Resistance-inductor-capacitor
SOC	State of charge
VPP	Virtual power plant
V2G	Vehicle to grid

Chapter 1 Introduction

1.1 Background and Motivations

A growing number of governments are setting ambitious targets to achieve net-zero carbon emissions to combat climate change [1]. For example, China legislators have set out a timetable for achieving carbon neutrality by 2060 [2]. To minimize the greenhouse effect and reduce carbon emission, as one of the large carbon emitters, the power industry has been actively promoting clean and renewable energies as promising alternatives to fossil fuels for electricity generation. European Union fixed a binding renewable energy target of at least 32% in the EU for 2030 [3]. China set a goal for renewables to account for at least 35% of electricity consumption by 2030 [4].

The deployment of a large number of distributed energy resource (DER) units is one of the practical approaches to integrating renewable energies in low-voltage networks, which can improve the network reliability and provide grid support, including voltage regulation, real and reactive power control, frequency stabilization [5]. Furthermore, the continuous increase of DER systems brings a significant transformation for the future low-voltage networks: *decentralization*. Contrary to conventional large-scale power plants that are centralized and require electricity to be transmitted over long distances through passive transmission and distribution networks to end-users, DER systems are smaller-scale and localized, which can be coordinated and managed to support the local loads in a decentralized manner efficiently.

While DERs bring many potential benefits to low-voltage networks, new challenges in terms of DER control and operation are posed due to the mass penetration of DERs, especially issues related to the intermittency of renewable energy resources. Moreover, with wide applications of information and communication technology (ICT), the low-voltage network is undergoing another transformation: *informatization*, making it a typical cyber-physical system (CPS). Furthermore, the realization of distributed operational schemes relies on information sharing among agents in the communication network. Hence, it is crucial to understand the impact of the communication network and address related issues.

In the light of the evolution of *decentralization* and *informatization* of the low-voltage network, reconstructing control strategies and developing new solutions is a challenging but necessary task to eliminate hazardous situations and maintain normal operating conditions, which will keep low-voltage networks growing fast in a sustainable, stable and economical way.

1.1.1 Control Architectures Revisited

The existing power network is a legacy system dating as far back as half a century, in which fully centralized control methods are predominantly employed resulting from centralized power plants [6]. A centralized control architecture relies on a single dedicated central controller, which collects the information from all supervised components, performs necessary computations, and determines control decisions. Once the control decision is made, the central controller sends the control signal to each component. During the centralized control process, extensive communications between the central controller and controlled components as well as significant

computations are required, making the implementation of a centralized control infeasible and inefficient in low-voltage networks with the geographically extensive integration of DERs.

Therefore, a noncentralized control scheme, either in the decentralized or distributed structure, is more suitable to provide the required functionality in low-voltage networks. In the structure of decentralized control, each component is controlled by its local controller. The main feature of decentralized control is that the local controller neither shares information with others nor accesses the information of system-wide variables [7]. In the power system application, such the feature may lead to poor system-wide performance if a strong coupling exists between the operations of various components [8]. The massive blackout across North America in August 2003 is an example revealing that the severe consequences of ignoring the interaction among the subsystems. In this blackout, each subsystem tripped and transferred the extra load to other subsystems to maintain its stability, which consequently causes a more severe overload and cascading failures [6][9].

As another form of noncentralized control, a distributed control has been drawn attention in recent power system research and applications considering the geographically dispersed nature of DERs. The distributed control method has been extensively applied in the multi-agent system (MAS), where the interactions among different agents significantly impact the overall control performance. In the structure of distributed control, each subsystem is controlled by a local controller and the local information is shared among controllers [10]. The autonomy of each subsystem can

be maintained and interactions among different subsystems can be achieved to raise the overall performance in a distributed control[6].

DER control structures in terms of the control mentioned above are visualized in Fig. 1.1, where the dashed lines represent the communication channel. Comparisons among three control architectures in terms of computational complexity, communication requirement, reliability, and scalability are summarized in Table 1.1.

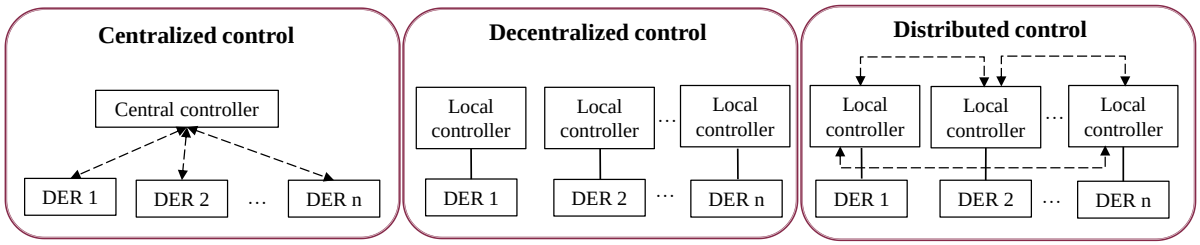

Fig. 1.1. Illustrative diagram of three control architectures for the DER control

Table 1.1. Comparisons of three control architectures

	Centralized	**Decentralized**	**Distributed**
Computational complexity	Significant computational complexity	Reduced computational burden	Reduced computational burden
Communication requirement	Communication infrastructure required	No communication required	Communication infrastructure required
Reliability	Low reliability, vulnerable to the single point of failure	Higher reliability	Better reliability
Scalability	Reduced scalability	Increased scalability	Increased scalability
Optimal solution	Global optimal solutions	No global optimal solutions	Sub-optimal solutions
Stability	Stability affected by the communication network		Stability affected by the communication network

The increasing demand for higher reliability, security and scalability requires distributed control and operational methods to be implemented for future low-voltage

networks. In summary, compared with centralized control, distributed control is preferred because of: 1) significantly reduced computational burden for the local processor [11]; 2) improved user data privacy and security, i.e., local information is prevented from being collected by central authorities, the decision can be made locally [12]; 3) increased scalability supporting the plug-and-play function and more flexible integration of DERs in the distribution network [13].

1.1.2 Distributed Secondary Control for Microgrid and Impact of Communication Network

The utilization of DERs provides a viable solution to reduce greenhouse emissions and increase the sustainability of power supplies. Notably, the microgrid (MG) contributes to the deployment of DERs by integrating them into the low- and medium-voltage distribution systems, which enhances the network reliability and controllability [14]. Through the electronic-interfaced inverter, DERs connected to the distribution network in the form of the MG can provide highly distributed and efficient support to the main grid. The MG can operate either in the grid-connected mode or islanded mode. When the MG is in the grid-connected mode, the frequency stability of the MG is guaranteed by the main grid, while it is more challenging to maintain the frequency stability due to its low-inertia characteristic in the islanded mode [8]. Besides, renewable-based DERs will cause uncertainties and fluctuations in the generation, which will pose a critical necessity for the demand-generation balance to maintain the system frequency as close to the reference value.

Adopting a hierarchical control structure consisting of inner control, primary (droop) control and secondary control has become a common practice to stabilize the

frequency and voltage and realize an accurate power sharing in islanded MGs [15]–[19]. Through the current and voltage control loop, inner control provides high frequency switching pulses for the power electronics-interface of the DER to produce the sinusoidal voltage with the desired frequency. Droop-based primary control aims to locally provide the power sharing among DERs and adjust the voltage and frequency reference provided to the inner control without the need for communication among DERs. Such a power sharing process is conducted based on the droop characteristics of each DER. However, the droop control often suffers the voltage and frequency deviation from the reference value. Therefore, secondary control is implemented to eliminate voltage and frequency deviations and maintain their amplitudes to the desired values via centralized or decentralized communications.

The centralized control structure that needs complex communication is designed for the conventional secondary control of MGs [15]–[17]. However, the network reliability can be adversely affected by it. As the MG is integrated with geographically dispersed DERs, a distributed secondary control without the existence of the central controller is highly desired to improve the controllability and reduce the computation burden [20]. With the advanced ICT, the local control action can be made cooperatively through peer-to-peer (P2P) information sharing among DERs.

As one of the distributed control techniques, pinning control is an efficient control method to drive the complex network to achieve a specific synchronization, where only a small fraction of nodes in the network can access the critical reference state [21]. Several studies have introduced the concept of pinning to different applications in power networks. Optimal power sharing within the grid-connected microgrid is

modeled as a pinning synchronization problem in [22]. In [23] and [19], secondary voltage control is formulated as a tracking synchronization problem. In [24] and [25], pinning-based distributed controls are developed for voltage and frequency regulation.

As one of the basic aspects of the distributed secondary control design, the structural topology of the cyber network has an impact on the dynamic performance of the islanded MG [26]. With the extensive usage of open communication mechanisms, the topology of the cyber network is not necessarily the same as the physical network of the MG [27]. Therefore, the communication topology can be regarded as an adjustable variable to improve the transient performance of the secondary frequency and voltage control. Like other distributed control methods, adopting the pinning technique in MGs requires cost-effective and robust P2P communications. How communication impairments impact pinning-based control dynamics has been investigated in some works. For example, in [28], the stochastic distributed pinning control is proposed for the voltage regulation considering the time-delay and noise disturbances of the communication network. The performance of the pinning-based consensus control for voltage and frequency regulation under uncertain communication topologies is examined in [29].

As a matter of fact, the communication graph, which contains the global structural information of the cyber network, has a prominent effect on the dynamics of pinning protocols [30][31]. The effectiveness of the pinning control is closely related to the spectral properties of the communication graph, such as the algebraic connectivity, eigenvalues of the Laplacian matrix, the number of communication links and the weighting of them, etc. [32]. Given an appropriate communication graph, the inherent

connectivity of the communication network will asymptotically force frequency and voltage across the MG to synchronize to the reference with a specific convergence rate. The authors of [33] investigate how the selection of the set of pinning DG influences the algebraic connectivity of the communication network. The impact of localization of pinning DGs on the algebraic connectivity of the communication network is analyzed in [34].

By reviewing existing literature on the employment of pinning technique in MGs, it is found that: 1) The topology of the communication network is prescribed in most of the studies; 2) Characteristics of the physical network and parameters of the controller are the main focus to improve the control performance [35]; 3) The investigation on the impact of the communication network on the dynamical performance is more focused on the local transient defects and mainly relied on time-domain simulations. Moreover, the effect of the overall communication topology on the dynamic performance of the pinning-based control has not been systematically analyzed. Communication cost, as an important evaluation index of the cost-effective network, has not been discussed.

1.1.3 Deregulated Electricity Market for Microgrid

Based on the P2P communication, not only the control of the MG can be reconstructed in the distributed structure, but also the electricity market can be deregulated. Moreover, the increasing employment of DERs restructures the electricity market where the owners of DER systems are proactive to participate in the market trading for benefit maximization. A deregulated and liberalized electricity market that allows the energy and ancillary service trading among DER systems will

be highly desirable. Driven by the technology trend of consumer-level communication and control, the entities with small-scale DERs in the MG can become prosumers to actively manage their energy generation, consumption, and energy storage [36]. Hence, apart from the technical requirements of MG control, a dedicated energy market, providing a platform for local prosumers to trade energy within the MG, should be designed for the MG to maximize overall economic benefits. The existing mechanisms in transmission-level wholesale markets cannot be directly adopted for the participation of small-scale DERs because of two main reasons: firstly, the capability to react in real-time to fluctuated generations from renewables-based DERs is missing [37]; secondly, an individual prosumer has little impact on the higher network level and transaction costs usually offset the potential benefits [36]. Compared with the conventional wholesale markets, an energy market implemented explicitly in the MG has the following advantages [38]: 1. Reduce the cost of energy transportation and losses through the localized trading; 2. Decrease managing congestion and the possibility of distribution faults through the distributed communication and control architecture; 3. Encourage reinvestments in DERs and the engagement of prosumers.

To promote efficient usage of local resources, P2P trading, as an emerging approach that enables participants of the network to share their resources, has become a research hotspot [39]. Sufficient prosumer participation is of vital importance for successful P2P trading. The authors of [40] make an overview of motivational psychology that can support P2P trading by increasing users' participation. In general, the P2P sharing market is divided into three categories depending on how the trading

is done and how the information is transmitted among the participants: coordinated market, decentralized market and community market [41]. Notably, an increasing number of studies integrate P2P trading mechanisms into the MG energy market. How to setting P2P trading price in the MG market is dedicatedly studied in [42]. [43] proposes a four-layer system architecture of P2P energy trading for grid-connected MG, consisting of business layer, control layer, ICT layer and power grid layer, while the business layer is the focus of this paper and a P2P energy trading platform 'Elecbay' is introduced. In [44], prosumers are grouped into virtual MGs and the social benefits of P2P energy trading in virtual MGs are optimized by using a Stackelberg game. Sharing problem of energy storage capacity between the residential community and shared facility controllers is formulated as the Stackelberg game as well in [45]. An aggregated battery control framework is proposed in [46] for P2P energy sharing in a community microgrid. In [47], P2P energy trading for a community MG is built based on the game-theoretic model, where the interaction between sellers and buyers is modeled as Stackelberg game and the pricing competition among sellers is modeled as a noncooperative game. The authors of [48] consider the network constraints to develop a decentralized P2P energy trading method in the low-voltage network. Based on cooperative game theory, the energy exchange is optimized in a distributed MG in [49]. P2P trading among plug-in electric vehicles is investigated in [50] to balance local electricity demand. [51] presents a comparative analysis of auction mechanisms and bidding strategies for the solar transaction energy market. P2P energy sharing among smart homes is evaluated in [52] and the total costs of all households are minimized. Based on a game-theoretical approach, a long-term planning for connected

industrial MGs is proposed in [53] for the daily energy exchanges. A P2P energy sharing model for PV prosumers in the MG is proposed in [54] considering the price-based demand response. An optimization model is developed to maximize the economic benefits for PV-battery DG system in the P2P energy trading environment in [55].

Table 1.2. Summary and comparison of P2P MG markets in the existing literature

Reference	P2P trading environment	The general objective of the work	Transactive commodity
[43][45][48][50][53]	Grid-connected network	Energy sharing and balance of supply and demand	Energy
[46][47][49][51][52] [54][55]	Islanded microgrid	Energy sharing and prosumer cost minimization	
Proposed work	Partitioned islanded microgrid	Energy sharing and frequency regulation	Energy and ancillary service

Table 1.2 gives the summary and comparison of the literature as mentioned earlier about the P2P MG market. It is found that most existing studies only consider 'energy' as the main transactive commodity in the P2P energy market. As a matter of fact, the coalitions of small-scale prosumers can provide flexible ancillary service, which means the transactive commodities should not be only limited to energy [56]. It is worth studying how both energy and ancillary service can be coordinately traded. According to the report of National Grid UK, the frequency response can be categorized into two types of service: dynamic and non-dynamic. Dynamic frequency response is a continuously provided service to control the normal second by second changes, while non-dynamic frequency response is usually referred to the discrete service triggered at a defined frequency deviation [57]. In the MG, entities such as

dispatchable generation units, energy storage systems and demand-responsible loads can adjust their power generation or demand to flexibly offer the frequency response service [58][59]. A comprehensive P2P trading mechanism for the MG should include ancillary service as a small but critical part of the entire trading process.

Some works have incorporated ancillary service into energy markets at the distribution or transmission level. In [60], multiple MGs, which can be regarded as balancing service providers to the transmission system, participate in the real-time balancing market bidding. A day-ahead scheduling strategy is proposed in [61] for the integrated community energy system to participate in the joint energy and ancillary service markets. Nevertheless, this joint market is still implemented at the level of wholesale markets. In [56], MGs are considered active prosumers to provide energy and ancillary service to the distribution network. Although the incorporation of joint energy and ancillary service exchanges is discussed, the focus of this research lies in the optimal management of the distribution system. An incentive contract between the independent system operator and frequency regulation service providers is designed in [62] to purchase energy and ancillary service simultaneously. The energy and frequency reserve are optimally allocated among regulation service producers. However, the contract design between two parties is the thesis's focus, without further comprehensive consideration in the view of the market design.

1.1.4 Distributed Voltage Regulation for Active Distribution Network

The concept of active distribution network (ADN) has been proposed to cooperate with the integration and regulation of DERs. Distributed generation (DG) and controllable load are considered as two main types of DERs which can be coordinated

to contribute to different types of ancillary services [11][63]. According to [64], ADN is referred to the distribution network integrated with DGs, which could control and monitor the status of DGs and loads. The flexibility of DG can be utilized to achieve a stable and secure system operation through a variety of sensing technology and a two-way communication network.

While many benefits can be achieved by the growing integration of DERs in ADNs, new challenges are also posed, particularly those related to optimal voltage regulation [65]. Due to the intermittent nature of renewable energy resources, such as solar photovoltaics (PVs), or wind farms, an increasing number of minor and temporary voltage violations will be experienced in a highly renewable penetrated distributed network. Conventional voltage regulation schemes, including on-load tap changer, thyristor-controlled Static VAR Compensator, or under-voltage load shedding, are predominantly deployed during extreme violations of voltage limits [66][67]. It is undesirable to frequently operate such control devices to regulate fast voltage deviations caused by renewable-based power variations, considering the cost and lifespan of the devices.

As a supplement to the conventional voltage regulation schemes, distributed control of DERs is a promising solution to deal with undervoltage and overvoltage problems in distribution networks. Resulting from advanced communication infrastructure, including high-speed communication links and secure protocols, distributed control architectures using DERs have been thoroughly discussed in the past to address the voltage problems [11], [27], [68]–[73].

To date, most of the existing distributed regulation schemes have considered either real or reactive power for voltage improvement. Reactive power *Q* support is the main approach to voltage control in most of the solutions. In [11], the reactive power provided by DERs can be collectively injected for the voltage regulation relying on the local exchange of information among neighboring controllers. A two-level distributed Volt/Var control method using PV inverters for the voltage regulation in the distribution network is proposed in [74]. Three-layer hybrid architecture is developed for Volt/Var control of distributed grids in [75], where fast-response DERs are employed together with load tap changers and voltage regulators for reactive power provision. [76] proposes an identification method to group the most effective control variables of reactive provision for voltage regulation in distribution networks. In practice, though, the ratio of line resistance to line reactance of a typical distribution network, i.e., *R/X* ratio, is usually much higher than that in transmission networks [73]. The impact of *R/X* on the effectiveness of reactive power support was examined in [77]. In [70], the bus voltage is considered much more sensitive to the change of real power *P*, which thus can be regulated by the real power provided by thermostatically controlled loads.

Jacobian matrix-based analysis has been used as a common tool to acquire the voltage sensitivity and calculate the needed power for the voltage restoration. For example, [72] utilizes the inverse Jacobian matrix for the sensitivity calculation to quantify the relationship between the voltage and injected power. However, such an approach requires global network information or at least prior knowledge about the network configuration. In [11], a distributed voltage control strategy is proposed, but

with a critical assumption that the local controller at each bus has an offline database, i.e., the voltage sensitivity of a certain bus being calculated according to a pre-defined network configuration. The topological approach to constructing a sensitivity table is proposed based on the Jacobian matrix in [78] for voltage regulation. However, such an approach lacks flexibility and scalability and is only suitable for a single network with fixed topology. In real life, the topology of an active distribution network will frequently change due to a need to integrate available DERs optimally. Therefore, it is impractical to update network topology information to all buses whenever a change happens.

Among a wide variety of DERs, EVs are considered one of the important parts of future active distribution networks under the development of vehicle-to-grid (V2G) technology. Many EVs can be used as flexible storage or controllable loads to participate in different ancillary services in the electrical network [79]. In [80], PV fluctuations are mitigated through the charging process of EVs in the distribution network. Fluctuations of wind generation are smoothed in [81] by developing a real-time charging strategy for plug-in EVs and in [82] by developing an optimized dispatch strategy for EVs. The load profile of the distribution network is flattened in [83] by utilizing large-scale V2G-enabled EVs. A smart charging strategy is proposed in [84] for EV charging stations to address the issue of finding an optimal charging station. The impact of EV load profiles on the distribution network under the stochastic charging behavior is assessed in [85], showing that EV charging should be appropriately coordinated and planned to avoid the voltage drop. Moreover, EV chargers can stabilize electrical network voltage and frequency by regulating both *P*

and *Q* with the appropriate charging solutions and control algorithms [86]. Particularly, on-board EV bidirectional chargers can supply reactive power support without the need of engaging the battery, and thus battery lifetime is not affected [87]. This feature makes EVs suitable candidates for voltage regulation in distribution networks, especially those with a higher *R/X* ratio.

1.1.5 Cybersecurity Considerations in Distributed Schemes

The deployment and integration of digital smart sensing, communication infrastructure, and control technologies have been accelerated in the past few decades to support smart power system applications and the optimal operation of modern ADNs. On one hand, it extensively boosts the growing functionalities of the power grid while maintaining its reliable operations. On the other hand, the successful realization of distributed operation requires advanced ICT, such as Internet of Things (IoT), 5G and edge computing. As work progresses on the digitalization transformation of the smart energy system, cybersecurity concerns continue to be raised. From another hand, a wide range of cybersecurity threats is posed to network components. To combat these threats, three main cybersecurity requirements: confidentiality, integrity, and availability, must be satisfied for system information security [88].

The resilience of power networks, which are subject to cyber-attacks, has been extensively investigated in the existing literature to satisfy cybersecurity requirements related to availability and integrity. Efforts have been devoted to detect and mitigate the adverse impacts of denial-of-service (DoS) attacks, which jeopardize the availability of information and power in smart grids [89]. For example, distributed

filters are developed for the power system affected by DoS in [90]. Resilient distributed control schemes for microgrids under DoS attacks are proposed in [91]–[93] using different advanced techniques. In terms of the integrity requirement of data and control actions, several works have been conducted to deal with false data injection (FDI) and data manipulation attacks. In [94], a consensus-based distributed EMS is proposed to maintain the correctness of local information under data integrity attacks. Secure secondary control strategies are developed in [95]–[97] to address FDI attacks in microgrids.

However, so far, insufficient attention has been paid yet to preserve the confidentiality of power system information. Confidentiality is an essential cybersecurity requirement to prevent unauthorized entities from obtaining confidential or private information of legitimate components [88]. The adversary actions, the so-called eavesdropping attacks, include stealing power usage data and price information, disclosing important decisions or control actions [98][99]. In a multi-agent cyber-physical system (CPS), eavesdropping attacks can be provoked by a curious and corrupted agent in the cyber network or an extraneous observer during data transmission and processing.

There are generally two approaches for preventing privacy disclosure. One approach is to implement differential privacy to protect data, and the other is to use cryptographic techniques. For the first approach, the so-called differential privacy, randomized noises are added into an individual's data such that an eavesdropper cannot infer the original information. In [100]–[102], privacy-preserving algorithms are developed based on differential privacy for energy management and economic

dispatch problems in smart grids and microgrids. In order to protect the confidentiality of private loads, differential privacy is also implemented in [103] for optimal power flow calculation. However, by utilizing differential privacy, the injected perturbations will potentially affect the exact accuracy of the algorithm convergence and deteriorate the control system performance. There exists an inherent tradeoff between correctness and privacy in the differential privacy scheme [104]. The injected noise should follow strict mathematical requirements, otherwise the convergence cannot be ensured.

By contrast, cryptographic techniques originated from cryptology, doe1s not inject any perturbation in the network and can find the exact solution of the problem after the decryption [98]. In particular, a homomorphic cryptosystem has desirable features which allow certain computations to be carried out on the ciphertext, i.e., the encrypted or encoded information, to maintain the confidentiality of the original information. After decrypting the encrypted result, it exactly matches the computation results performed on the plaintext [105]. With the advantage of semantically secure encryption and efficient decryption, the homomorphic cryptosystem has been employed in the field of distributed consensus-based control for creating privacy-preserving control schemes. In [106] and [107], privacy-preserving average consensus algorithms are developed to ensure the accurate average consensus without disclosing the initial states of agents. In [108], a distributed ratio consensus algorithm based on homomorphic encryption is developed.

With the incorporation of ICT, the ADN is a typical multi-agent CPS that includes different agents, e.g., DGs and load customers. Due to the dispersed nature of agents in the ADN, various distributed control and optimization schemes have been proposed

and favored to drive agents to different network-wide objectives, e.g., cost minimization, loss minimization, or accurate power sharing in [109]–[112]. Nevertheless, the collaborative nature of agents in a distributed scheme causes private information leakage easily. The data is transmitted and received directly between agents via communication links, which can be eavesdropped on by a corrupted agent or an extraneous observer. The confidential information of the agent that should be kept secret might be inferred and collected during the distributed decision-making process. For instance, the data of power usage is confidential as it can imply personal preference and activities. Therefore, measures to keep agents' private data secure in the distributed operation and control are essential to improve the resiliency of the ADN.

1.2 Research Challenges and Objectives

Although different distributed solutions have been investigated and applied in the low-voltage network, including secondary voltage and frequency control for the MG, P2P trading, distributed voltage regulation and distributed energy management system for the ADN, some drawbacks and research gaps are still needed to be addressed, which are concluded as:

1. As the distributed control relies on the information sharing among agents in the communication network, how the topology of the communication network of the MG impacts the distributed control? How to analytically formulate the relationship between the communication topology and the distributed control in the MG?

2. An appropriate P2P marketing mechanism for the MG should be put in place to facilitate not only the energy trading but the frequency response provision. However,

in the existing literature on the P2P market, the frequency regulation as an essential tradable ancillary service in the MG level to maintain the local balance of generation-demand and frequency stability has not been addressed carefully. The regulation effect, which could be closely related to the market mechanism, has not been clearly investigated.

3. Few studies have taken both *P* and *Q* into account to regulate the voltage, and their regulation effect has not been demonstrated in this regard. In addition, existing voltage regulation schemes using DERs are mostly investigated from the viewpoint of the technical side. Economic considerations related to voltage regulation ancillary service from the provider's side have not been adequately explored in the research as mentioned above. As a matter of fact, the financial incentive is a critical factor to encourage more providers to participate in the regulation scheme, which should not be neglected.

4. The distributed voltage regulation schemes in the distribution network are mainly based on the Jacobian matrix, which needs each bus to know the entire network. However, considering DERs' plug-in-play function and the frequent change of the physical topology, how to make sure each bus still contributes appropriately to the voltage regulation without prior knowledge about the network configuration?

5. So far, insufficient attention has been paid yet to preserve the confidentiality of power system information. However, the collaborative nature of agents in a distributed scheme causes private information leakage easily. How to protect the private information of each agent against eavesdropping attacks during iterative communications in distributed schemes is needed to be addressed.

Based on the above research gaps, the research objectives of the thesis, are summarized as follows:

1. The impact of the communication topology on the pinning-based secondary voltage and frequency control is examined analytically. A topology designing model is developed and can be used by the network designer to properly plan the communication network of the MG in the planning stage.

2. A deregulated trading framework that enables prosumers in the MG to trade energy and frequency regulation service simultaneously is proposed, economically coping with the balancing and frequency stability issue in the islanded MG. The regulation effect closely related to the market mechanism is investigated.

3. A fully distributed voltage regulation scheme for dominantly resistive distribution networks by utilizing both *P* and *Q*, considering the financial incentives of the EVFs, is proposed. It includes an optimal planning stage for the planning of EVF optimal charging/discharging and a distributed regulation stage for the real-time voltage regulation.

4. A privacy-preserving EMS for ADN based on the homomorphic cryptosystem is developed, fulfilling the core task to prevent information disclosure of each agent during the information exchange needed for distributed optimization and coordination.

1.3 Thesis Outline

The remainder of the thesis is organized as follows. The main object of Chapter 2 and Chapter 3 is the islanded MG. Chapter 2 analytically examines how the communication network topology influences distributed pinning-based secondary control performance for islanded MGs. A designing model is proposed to find the

optimal communication network topology with the lowest communication cost, and the desired control performance can be achieved. Following the P2P communication structure, Chapter 3 proposes a multi-market trading framework that enables the transaction of energy and ancillary service among participating DERs. The real-time distributed frequency regulation based on the pining control is provided according to the market trading results. Chapter 4 and Chapter 5 are dedicated to the secure and reliable operation of the distribution network. Chapter 4 provides a distributed voltage regulation scheme through incentivized EV charging. An optimal EV charging model is formulated so that both real power P and reactive power Q can be utilized to support the voltage. A distributed parallel-consensus algorithm is developed for the online voltage regulation stage. Chapter 5 describes the privacy concerns in distributed operation schemes due to the direct data flow among different agents. A secure and privacy-preserving EMS is proposed based on the homomorphic cryptosystem to prevent privacy breaches against eavesdropping attacks. Chapter 6 concludes the research and provides possible research extensions.

Chapter 2 Cost-Effective Communication Network Planning Considering Performance of Pinning-Based Secondary Control in Microgrids

Driven by the fact that the structural topology of the communication network has a significant effect on the dynamical performance of the related physical network, this Chapter addresses the communication network planning problem for islanded MGs. The optimal communication topology with the lowest communication cost, which supports the desired performance of pinning-based distributed control is designed in the MG planning stage. To achieve that, firstly, pinning synchronization control (PSC) is developed to regulate the voltage and frequency at each DG to the reference state. Then the criteria of the algebraic connectivity of communication network to fulfill the convergence requirement of PSC protocols are derived analytically using spectral graph properties and Lyapunov theory. Finally, a communication network planning model is formulated as Mixed Integer Semidefinite Program (MISDP) by using Linear Matrix Inequalities (LMI) techniques. The convergence speed requirement of PSC, communication time delay and the importance of connections between DGs are considered as constraints. The optimal communication network with the lowest communication cost can be acquired and the satisfactory dynamical performance of PSC protocols can be guaranteed. The case studies are designed to evaluate how the planning model can practically facilitate the pinning-based control in the islanded MG. The simulation results effectively verify that the dynamical control convergence can be improved under the properly designed communication network. The control

performance of the proposed protocol is validated experimentally based on a two-DG MG prototype.

2.1 Pinning Synchronization Control Protocols for Distributed Secondary Voltage and Frequency Control

A typical MG generally is comprised of two main functional systems: physical system and cyber system, which collaborates with each other to ensure a reliable and stable operation. The information flow among DGs in the cyber system plays a key factor in achieving control goals and reflecting the dynamical performance of the secondary control in the physical system. In this section, the communication graph, which is used to describe the structural topology of the cyber system, is introduced firstly. Then the primary and pinning based secondary control of the physical system is presented.

2.1.1 Preliminary on the Communication Graph

The topology of the communication network can be depicted by a weighted graph, $\mathcal{G} = (\mathcal{V}, \mathcal{E}, \mathcal{A})$, containing a set of nodes $\mathcal{V} = \{v_1, v_2, \dots, v_N\}$ and edges $\mathcal{E} \subseteq \mathcal{V} \times \mathcal{V}$. For a MG, one DG unit and the communication link between two DGs can be regarded as a node and an edge of the corresponding communication graph $\mathcal{G}$, respectively. $\boldsymbol{A} = (a_{ij}) \in \mathbb{R}^{N \times N}$ is defined as the weighted *adjacency matrix* to describe the weight of the communication link. If i^{th} node can receive the information from j^{th} node, a_{ij} is a positive number; otherwise $a_{ij} = 0$. The set of neighboring nodes of i^{th} node is denoted as $N_i = \{v_j \in \mathcal{V} | (v_i, v_j) \in \mathcal{E}\}$. In-degree and out-degree of i^{th} node is defined as follows in a weighted graph:

$$deg_{in}(v_i) = \sum_{j=1}^{N} a_{ji} \qquad deg_{out}(v_i) = \sum_{j=1}^{N} a_{ij} \tag{2.1}$$

Degree matrix $\boldsymbol{D}$ of the graph $\mathcal{G}$ is a diagonal matrix with the i^{th} diagonal entry as the out-degree of the i^{th} node. Matrix $\boldsymbol{L_N} = \boldsymbol{D} - \boldsymbol{A}$ is defined as *Laplacian matrix* of the graph $\mathcal{G}$, with entry $l_{ij} = -a_{ij}$ for $i \neq j$ and $l_{ij} = \sum_{j=1, j\neq i}^{N} a_{ij}$ for $i = j$. It is irreducible with eigenvalues $0 = \lambda_1(\boldsymbol{L_N}) < \lambda_2(\boldsymbol{L_N}) \leq \cdots \lambda_N(\boldsymbol{L_N})$ for a strongly connected network. The eigenvalues of the Laplacian matrix contain the structural information of the communication network. Importantly, $\lambda_2(\boldsymbol{L_N})$ is referred as *algebraic connectivity* of the graph, which characterizes the performance of network dynamics and determines the convergence rate.

2.1.2 Modelling of DER Inverter Controller

A typical inverter-based MG is shown in Fig. 2.1, which consists of three modules: inverter-based DGs, inverter controllers and load. Each DG is connected to the main grid through a power electronic-based interface, which consists of a DC voltage source, an inverter bridge, and a resistance-inductor-capacitor (RLC) filter. The inverter controller including power control, voltage and current control aims to regulate the output voltage and frequency of the inverter, which is shown in Fig. 2.2. The accuracy of assessment of MG stability is closely related to the precision of its dynamical model. The small-signal analysis of MG has been studied in most of the existing works and the eigenvalue analysis is used to evaluate the system stability, which however, only ensure the small signal stability. The system stability with the large signal disturbances cannot be guaranteed [114]. Alternatively, the large-signal dynamical model can be used to evaluate the dynamic performance of the network under the large signal

disturbances [23], [28]. Generally, both two modelling techniques are capable of the analysis of fast transient dynamics of DG and MG.

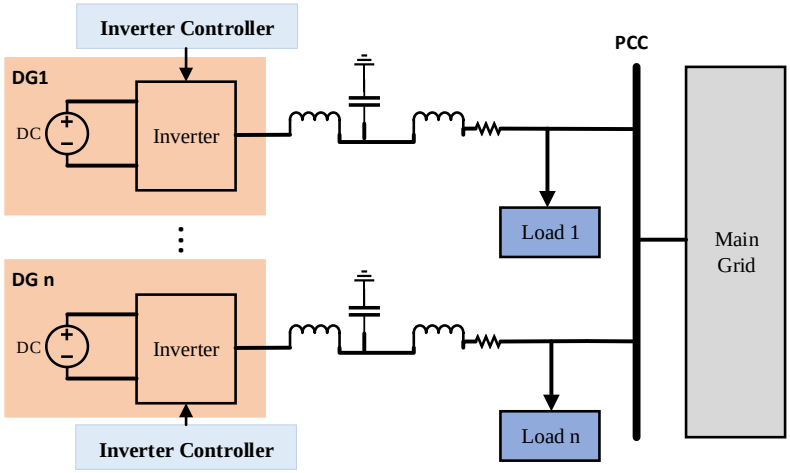

Fig. 2.1. Network diagram of a typical inverter-based MG

For the hierarchical control system of MGs, power control has slower dynamics comparing to the voltage and current control [18]. As the voltage and frequency restoration is of our interest in this work, faster loops are neglected, and only power controller is considered for the inverter-based DG model. Moreover, switching dynamics is neglected due to the relatively high switching frequency of the inverter bridge and an ideal DC source is assumed for each DG which means the DC-bus dynamics can also be neglected. The dynamics of each inverter is formulated based on their individual rotating reference frames at rotational frequency ω_i , i.e., $(d-q)_i$. In the controller module, all quantities in three-phase are transformed to *d*-*q* quantities. After the control actions are conducted, all *d*-*q* quantities are transformed back to three-phase quantities. As a MG consists of more than one inverter, the frame attached to one of the inverters is regarded as the common reference frame $d-q$ with rotating frequency ω_{com}.

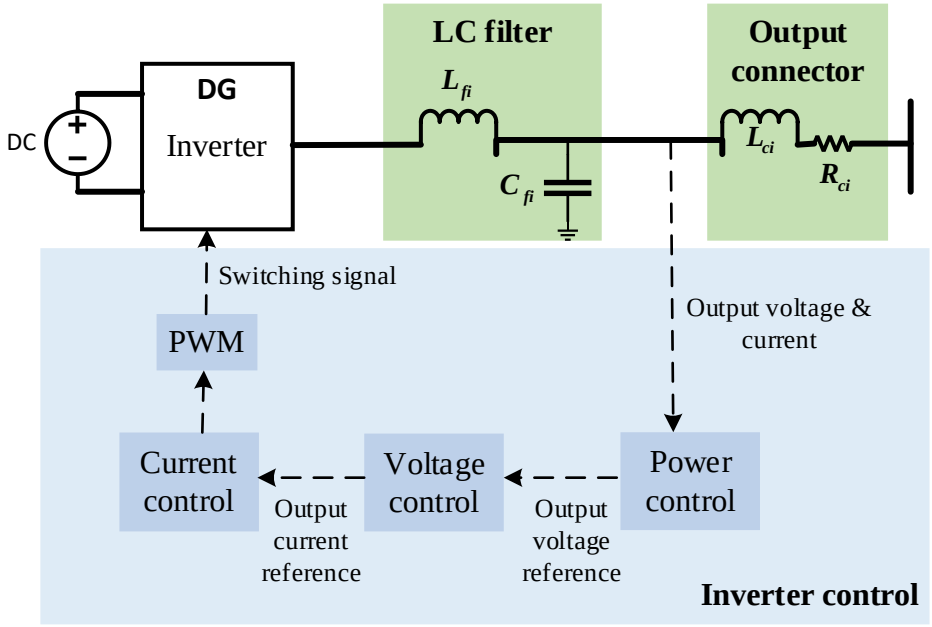

Fig. 2.2. Functional blocks of the inverter control

The droop technique is adopted in the power controller to regulate the angular frequency ω_i and voltage magnitude V_i through local real and reactive power measurements. Fig. 2.3 shows its internal working mechanism. The primary droop control keeps voltage and frequency in the pre-defined ranges, however, there exists inherent voltage deviation of each inverter output voltage from its nominal value. As an additional control level to compensate voltage deviations resulted from the primary control, secondary control is required to restore the voltage [15][16].

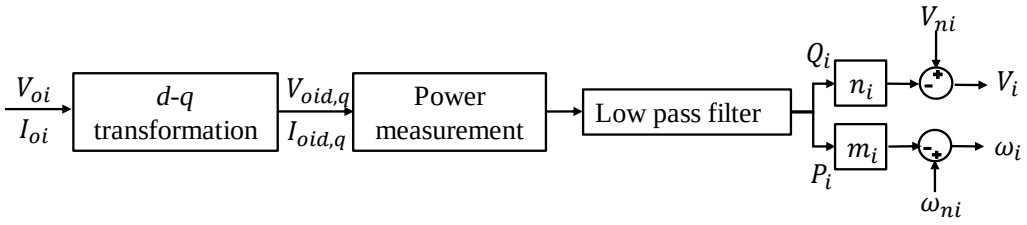

Fig. 2.3. Diagram of droop control

2.1.3 Development of PSC Protocols for Distributed Secondary Voltage and Frequency Control

As shown on the left-side of Fig. 2.4, an inverter-based DG i consisting of a DC voltage source, an inverter bridge and a RLC filter, is connected to the main grid via a point of connection (PoC). The dynamics of each DG are formulated based on a common $d-q$ frame. The primary control of each DG includes droop controller, PI voltage controller and PI current controller. Detailed modeling of the voltage and current controller can be referred to [23]. The droop technique is adopted to regulate the angular frequency ω_i and voltage magnitude V_i through local real and reactive power measurements:

$$\omega_i = \omega_{ni} - n_i P_i \tag{2.2a}$$

$$V_i = V_{ni} - m_i Q_i \tag{2.2b}$$

where ω_i is the frequency reference provided to the inverter; ω_{ni} and V_{ni} are the nominal frequency and voltage magnitude, respectively; n_i and m_i are the droop gains which are set according to the power rating of the DG; P_i and Q_i are the average output active and reactive power acquired by passing instantaneous power measurements through a low-pass filter with the cutoff frequency ω_c:

$$\dot{P}_i = -\omega_c P_i + \omega_c (V_{oid}\, I_{oid} + V_{oiq}\, I_{oiq}) \tag{2.3a}$$

$$\dot{Q}_i = -\omega_c Q_i + \omega_c (V_{oiq} I_{oid} - V_{oid} I_{oiq}) \tag{2.3b}$$

where V_{oid} (I_{oid}) and V_{oiq}(I_{oiq}) donate the output voltage (current) along the d axis and q axis, respectively. As the output voltage of the inverter is adjusted to d-axis of the reference frame, the magnitude V_i along d-axis and q-axis can be written as

$$\begin{cases} V_{oid}^{ref} = V_{ni} - m_i Q_i \\ V_{oiq}^{ref} = 0 \end{cases} \tag{2.4}$$

where V_{oid}^{ref} is the reference value for the voltage controller.

As shown on the right-side of Fig. 2.4, to eliminate the deviations of V_{di} and ω_i from its nominal value, correction terms $\Delta\delta_{V_i}$ and $\Delta\delta_{\omega_i}$ are embedded into droop mechanisms (2.2):

$$V_{di} = V_{ni} - m_i Q_i + \Delta\delta_{V_i} \tag{2.5a}$$

$$\omega_i = \omega_{ni} - n_i P_i + \Delta\delta_{\omega_i} \tag{2.5b}$$

The following control objectives are expected to achieve for each DG when the MG is disconnected from the main grid:

$$\lim_{t\to\infty} V_{di}(t) = V_{ref} \tag{2.6a}$$

$$\lim_{t\to\infty} \omega_i(t) = \omega_{ref} \tag{2.6b}$$

PSC protocols are employed to formulate secondary control where a small group of DGs is selected to be controlled so that (2.6) can be realized by forwarding proper correction terms from secondary control to the droop level. Only pinning DGs are injected with the reference signal. Through the local information exchange in the neighbor-to-neighbor communication network, dynamical frequency and voltage disagreement of DG *i* with neighboring DGs is formulated as follows:

$$\dot{\omega}_i(\mathrm{t}) = c\{\textstyle\sum_{j\in N_i} l_{ij} Z\left[\omega_j(\mathrm{t}) - \omega_i(\mathrm{t})\right] + d_i\left[\omega_{ref} - \omega_i(\mathrm{t})\right]\} \tag{2.7a}$$

$$\dot{V}_{di}(\mathrm{t}) = \mathrm{c}\{\textstyle\sum_{j\in N_i} l_{ij}\, Z\left[V_{dj}(\mathrm{t}) - V_{di}(\mathrm{t})\right] + d_i\left[V_{ref} - V_{di}(\mathrm{t})\right]\} \tag{2.7b}$$

where c is the coupling strength of the communication network; l_{ij} indicates the weight of the communication link between any pair of DGs; $d_i > 0$ denotes the

pinning control gain, $d_i = 0$ if DG is not pinned. $Z = diag(z_1, \dots, z_N) > 0$ is the inner coupling matrix. By applying protocols (2.7), pinning DGs regulate own output voltage and frequency to V_{ref} and ω_{ref} while the non-pinning DGs minimize the disagreement with their neighboring DGs. The correction terms can be acquired by employing feedback actions:

$$\Delta\delta_{V_i} = -k_{V_i} \int \dot{V}_{dl}(t) \tag{2.8a}$$

$$\Delta\delta_{\omega_i} = -k_{\omega_i} \int \dot{\omega}_{l}(t) \tag{2.8b}$$

where k_{V_i} and k_{ω_i} are the positive feedback gains.

Pinning DGs will be determined by the network operators in the planning stage. After obtaining the planning results, the most highly connected DG, i.e., DG with the largest degree, is selected to pin and access the reference value of the frequency and voltage. In real-time operation if there is the communication failure that makes the topology changes, the entire network can still operate as normal if the pinning node is still in the connection. Besides, the selected pinning DGs will be planned with the backup communication links and the backup ones can be activated in time in case of emergency.

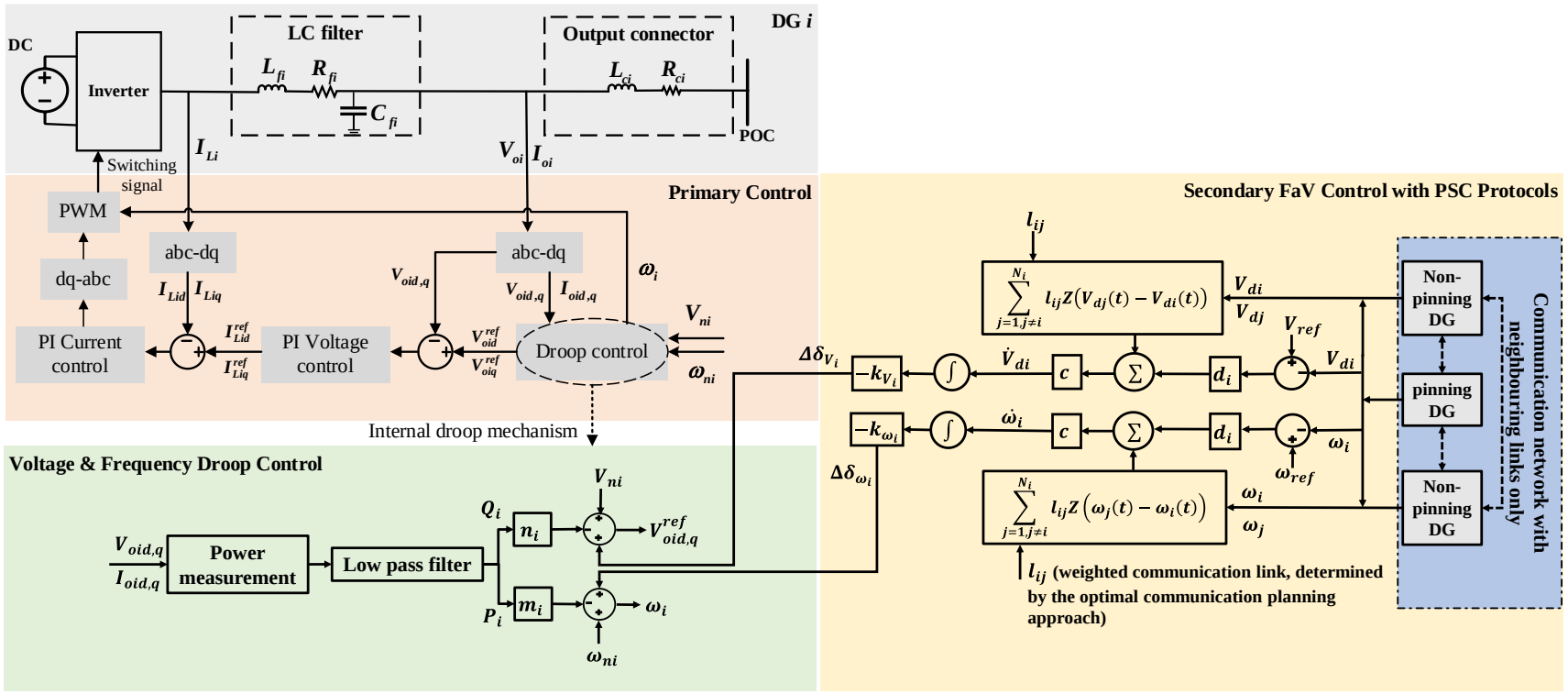

Fig. 2.4. Schematic diagram for primary control and secondary control with PSC protocols of i^{th} DG

2.2 Pinning Controllability Analysis Based on the Algebraic Graph-theoretic Properties

In this section, the criteria for the pinning controllability of the proposed PSC are investigated using algebraic graph-theoretic properties. Two assumptions in terms of the communication network are made to accelerate the analysis of the pinning controllability: 1) The information can be exchanged bi-directionally via the communication link, which gives an undirected communication graph $\mathcal{G}$. As such $deg_{in}(v_i) = deg_{out}(v_i)$ for each DG, i.e., the graph is balanced. 2) For any non-pinning DG i, there is always a path connecting pinning DG and DG i in the network, i.e., the undirected graph is strongly connected.

For a MG with the communication graph $\mathcal{G}$, the set comprising the pinning DGs is denoted as *J* and $|J| = p$ is the number of DGs in set *J*. Without loss of generality, it is assumed that the first p DGs are pinned. By removing the rows and columns corresponding to *J* of the Laplacian matrix $\boldsymbol{L_N}$, a $(N-p)\times(N-p)$ submatrix $\boldsymbol{L_{N-p}}$ can be obtained, which is referred to *Grounded Laplacian matrix* [116].

Lemma 1 [117]: Let C_n be a symmetric $n \times n$ matrix and $B = diag\left(b_1, \dots, b_P, \underbrace{0, \dots, 0}_{n-p}\right)$ with $b_i > 0, i = 1, \dots, p$. When $b_i > 0$ is sufficiently large, $C - B < 0$ is equivalent to $C_{n-p} < 0$, where C_{n-p} is the submatrix of *C* by deleting its first p row-column pairs.

Lemma 2 [117]: Let *B* and *C* are $n \times n$ *Hermitian* matrices, If $\lambda_1 \le \cdots \le \lambda_n$, $\mu_1 \le \cdots \le \mu_n$ and $\gamma_1 \le \cdots \le \gamma_n$ are the eigenvalues of *B*, *C* and *B*+*C*, respectively. Then for $i = 1, \dots, n$, one has $\lambda_i + \mu_1 \le \gamma_i \le \lambda_i + \mu_n$.

Let $e_{V_i}(t) = V_{di}(t) - V_{ref}$ and $e_{\omega_i}(t) = \omega_i(t) - \omega_{ref}$ denote the voltage and frequency tracking error, respectively. The tracking error dynamics can be formulated as:

$$\dot{\varepsilon}_i = f\left(\varepsilon_i + V_{ref}\right) - f\left(V_{ref}\right) + c\sum_{j\in N_i} l_{ij}\, Z\varepsilon_j - d_i Z\varepsilon_i \tag{2.9}$$

where $\varepsilon_i = [{e_{V_i}}^T, {e_{\omega_i}}^T]$ is the compact form of the tracking errors.

Assumption 1 [118]*:* For any two different vectors $x, y \in \mathbb{R}^N$, there exists a sufficiently large positive α, such that nonlinear function f satisfies

$$(x-y)^T[f(x) - f(y)] \le \alpha(x-y)^T Z(x-y) \tag{2.10}$$

Theorem 1: Suppose that Assumption 1 holds, by employing the feedback controller (2.8), the states of all DGs globally synchronize to the reference state, provided that

$$\lambda_1\left(L_{N-p}\right) > \alpha/c \tag{2.11}$$

Proof: Construct the Lyapunov functional candidate

$$V = \frac{1}{2}\sum_{i=1}^{N} {\varepsilon_i}^T \varepsilon_i \tag{2.12}$$

Then

$$\dot{V} = \sum_{i=1}^{N} {\varepsilon_i}^T \left[f(\varepsilon_i + s) - f(s) + c\sum_{j\in N_i} l_{ij}\, Z\varepsilon_j - d_i Z\varepsilon_i \right]$$

$$\le {\varepsilon_i}^T \left[\alpha Z + c\sum_{j\in N_i} l_{ij}\, Z\varepsilon_j - d_i Z\varepsilon_i\right] \tag{2.13}$$

Rewrite (2.13) in the compact matrix form:

$$\dot{V} \le \boldsymbol{E}^T[(\alpha \boldsymbol{I_N} + c\boldsymbol{L} - \boldsymbol{D}) \otimes \boldsymbol{Z}]$$

$$= \boldsymbol{E}^T[(\boldsymbol{M} - \boldsymbol{D}) \otimes \boldsymbol{Z}] \tag{2.14}$$

where $\boldsymbol{D} = diag(d_1, \dots, d_p, \underbrace{0, \dots, 0}_{N-p})$ and $\otimes$ represents the Kronecker product of two matrices. From Lemma 1, it is known that $\boldsymbol{M} - \boldsymbol{D} < 0$ is equivalent to the $\boldsymbol{M}_{N-p} < 0$, which is the submatrix of *M* by deleting the corresponding p row-column pairs. By using Lemma 2, the following result holds

$$\lambda_1(\boldsymbol{M}_{\boldsymbol{N-p}}) = \lambda_1((\alpha \boldsymbol{I}_{\boldsymbol{N}} + c\boldsymbol{L})_{N-p}) \leq \alpha + c\lambda_1(\boldsymbol{L}_{\boldsymbol{N-p}}) \tag{2.15}$$

According to the given condition (2.11) in Theorem 1, we know $-c\lambda_1(\boldsymbol{L}_{\boldsymbol{N-p}}) < -\alpha$ and $\alpha + c\lambda_1(\boldsymbol{L}_{\boldsymbol{N-p}}) < 0$ hence. Given (2.15), we have $\lambda_1(\boldsymbol{M}_{\boldsymbol{N-p}}) < 0$ which reveals $\boldsymbol{M}_{\boldsymbol{N-p}} < 0$. Then, it can be concluded that $\boldsymbol{M} - \boldsymbol{D} < 0$ and therefor $\dot{V} < 0$ which indicates that the tracking errors would asymptotically go to zero, i.e., $\lim_{t\to\infty} V_{di}(t) = V_{ref}$ and $\lim_{t\to\infty} \omega_i(t) = \omega_{ref}$. This completes the proof.

Remark: Theorem 1 provides the algebraic graph-theoretic condition of controllability of the proposed PSC protocols under the feedback control. Given the coupling strength of the network, the larger $\lambda_1(\boldsymbol{L}_{\boldsymbol{N-p}})$ the faster convergence of PSC. Compared to the controllability index proposed in [33][119], the condition is independent of pinning gains.

Theorem 2 *(Cauchy interlacing theorem* [120]*):* Let *B* be a $n \times n$ matrix and *C* a submatrix of *B* with order *n*-1. If $\lambda_1 \leq \cdots \leq \lambda_n$ and $\mu_1 \leq \cdots \leq \mu_{n-1}$ are the eigenvalues of *B* and *C*, respectively, then

$$\lambda_1 \leq \mu_1 \leq \lambda_2 \dots \leq \lambda_{n-1} \leq \mu_{n-1} \leq \lambda_n \tag{2.16}$$

By Theorem 2, the following relationship can be found

$$\lambda_i(\boldsymbol{L_N}) \leq \lambda_i(\boldsymbol{L_{N-p}}) \leq \lambda_{p+\mathrm{i}}(\boldsymbol{L_N}) \tag{2.17}$$

Let $i = 1$, then

$$\lambda_1(\boldsymbol{L_{N-p}}) \leq \lambda_{p+1}(\boldsymbol{L_N}) \tag{2.18}$$

Based on the conclusions in [32], $\lambda_{p+1}(\boldsymbol{L_N})$ is equal to $\lambda_1(\boldsymbol{L_{N-p}})$ when a small portion of nodes are pinned ($\frac{p}{N} \leq 50\%$). Supposing only one DG in the MG is pinned, i.e., $p = 1$, a good estimation of synchronization measure can be made by the algebraic connectivity of the corresponding communication network, and the following equivalence is established

$$\lambda_1\big(\boldsymbol{L_{N-p}}\big) = \lambda_2(\boldsymbol{L_N}) \tag{2.19}$$

The condition (2.11) is adopted to $\lambda_2(\boldsymbol{L_N})$ and thus the following result holds to guarantee the pinning synchronization when only a single DG is pinned:

$$\lambda_2(\boldsymbol{L_N}) > \frac{\alpha}{c} = \lambda^* \tag{2.20}$$

where $\lambda^* = \alpha/c$ is the lower bound for the algebraic connectivity of a communication graph for the MG to achieve the minimum convergence requirement of the PSC.

Remark: Now the relationship between the communication network topology and the convergence speed of the PSC is established: larger the second smallest eigenvalue of the Laplacian $\lambda_2(\boldsymbol{L_N})$, the faster convergence speed of the PSC protocols. It should be mentioned that the effectiveness of the PSC also depends on the physical parameters of the individual DG and corresponding controller parameter setting. Extensive studies have been done to investigate how physical control parameters and the physical network influence the dynamics of the MG, which however is not our

focus in this chapter. We target the MG which is under construction at the planning stage. How to design an optimal communication network with the lowest cost whilst ensure the performance of the control protocol is of our interest.

2.3 Cost-Effective Communication Network Planning

A dedicated communication network with proper structural topology can largely facilitate the implementation of distributed secondary control operations within a MG. Specifically, in the planning stage of the construction of MGs, the comprehensive design of the communication network is vital for the future reliable and stable operation of the MG when it goes in-service. Fig. 2.5 shows the interdependence between the communication network planning and the real operation of the MG including the physical and cyber system.

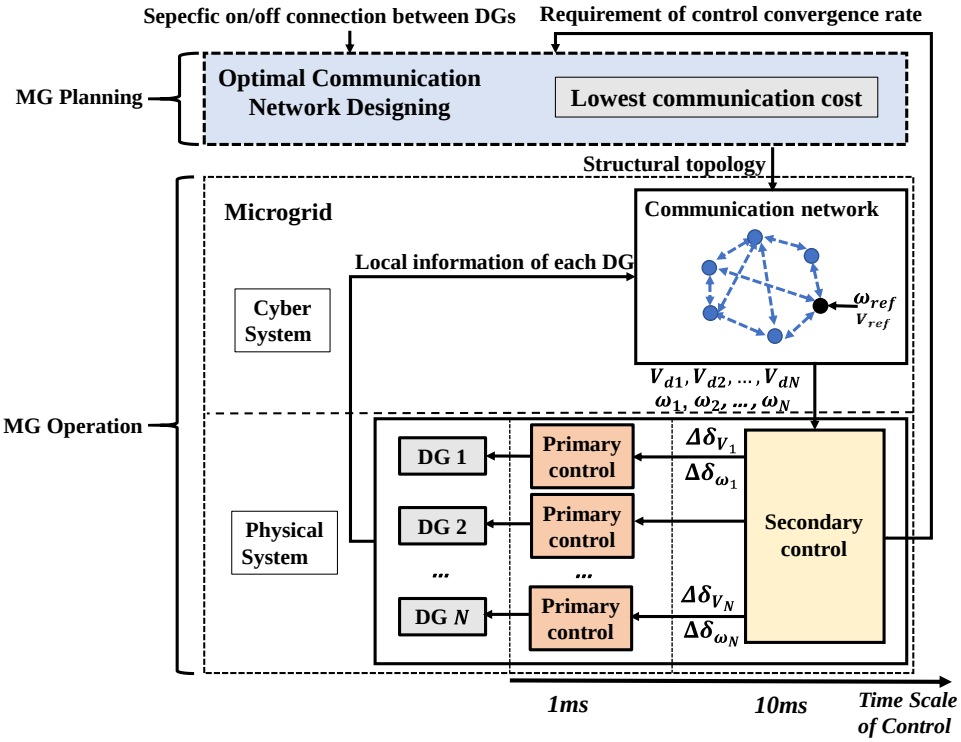

Fig. 2.5. System and control formulation of the MG with communication network design strategies

2.3.1 Problem Formulation

As the planning problem for the MG communication network is of our great concern in the chapter, the number of DG connection point and the importance of DG are considered as known parameters for the designing. In practice, the utility or grid operator will evaluate DGs based on some factors (e.g., economic factor, reliability factor). The generator with higher reliability or larger investment return will be recognized with a higher priority. Besides, the importance of DGs can be determined considering the priority level of their directly connected loads by the grid operator. The DG responsible for the power supply for the load or customer with a higher priority will be treated to be more important and thus it should equip with more communication links to speed the data exchanging. For some pairs of DGs there is no need to build the connection between them due to the practical considerations of the privacy concern or the geometrical distance. Hence, on/off connection between certain pair of DGs is one of the important factors that must be considered by the network designer. Besides, the weight of the communication link, which can be determined by the required size of data packet or the rate of data transfer in practice, should also be considered for the communication network designing as it affects the communication quality or speed. For the cooperative operation of multiple DGs in a distributed fashion heavily relying on communication, it is desirable to keep the communication cost as low as possible while ensuring the convergence speed of protocols fast enough to realize the satisfying synchronization performance. The total communication cost for the communication network is defined:

$$C = \sum_{i,j=1}^{N} \mathrm{sgn}(a_{ij}) \tag{2.21}$$

This equation physically represents the total number of undirected communication links of a weighted graph, where the sign function in the equation takes negative a_{ij} to -1, zero a_{ij} to 0 and positive a_{ij} to 1. Based on the result from the previous section, the second largest eigenvalue λ_2 of the Laplacian matrix of the communication graph, known as algebraic connectivity, is an important measure of the network synchronization performance. Therefore, in view of graph-theoretic conditions, the algebraic connectivity of the communication graph must be taken into consideration as a critical constraint to ensure the control convergence performance when planning the communication topology.

Besides, the communications among DGs would inevitably experience time delays which deteriorate the system dynamic performances. Therefore, it is important to incorporate time delays when designing the optimal communication network topology. If all communication links suffer a time delay τ, a sufficient condition for the convergence of the synchronization protocol is $\tau \leq \pi/2\lambda_{max}(L_N)$ [121], where $\lambda_{max}(L_N)$ denotes the maximum eigenvalue of Laplacian matrix of the communication graph. The network delay margin is directly related to the maximum eigenvalue of Laplacian matrix of its communication graph.

Given the lower bound of the algebraic connectivity λ^*, the network design goal is to obtain the lowest communication cost while the required convergence speed condition is fulfilled. Time delay τ is also considered as one of the constraints to design the communication topology. One can formulate as:

$$\min_{C \in \mathbb{R}} \mathrm{C} \tag{2.22}$$

s.t $$l_{ij} \leq 0 \quad \forall\, i,j = 1,2,\dots,N, i \neq j \tag{2.22a}$$

$$l_{ii} \geq 0 \quad \forall\, i = 1,2,\dots,N \tag{2.22b}$$

$$L_N \mathbf{1} = 0 \tag{2.22c}$$

$$\mathbf{1}^{\boldsymbol{T}} L_N = 0 \tag{2.22d}$$

$$\lambda_2(\boldsymbol{L_N}) \geq \lambda^* \tag{2.22e}$$

$$\tau \leq \pi/2\lambda_{max}(L_N) \tag{2.22f}$$

where $\mathbf{1}$ represents a n-by-1 vector with all coefficients equal to one. Constraint (2.22a) - (2.22c) ensure L_N is a legal Laplacian matrix. Particularly, (2.22a) indicates the on/off connection relationship between any pair of DGs. Constraint (2.22d) makes sure the communication graph is balanced, i.e., $deg_{in}(v_i) = deg_{out}(v_i)$ for each DG. Constraint (2.22e) is imposed to ensure the convergence of the proposed PSC protocols. Constraint (2.22f) must be fulfilled to ensure the convergence of the protocols if there is a time delay τ existing on all communication links.

2.3.2 Reformulation and Relaxation

As such the optimization involves eigenvalue calculation, it is inherently a NP-hardness problem that is computationally complex [33]. In order to transform the original problem into a solver-efficient convex problem, binary variables are introduced to transform the above problem to the *Mixed Integer Semidefinite Program* (MISDP) based on the *Linear Matrix Inequalities* (LMI).

The transformation starts with the constraints such that all constraints are transformed to LMIs. Boolean binary variable $\chi_{ij} \in \{0,1\}$ is introduced to

substitute$l_{ij} \leq 0, i, j = 1, \dots, N, i \neq j$. Hence, constraint (2.22a) can be replaced by the following series of new constraints:

$$l_{ij} \leq 0 \quad \forall\, i, j = 1,2, \dots, N, i \neq j \tag{2.23}$$

$$l_{ij} \leq 1 - \chi_{ij} \quad \forall\, i, j = 1,2, \dots, N, i \neq j \tag{2.24}$$

$$l_{ij} \geq \chi_{ij} M \qquad \forall\, i, j = 1,2, \dots, N, i \neq j \tag{2.25}$$

where $M < 0$ is a small lower bound on l_{ij} to limit the weight of the communication link, i.e., $l_{ij} \leq |M|$. Defining $\mathbf{\Gamma} \in \{0,1\}^{N \times N}$ as a binary matrix with entry $\Gamma_{ij} = \chi_{ij}$ and $\Gamma_{ii} = 0$ for $i, j = 1, \dots, N$, the following constraint can be used to define a strongly connected graph of $\boldsymbol{L_N}$:

$$\mathbf{\Gamma 1} = \mathbf{\Gamma}^T \mathbf{1} \tag{2.26}$$

$\sum_{i,j=1, i \neq j}^{N} \chi_{ij} = \mathbf{1^T \Gamma 1}$represents the total number of communication links, and thus communication cost *C* in the objective function (2.22) can be reformulated as:

$$C = \mathbf{1^T \Gamma 1} \tag{2.27}$$

Constraint (2.22f) can be reformulated as [122]:

$$l_{ii} \leq 1/2\tau \tag{2.28}$$

Now the reformulation is left with the constraint (22e) which is also needed to be transformed to LMI. For a connected and undirected graph, $\lambda_2(\boldsymbol{L_N})$ can be written as [123]:

$$\lambda_2(\boldsymbol{L_N}) = \min_{z \neq 0} \frac{x^T \boldsymbol{L_N} x}{\|x\|^2} \tag{2.29}$$

We define $\boldsymbol{H} = xx^T$and the following formulation exists [122]:

$$\lambda_2(\boldsymbol{L_N}) = \min_{H \in S^n} \langle \boldsymbol{H}, \boldsymbol{L_N} \rangle \tag{2.30}$$

s.t. $$\boldsymbol{H} \succcurlyeq 0 \tag{2.31}$$

$$\mathrm{Tr}\boldsymbol{H} = 1 \tag{2.32}$$

$$\boldsymbol{H1} = [0]_{n \times 1} \tag{2.33}$$

$$\mathrm{rank}(\boldsymbol{H}) = \boldsymbol{1} \tag{2.34}$$

where $\langle \boldsymbol{H}, \boldsymbol{L_N} \rangle$ represents the inner product between matrix $\boldsymbol{H}$ and $\boldsymbol{L_N}$ .The rank constraint (2.34) needs to be relaxed and the dual problem is written as follows:

$$\mathcal{L}(\boldsymbol{H}, \boldsymbol{K}, k_1, k_2) = \langle \boldsymbol{H}, \boldsymbol{L_N} \rangle - \langle \boldsymbol{H}, \boldsymbol{K} \rangle + k_1(1 - \mathrm{Tr}\boldsymbol{H}) + k_2^T \boldsymbol{H}1 \tag{2.35}$$

where $\boldsymbol{K} \in S_+^{\boldsymbol{n}}, k_1, k_2 \in \mathbb{R}$.

$$g(\boldsymbol{K}, k_1, k_2) = \min_{H \in S^n} \langle \boldsymbol{H}, \boldsymbol{L_N} - \boldsymbol{K} - k_1 \boldsymbol{I} + k_2 \boldsymbol{1^T} \rangle + k_1 =$$

$$\begin{cases} k_1, if\ \boldsymbol{L_N} - \boldsymbol{K} - k_1 \boldsymbol{I} + k_2 \boldsymbol{1^T} = 0 \\ -\infty, otherwise \end{cases} \tag{2.36}$$

Furthermore,

$$g^* = \max_{\boldsymbol{K} \in S_{+,}^{\boldsymbol{n}} k_1, k_2 \in \mathbb{R}} g(\boldsymbol{K}, k_1, k_2) \tag{2.37}$$

$$= \max_{\boldsymbol{K} \in S_{+,}^{\boldsymbol{n}} k_1, k_2 \in \mathbb{R}} k_1 \tag{2.38}$$

s.t. $$(k_2)_1 = \cdots = (k_2)_n = \beta \tag{2.39}$$

$$k_2 \boldsymbol{1^T} - k_1 \boldsymbol{I} + \boldsymbol{L_N} \succcurlyeq 0 \tag{2.40}$$

Then $$g^* = \max_{\boldsymbol{K} \in S_{+,}^{\boldsymbol{n}} k_1, k_2 \in \mathbb{R}} k_1 \tag{2.41}$$

s.t. $$\beta \boldsymbol{11^T} - k_1 \boldsymbol{I} + \boldsymbol{L_N} \succcurlyeq 0 \tag{2.42}$$

The primal-dual variables (H^*, k_1^*, β^*) are introduced to form the primal and dual problem. KKT conditions are necessary for the optimum as the primal and dual problem is both strictly feasible, which are as follows [124]:

Primal feasibility: $\boldsymbol{H}^* \succcurlyeq 0$,Tr$\boldsymbol{H}^* = 1$, $\boldsymbol{H}^*\mathbf{1} = [0]_{n\times 1}$

Dual feasibility: $\beta^*\mathbf{1}\mathbf{1}^{\boldsymbol{T}} - {k_1}^*\boldsymbol{I} + \boldsymbol{L_N} \succcurlyeq 0$

Complementary slackness: $(\beta^*\mathbf{1}\mathbf{1}^{\boldsymbol{T}} - {k_1}^*\boldsymbol{I} + \boldsymbol{L_N})\boldsymbol{H}^* = \mathbf{0}$

Consider $\boldsymbol{H}^*$ as the primal optimal solution and thus $(\beta^*\mathbf{1}\mathbf{1}^{\boldsymbol{T}} - {k_1}^*\boldsymbol{I} + \boldsymbol{L_N})h^* = \mathbf{0}$ holds for any column h^* of $\boldsymbol{H}^*$.By normalizing h^*, it is concluded that $h^*(h^*)^T \succcurlyeq 0, \mathrm{Tr}h^*(h^*)^T = 1, h^*(h^*)^T = [0]_{n\times 1}$. Therefore, $h^*(h^*)^T$is a primal optimal solution whose rank is 1. Now it has proved that the rank relaxation of (2.34) is exact.

2.3.3 MISDP Model for Designing Communication Topology

After completing the relaxations, the problem (2.22) can be rearranged into the MISDP model:

$$\min_{L\in\mathbb{R}^{N\times N},\Gamma\in\{0,1\}^{N\times N},\beta,k\in\mathbb{R}} \mathbf{1}^{\boldsymbol{T}}\boldsymbol{\Gamma}\mathbf{1} \tag{2.43}$$

$$l_{ij} \le 0 \quad \forall\, i,j = 1,2,\dots,N, i \ne j \tag{2.43a}$$

$$k > \lambda^* \tag{2.43b}$$

$$l_{ii} \le 1/2\tau \tag{2.43c}$$

$$\boldsymbol{L_N}\mathbf{1} = 0 \tag{2.43d}$$

$$\mathbf{1}^{\boldsymbol{T}}\boldsymbol{L_N} = 0 \tag{2.43e}$$

$$\beta\mathbf{1}\mathbf{1}^T - k\boldsymbol{I} + \boldsymbol{L_N} \succcurlyeq 0 \tag{2.43f}$$

$$l_{ii} \geq 0 \quad \forall\, i = 1,2,\dots,N \tag{2.43g}$$

$$\chi_{ii} = 0 \;\forall\, i = 1,2,\dots,N \tag{2.43h}$$

$$l_{ij} \leq 1 - \chi_{ij} \quad \forall\, i,j = 1,2,\dots,N, i \neq j \tag{2.43i}$$

$$l_{ij} \geq \chi_{ij} M \qquad \forall\, i,j = 1,2,\dots,N, i \neq j \tag{2.43j}$$

$$\boldsymbol{\Gamma 1} = \boldsymbol{\Gamma}^T \mathbf{1} \tag{2.43k}$$

The MISDP reformulation can be solved efficiently by the solver. The optimal communication topology can be found by determining the Laplacian matrix of optimal communication graph with the lowest communication cost. Specifically, network constraints (2.43a) - (2.43c) can be adjusted according to the practical requirement. Constraint (2.43a) is used to determine on/off connection. For example, if DG i does not directly communicate with DG j due to privacy concern, then $l_{ij} = 0$ should be set as the constraint of the above program to accommodate this requirement. Constraint (2.43b) indicates that a certain requirement for the convergence speed must be satisfied. Constraint (2.43c) makes sure the communication network is robust to a time delay τ. Constraint (2.43d) - (2.43k) are non-adjustable constraints that incorporate the necessary conditions for the strongly connected and balanced communication graph.

Remark 1: There exists a tradeoff between achieving a high convergence rate and keeping a low communication cost. The constraint (2.43b) has a significant impact on the optimal solution. In real MG application scenarios, how to balance these two contradictory objectives in terms of communication network planning depends on many practical factors. Here we take the geographical span of the MG as an example

to briefly discuss. Usually, for the MG with a large geographical span, where the physical distance between DGs is relatively long, a communication network with lower algebraic connectivity is more desirable. In other words, the construction cost of the communication network can be reduced with the decreased convergence speed by setting smaller λ^*. For the small-scale MG, larger algebraic connectivity can be achieved without costing too much on the communication network. No matter which is the case, the dynamical performance of the secondary control can be guaranteed by the proposed planning model.

Remark 2: It is worth noting that the proposed planning model aims to provide more options on the available communication topology for network operators to choose in the planning stage. In real applications, only the designing communication network satisfying the *N-1* rule (which means there will be no isolated DG even if one communication link fails) could be implemented in practice for the sake of reliability.

2.4 Case Studies

In this section, the proposed MISDP model (2.43) is applied to design the communication network for two MGs in different scales. The weight of the communication link which is restricted by a negative ancillary parameter M in (2.25) is set to -2.5. The MISDP model is solved by MOSEK through YALMIP interface in MATLAB. Then the effectiveness of PSC protocols is validated and the improvement on the dynamical performance under the optimal communication network is evaluated in MATLAB/Simulink.

2.4.1 Communication Network Planning for Four-DG MG

The communication network for the MG consisting of four DGs is first considered. Time delay $\tau = 0\text{s}, 0.01\text{s}$ and 0.1s is incorporated into the planning model as the constraint, respectively, to design the communication network. The scenario that no connection limitations among DGs is investigated. Under different algebraic connectivity λ^* (convergence speed requirement), the minimum cost of the optimal communication network is demonstrated in Fig. 2.6.

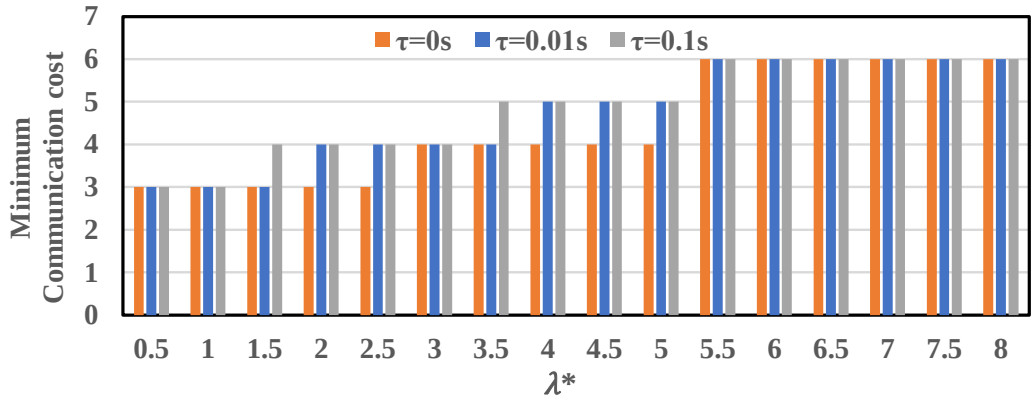

Fig. 2.6. Communication cost of 4-DG MG under different convergence speed requirement

As illustrated in Fig. 2.6, three minimum communication costs are found: C = 3, 4 and 6. The corresponding topology is shown in Fig. 2.7. Notably, the communication cost remains unchanged within a certain range of dynamical convergence requirements. Taking the case with $\tau = 0\text{s}$ as an example to analyze, the communication cost is doubled if the convergence rate is increased from $\lambda^* = 2.5$ to $\lambda^* = 5.5$ while it is only increased by around 33% if the convergence rate is increased to $\lambda^* = 5$. Such observation helps the communication network planning: a faster convergence speed can be acquired without increasing the communication cost to some extent. Besides, it is found that a longer time delay generally results in a higher

communication cost. Hence, it can be concluded that the communication cost might be sacrificed to compensate for the adverse effect of time delay on the communication links.

As the communication cost of the optimal topology keeps unchanged under three time-delay settings when $\lambda^* \geq 5.5$, the average weight of the communication link is investigated, which is shown in Table 2.1. It is observed that a higher convergence speed can be satisfied by increasing the weight of the communication link. Notably, a larger weight of the communication link improves the robustness of the communication network to the time delay, even without the need to increase the communication cost. The largest average weight is 2.5, which is consistent with the bound M. A feasible solution cannot be found when $\lambda^* \geq 11$, 10 and 9 when time delay is 0, 0.01s and 0.1s, respectively, as the weight is over the defined bound M. Obviously, in addition to the total number of links, the weight of the communication link is another critical factor that affects the convergence speed of the PSC protocols, which must be designed carefully.

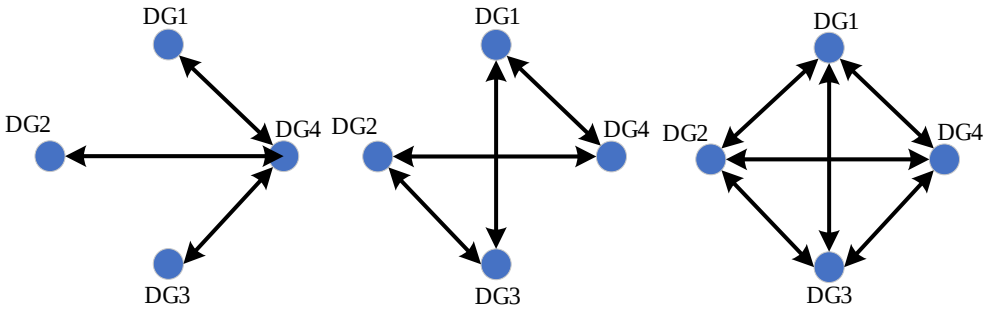

(a) cost=3 (b) cost=4 (c) cost=6

Fig. 2.7. Optimal communication topology planning for 4-DG MG

Table 2.1. Average weight of communication links with various time delays

Optimal Communication Cost = 6							
λ^*	5.5	6	7	8	9	10	11
$\tau = 0$	1.325	1.375	1.75	2	2.25	2.5	NA
$\tau = 0.01$s	1.375	1.515	1.85	2.15	2.45	NA	NA
$\tau = 0.1$s	1.405	1.525	1.95	2.35	NA	NA	NA

2.4.2 Communication Network Planning for Larger MG

To further demonstrate how the communication topology is designed considering the communication constraints and the convergence requirement, the proposed communication network planning approach is applied to a larger MG with eight DGs. The effect of time delay is not considered here. As shown in Fig. 2.8, similar results are acquired in terms of the minimum communication cost under different λ^*.

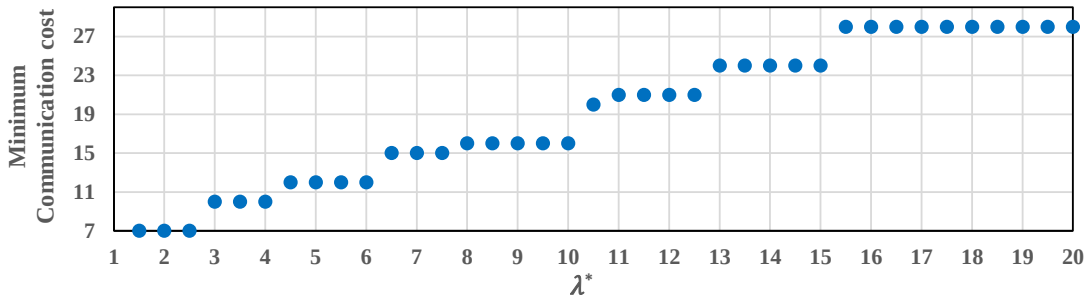

Fig. 2.8. Communication cost of 8-DG MG under different convergence speed requirement

Again, we find that the faster control convergence speed does not contribute to a higher communication cost. Therefore, when designing the potential communication network for the MG, the proposed planning approach is useful to avoid the extra communication cost.

Various communication topologies designed by the proposed planning approach under different requirements are given in Fig. 2.9. The specific weight of the

communication link is displayed on the graph, otherwise, it is 2.5. Generally, with the increasing of algebraic connectivity λ^*, the total number of communication links is larger. The topology displayed in (a) is the simplest graph when DG1 is appointed as the pinning DG with the highest priority. Although this topology has the lowest communication cost, it is the least robust network subjecting to single-point communication failure, which is not a desirable design for the real application. The networks displayed in (c) and (d) have the same communication cost but different algebraic connectivity. This is because that the weight of the communication link is different. Again, this shows the importance of the determination of the communication weight. For topology (e), the link between DG1 and DG5 is configured to be disconnected. After imposing this constraint on the planning model, the topology with no direct link between these two DGs is acquired. For topology (f)-(j), the communication link between DG1 and DG5 is prescribed to be connected. Particularly, when $\lambda^* > 20$, there is no feasible solution of the planning model, which means 20 is the largest algebraic connectivity can be attained by the communication graph of 8-DG MG (displayed in (j)).

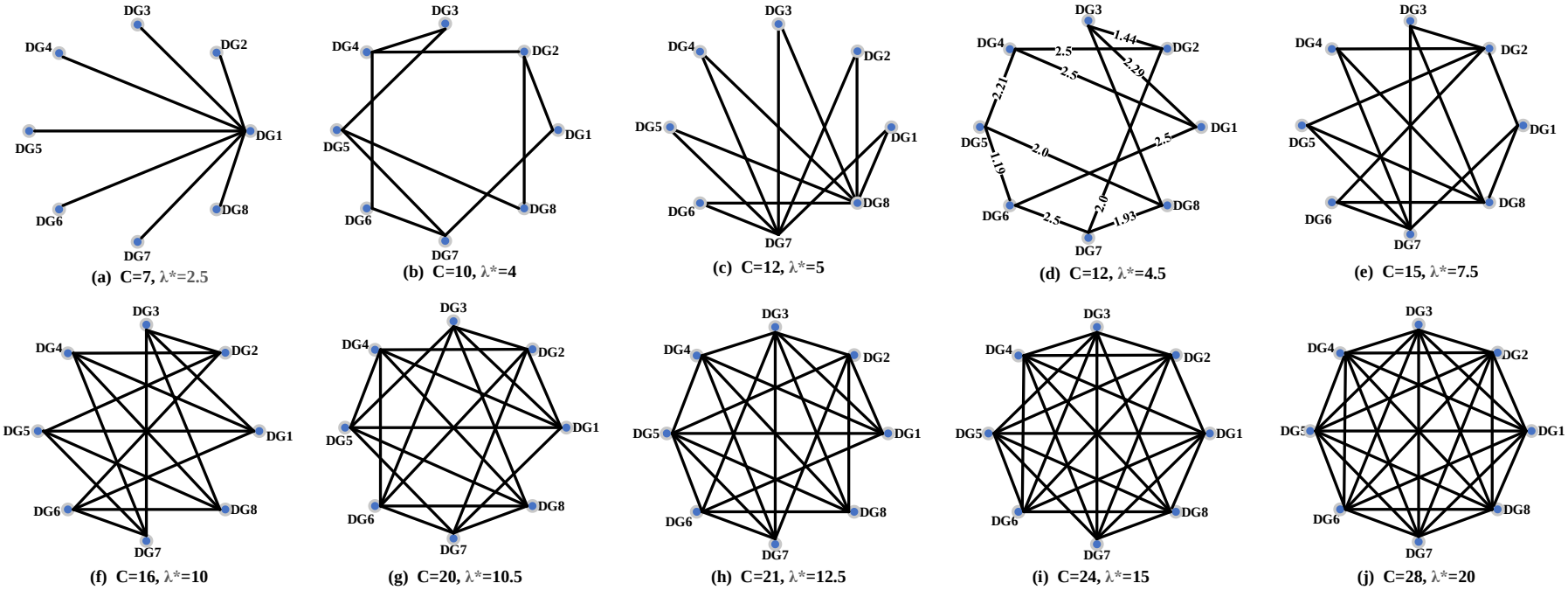

(a) C=7, λ*=2.5 (b) C=10, λ*=4 (c) C=12, λ*=5 (d) C=12, λ*=4.5 (e) C=15, λ*=7.5

(f) C=16, λ*=10 (g) C=20, λ*=10.5 (h) C=21, λ*=12.5 (i) C=24, λ*=15 (j) C=28, λ*=20

Fig. 2.9. Optimal communication topology planning for 8-DG MG

2.4.3 Validation of PSC Protocols under Designed Communication Networks

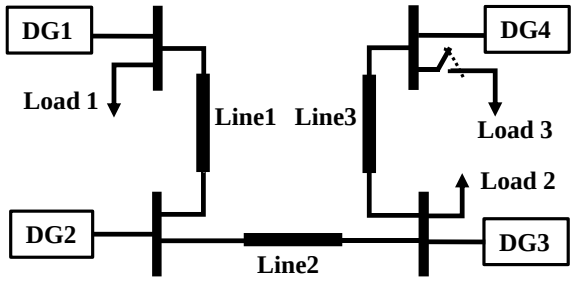

Fig. 2.10. Single-line diagram of 4-DG MG

The MG shown in Fig. 2.10 is used to validate the effectiveness of PSC protocols and the proposed communication planning model. The MG is disconnected from the main grid at 0s and secondary PSC protocols are initiated once the MG goes to islanding mode. Load 1 and Load 2 are the permanent local loads while Load 3 is connected/disconnected to the MG upon request. The specifications of DGs, loads and lines are shown in Table 2.2. As the controller design is not the focus of this chapter, parameters of PSC protocols are prescribed for optimal control performance. Coupling strength *c* and pinning gain *d* is set to 200 and 10, respectively. Feedback gain k_{V_i} and k_{ω_i} are both set to 1.2.

Table 2.2. Test MG specifications

DG	R_f	0.01Ω	DG 1&3 (40kVA rating)	m_p	1×10^{-5}
	L_f	0.6 mH		n_q	3×10^{-4}
	C_f	1.5 mF	DG 2&4 (45kVA rating)	m_p	1.5×10^{-5}
	R_c	0.005 Ω		n_q	4.5×10^{-4}
	L_c	0.1 mH			
Load	Load 1		25kW+10kVar		
	Load 2		25kW+15kVar		
	Load 3		10kW+10kVar		
Line	Line 1 & 3		0.23 Ω +0. 3mH		
	Line 2		0.35Ω+1.84 mH		

As single pinning is the main interest in this chapter, the most highly connected DG, i.e., DG with the largest degree, is selected to pin and access the reference value of the frequency and voltage. For the optimal communication network (b) and (c) shown in Fig. 2.7, the symmetrical topology makes each DG have the same degree, which means any one of them can be pinned. DG1 is pinned for simplicity in the following simulation studies. But for the unsymmetrical network as shown in Fig. 2.7 (a), the DG with the largest degree is pinned, which is DG4. In the real application scenario, the DG with the highest priority is planned to have more communication links with the rest of the DGs in the MG and is usually selected as the pinned DG to access the reference signal.

To verify the effectiveness of the PSC protocols with optimized communication topology, two cases are conducted in the following. In *Case One*, two reference signals are provided to the pinning DG at different times: at t = 0s, V_{ref}=220 V (RMS phase voltage), ω_{ref} =314 rad/s (50Hz); at t = 0.4s, V_{ref} = 215.6 V, ω_{ref} =313 rad/s (49.85Hz). The simulation results are demonstrated in Fig. 2.11, where the optimal topology shown in Fig. 2.7 (b) is applied. It can be observed that the reference is tracked precisely by all DGs. The transient response for the reference change is less than 0.1s. Not surprisingly, DG1 has the fastest convergence rate as it is pinned.

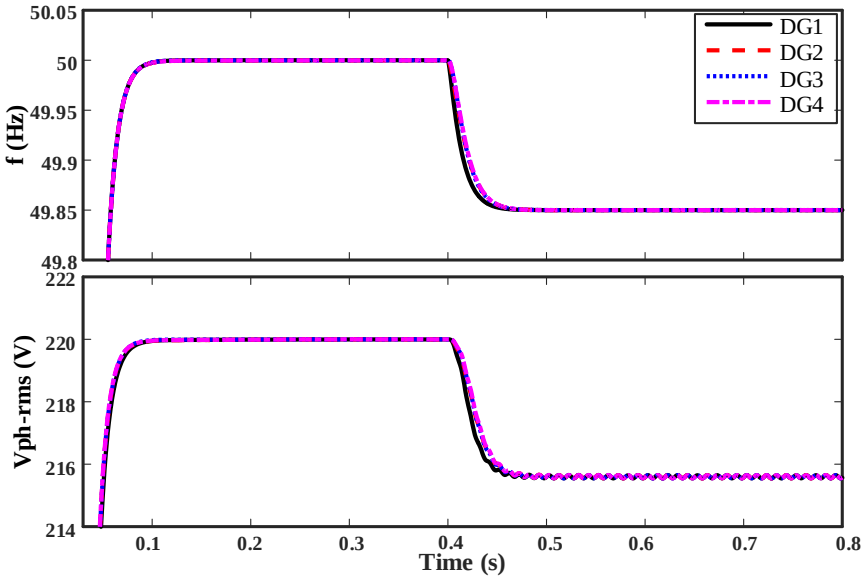

Fig. 2.11. Reference synchronization by using PSC protocols

In *Case Two*, the dynamical response of frequency and voltage to load variations is investigated. Load 3 is connected to the MG at t = 0.3s and removed at t = 0.7s. Time delay is considered here and set to 0.01s for all communication links. The simulation results under the same communication topology as the one used in *Case One* are demonstrated in Fig. 2.12. The frequency and voltage of all DGs experience a transient drop/surge when the extra load is connected/disconnected, where DG4 has the most severe changes as Load 3 is located close to DG4. By utilizing the proposed PSC protocols, both voltage and frequency can be restored fast, which means the MG is robust to the severe load variations and time delay under the optimized communication topology.

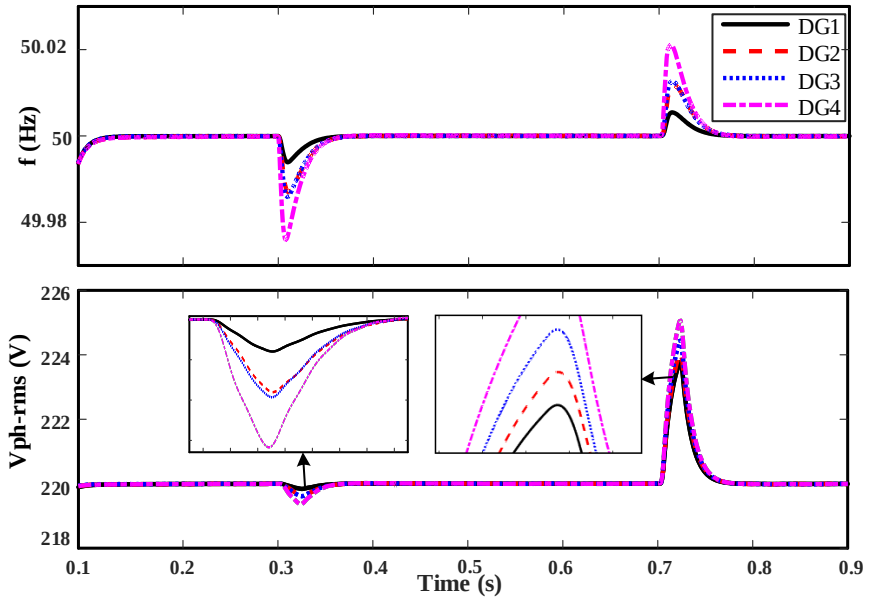

Fig. 2.12. Frequency and voltage response to dynamical load variations with 10ms time-delay

2.4.4 Comparison of Dynamical Performance of Secondary Control under Different Designed Communication Networks

Next, the improvement in the dynamical performance of PSC protocols with the implementation of different designed communication networks is demonstrated. Communication topologies shown in Fig. 2.7 (b), (c) and a normal circle graph are used for the test MG. As we aim to compare the dynamical performances under different communication topologies, the effect of time delay is not examined and set to 0s here. The dynamical voltage and frequency performance of non-pinning DG2 is examined. Fig. 2.13 verifies that the communication network with larger algebraic connectivity leads to a better dynamical profile of the frequency and voltage.

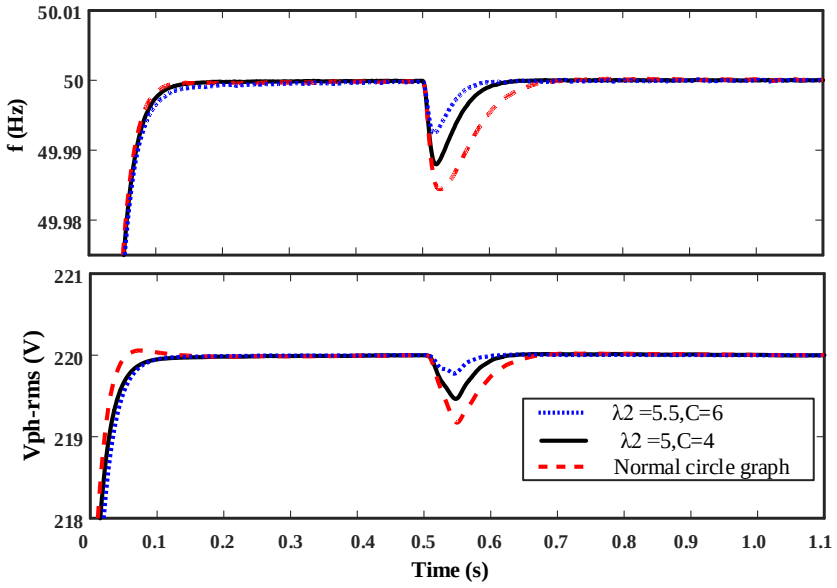

Fig. 2.13. Frequency and voltage response of non-pinning DG2 to load variations under different communication networks

Then, to evaluate the impact of different communication topologies on the pinning DG, we investigate the dynamical performance of DG1. As shown in Fig. 2.14, the frequency evolution of DG1 under three communication topologies is almost the same and it is hard to see the apparent difference. It gives the fact that the dynamical performance of the pinning DG is not significantly affected by the algebraic connectivity of the communication network. Therefore, in the real application, DG with the highest importance should be planned as the pinning DG to avoid the adverse influence of the communications.

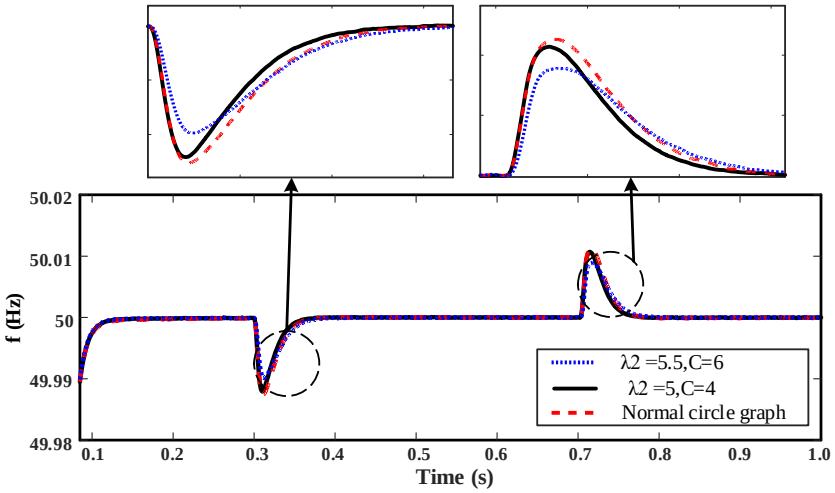

Fig. 2.14. Frequency response of pinning DG1 to load variations under different communication networks

2.5 Experimental Validation

An islanded MG consisting of two DGs was built and tested in the laboratory to validate the effectiveness of the proposed PSC protocol experimentally. The software parts are set up in RT-LAB, a real-time simulation platform allowing the Simulink model to interact with the hardware in real-time. The experimental setup includes two DC power supplies, two inverters, coupling feeders, a load box, and an OP4510 used to implement the control strategies and generate the switching signals for the inverters. The experimental results are extracted from the control desk and plotted in MATLAB. Fig. 2.15 shows the experimental hardware setup. The rated power of the two inverters is 3kVA and DC voltage is 400V. Other electrical parameters can refer to Table 2.3.

Table 2.3. DG Specifications in Experiments

Parameter	Value
Switching frequency	28kHz
Signal sampling frequency	50kHz
Allowed frequency deviation	0.2Hz
Allowed voltage deviation	8.25V
Cutoff frequency of LPF	30rad/s

Filter inductance	3mH, 0.12Ω
Filter capacitance	40μF
Feedforward gain of output current	0.6
Connecting feeder impedance of DG1	2mH, 0.3Ω
Connecting feeder impedance of DG2	2.5mH, 0.5Ω

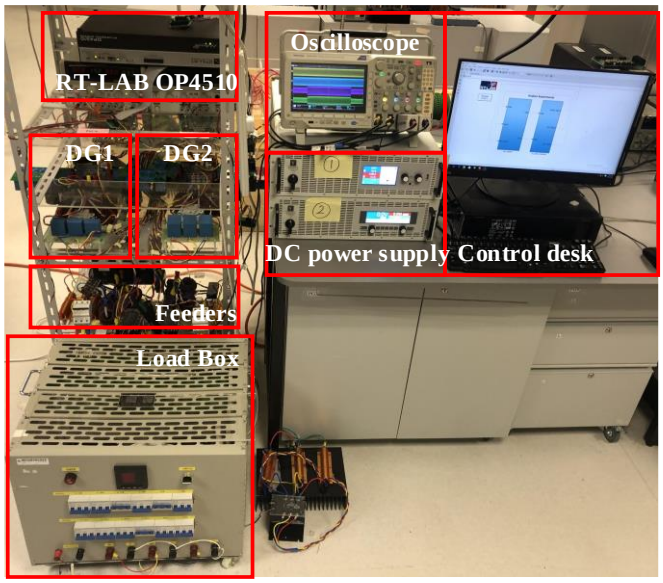

Fig. 2.15. Experimental platform

In the experiment, DG 1 is set as the pinning inverter with the reference $\omega_{ref} =$ 314.159 rad/s and V_{ref} = 156V. Coupling strength c and pinning gain d is set to 100 and 10, respectively. Feedback gain k_{V_i} and k_{ω_i} is both set to 1. The first test is conducted to validate the reference tracking performance of the proposed PSC protocol. At t = 0.1s, the proposed secondary control is enabled. At t = 4.2s and t = 9s, an extra 1kW load is connected and disconnected, respectively. The change of output currents of two DGs is shown in Fig.2.16, which is the captured result from the oscilloscope. The increase and decrease indicate the connection and disconnection of the load. The experimental results are recorded in Fig. 2.17. It can be observed that

once the secondary control is activated, the reference can be tracked precisely under the load variations.

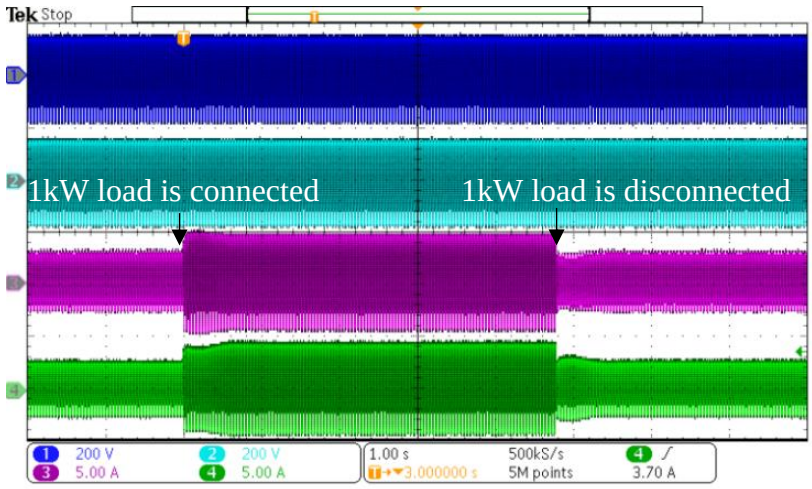

Fig. 2.16. Experimental results of the output currents of two DGs

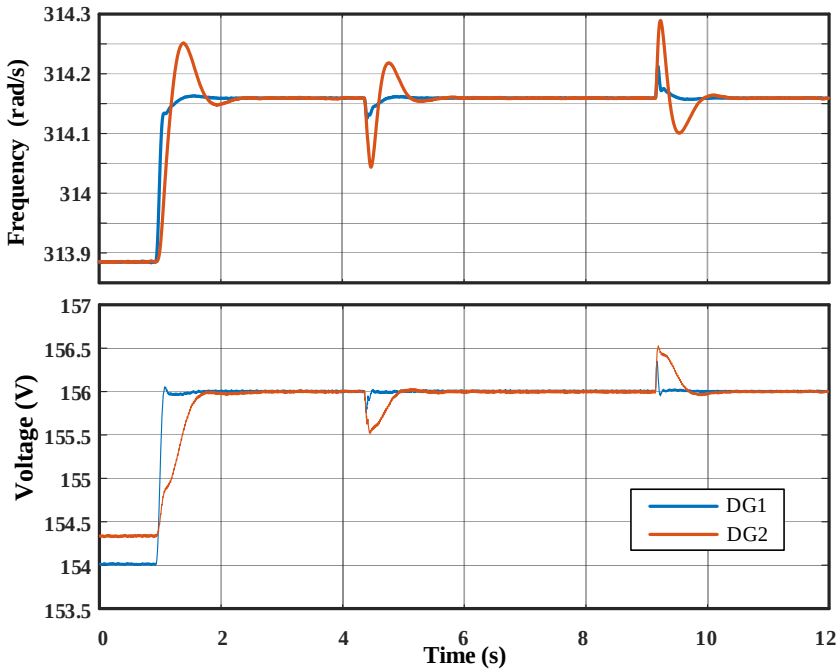

Fig. 2.17. Experimental results of the proposed PSC in tracking frequency and voltage reference

As there are only two inverters in the experimental MG prototype, the communication network is relatively simple with the cost $C = 1$ (one communication link). Therefore, only the impact of the weight of the communication link is

investigated in the second test. Similar to the first one, an extra 1kW load is connected into the MG and disconnected from the MG at t = 2.3s and t = 8.1s, respectively. Assigned communication weight is changed to compare dynamical performances under different weights. As shown in Fig. 2.18, the results prove that a larger weight will result in a faster response under the same communication topology. Overall, by implementing the proposed PSC on the laboratory MG prototype, the effectiveness of the PSC is validated successfully.

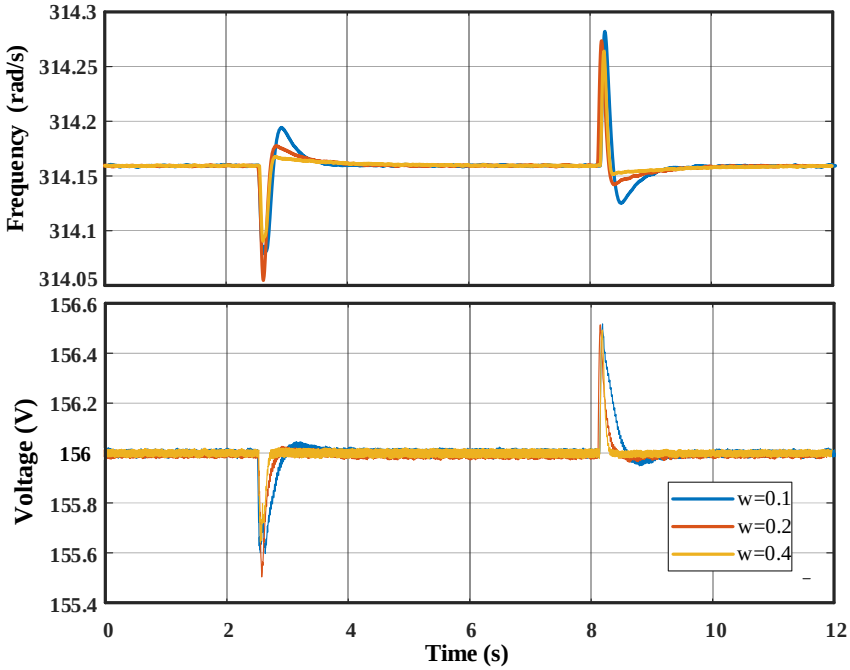

Fig. 2.18. Experimental results of the proposed PSC in regulating frequency and voltage under different communication weights

2.6 Chapter Summary

This chapter investigates how the topology of the communication network impacts real-time dynamical performance of the physical MG and develops a communication network planning model for the MG to guarantee the distributed secondary control performance. Firstly, a pinning-based control protocols are designed for the secondary

voltage and frequency control. Furthermore, a cost-effective communication network planning model for the islanded MG is developed. Using spectral graph properties, our work theoretically reveals how the communication network affects the pinning secondary control performance and analytically provides the critical criteria for the communication network designing. The planning model is then reformulated in the form of MISDP based on LMI so that the cost-effective communication topology that is robust to the time delay can be found efficiently. Meanwhile, the minimum requirement of dynamical convergence speed for secondary PSC can be guaranteed.

Case studies are given to demonstrate how the communication topology is designed for MGs in different sizes. Particularly, it is revealed that a faster convergence can be achieved without adding additional communication links. The results also indicate that the weight of the communication link is a critical factor that affects the convergence speed of the PSC protocols, which should be designed carefully. The planning model can be used to investigate how much the dynamical convergence performance of secondary PSC protocols can be improved if additional communication links are added. Such the model can help the network designer to properly plan the communication network of the MG in the planning stage to save the potential cost.

Chapter 3 A Multi-market Nanogrid P2P Energy and Ancillary Service Trading Paradigm: Mechanisms and Implementations

In the presence of geographically dispersed DERs, the MG can be organized into several nanogrids (NGs) which provides an efficient approach to aggregating DERs for the participation of ancillary service with a high level of efficiency and controllability. In this regard, this chapter presents a multi-market NG trading paradigm for simultaneous real-time imbalance elimination and frequency regulation procurement, based on the architecture of P2P trading and communication. It comprises three consecutive markets: P2P bilateral energy market, balancing market and ancillary service market. Optimal offering strategies are designed to maximize the profits of producer NGs and meanwhile to tackle the capacity allocation tradeoffs among three markets. When it is approaching to real-time, the market will be closed with completion of balancing, and selected NGs with reserved capacity for the ancillary service will provide the real-time frequency regulation in a fully distributed manner. A parameter so-called engagement factor is designed based on the market clearing results to determine the deployment of frequency regulation service of each participated NGs. Subsequently, the pinning-based distributed secondary control upon P2P information sharing among NGs is implemented to regulate the frequency and ensuring the power sharing. The results of case studies indicate the feasibility of the proposed paradigm and its good performance, while different remuneration mechanisms are compared for discussion of their pros and cons.

3.1 MG Partition and Set-up

To enhance reliability and flexibility, a MG can be grouped into a set of sub-networks, i.e., networked MG [125][126]. As it is not feasible for an individual small-scale DER to play a significant role in the market trading and to make an impact on the real-time operation due to its limited capacity, in this chapter, an islanded MG is partitioned into several sub-networks, so called 'nanogrids' (NGs). DERs and loads that are geographically close to each other can be grouped into one NG and each NG functions as a single entity for the energy trading and frequency regulation hereinafter.

Each NG locally contains uncontrollable loads and two types of DERs: non-dispatchable DERs (e.g., PV, wind turbine) and dispatchable DERs (e.g., gas turbines, energy storage devices). The NG can be categorized into two types: consumer NGs (N_c) and producer NGs (N_p). In a specific trading timeslot, if there is a power deficiency in a NG, it becomes a consumer NG; if there is a power surplus in a NG, then it becomes a producer NG. A single NG is the main trading and regulation entity hereafter in the chapter. Fig. 3.1 shows a schematic diagram of an islanded MG consisting of multiple NGs, where the important network components are displayed in the diagram. Apart from NGs, there exist other virtual agents and smart ICT-based infrastructures that facilitate the market implementation, which are introduced below.

Communication router

Every market participant in the MG has a communication router for the information sending and receiving. It is the fundamental infrastructure to enable P2P energy trading and information sharing among NGs.

Database

A cloud server is embedded in the top level of the NG energy management system, providing a data repository for the extraction of historical data of NGs and relevant components in the MG. The trading information for each trading would also be stored in the database.

Transactive meter

Each NG is equipped with a transactive meter to record the energy data, e.g., real-time demand and available power capacity, which is monitored and managed by the NG operator.

Balancing Responsible Party

Balancing responsible party (BRP) is a non-profit entity to ensure the ultimate power balance of the MG in real-time. In acting as a coordinator, BRP is responsible to validate and finalize the transaction and guarantee the security of the network operation by acquiring the knowledge of the trading among of NGs.

NG Operator

The main goal of the NG operator is to locally optimize the profit and ensure the secure operation of the individual NG. NG operator could be a virtual agent or platform that has the specific knowledge of the conditions of the NG, including the rated capacity of the generation units, storage devices and the loads inside the NG. It can access the real-time data through the transactive meter of the NG, determine and submit the bid/offer and send the control signal to DER controllers.

DER controller

The specific type of device (dispatchable DER) is equipped with the controller and it can respond immediately following the control signal from the NG operator.

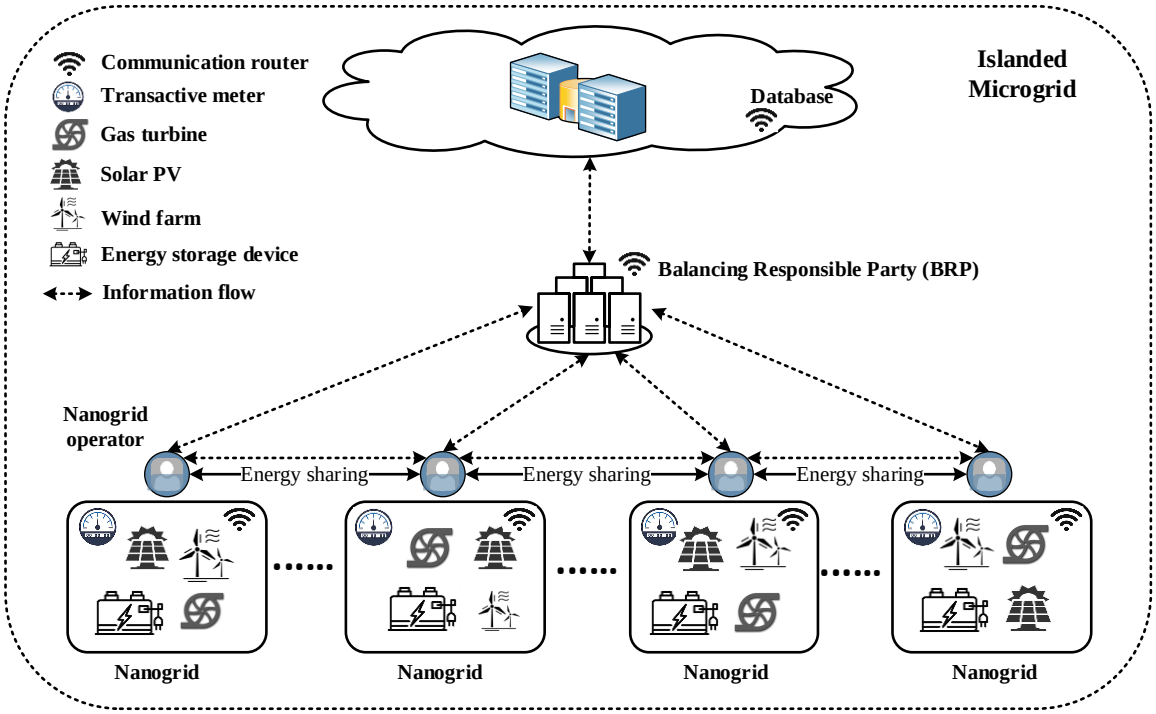

Fig. 3.1. An islanded MG consisting of multiple NGs with different DERs for P2P energy and ancillary service trading

In an islanded MG, the frequency stability of the MG is no more guaranteed by the conventional main grid and the power mismatches between generation and demand will result in severe frequency violations. Hence, it is critical to keep the balance of the generation and demand within the network and to maintain the frequency close to the reference value. The non-dispatchable DERs (PV, wind turbines) operating in a grid-following mode can provide the maximum available power, which are seen as the negative loads in the chapter. As the output of renewable-based DGs is intermittent and uncertain, it would be more complex to design the regulation and market mechanism if allow them to participate into the ancillary service. The dispatchable

DERs (gas turbines, energy storage devices), operated as voltage source inverters in a grid-forming mode, can participate in the system frequency regulation and power sharing to satisfy the network demand. The power sharing among NGs is conducted by implementing primary droop control, which is shown as:

$$f_i = f^* - k_{eq,i} P_i \tag{3.1}$$

where f^* is the reference value of frequency; f_i and P_i correspond to the measured frequency and power of NG *i*, respectively; $k_{eq,i}$ denotes the equivalent droop gain of NG *i* which is the sum of the droop gains of all dispatchable DERs in NG *i*. The main idea of the droop mechanism is to mimic the response capability of synchronous generators, where the system frequency can be regulated down or up when the power output is increased or decreased [127]. Once the load demand changes, the power output of grid-forming DERs would be adjusted instantaneously based on their droop characteristics to maintain the power balance. However, conventional primary droop control would cause frequency deviated from the reference value [5]. Secondary control is required to mitigate the frequency deviation. As such, the droop function is now formulated as:

$$f_i = f^* - k_{eq,i} P_i + \Delta f_i \tag{3.2}$$

where Δf_i is the frequency correction term, which is provided by the secondary control to ensure the frequency can be regulated to the reference value. Under the P2P communication structure, a distributed secondary control based on the neighboring information sharing is compatible with the P2P market. A market-enabled distributed secondary control considering the economic incentives for the frequency regulation will be introduced in Section 3.3.

3.2 Mechanisms of Multi-market Paradigm for NG P2P Energy and Ancillary Service Trading

3.2.1 Overview of Multi-market Trading Paradigm

The trading paradigm including three consecutive markets is proposed to facilitate the cost-effective real-time operation in the MG, addressing the issue of demand and generation balancing, while offering potential transaction opportunities for NGs to provide both energy deployment and real-time frequency regulation service. Fig. 3.2 shows the sequential implementation procedure of these three markets. In order to avoid uncertainties resulting from renewable generations, energy trading for balancing is encouraged to be conducted as close to real-time as possible. Therefore, the entire market trading procedure is conducted in a 15-minute timeline for the proposed paradigm, where the implementation of bidding, matchmaking and balancing are conducted. After the market gate closure, the responsibility of balancing and frequency regulation determined during the market trading will be deployed in the subsequent hourly real-time operation. Such a 15-min trading timeline is feasible for NGs consisting of flexible small-scale generators with fast response capability and without pre-defined annually/monthly/weekly start-up and shut-down schedule.

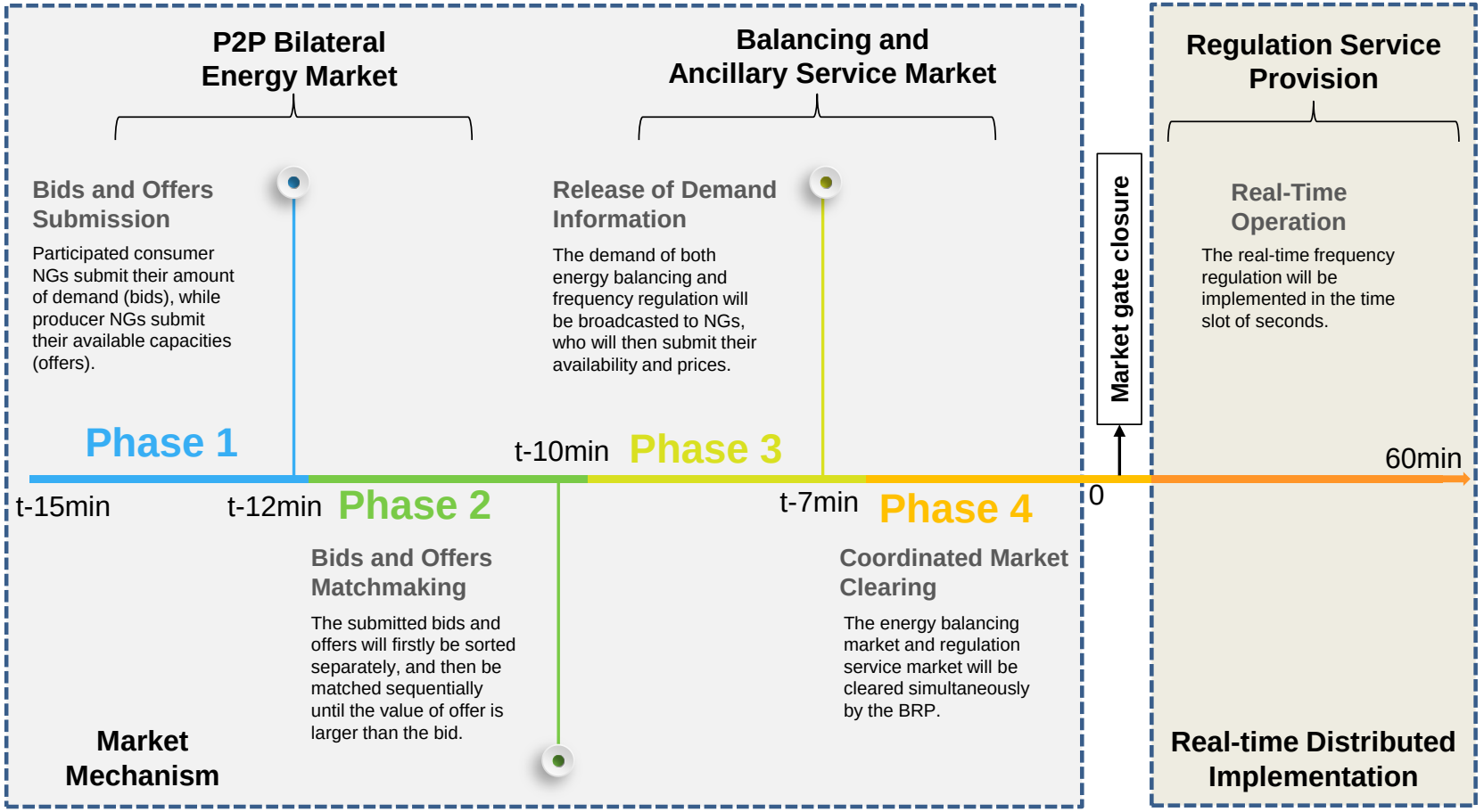

Fig. 3.2. The sequential implementation procedure of the proposed multi-market NG trading paradigm

In the bilateral P2P trading market (Phase 1&2), each NG will mitigate the power imbalance resulting from inaccuracy of prediction by participating in the bilateral P2P transaction, in which the matchmaking procedure is conducted by the BRP. In the balancing and ancillary service market (Phase 3&4), BRP will organize a centralized bidding procedure and coordinated market clearing for the deployment of both energy and regulation service, to enable available NGs to participate: 1) further elimination of the remaining imbalance due to failure of matchmaking at Phase 2; and 2) real-time frequency regulation service provision following the control signal. Details in terms of market mechanisms are discussed in the following sections.

3.2.2 Optimal Offering Strategy in P2P Bilateral Energy Market

From the perspective of producer NGs, the 'tradeoff' that needs to be tackled is: how much capacity should be offered to the bilateral P2P energy market and subsequent balancing and ancillary service market respectively, to achieve the maximum total profit? The expected unit price in the balancing and ancillary service market would apparently be higher than the bilateral market, as it is much more approaching the market closure time, and the 'willingness' of producers to sell such service would therefore be strengthened. However, devoting all the available capacity to the subsequent markets is also not the best decision, as producers cannot precisely foresee the actual demand of network balancing and ancillary service, and it would be possible that the value of submitted offers is much larger than the actual demand. According to the above descriptions, the optimal offering strategy for a producer NG to allocate its available capacity to different markets can be formulated as follows:

$$\max\left\{\begin{array}{c}\mu_{S1,i}\left[\lambda_{S1,i}(t)-C_i(t)\right]q_{S1,i}(t)+\\ +\mu^{B}_{S2,i}\left[\lambda^{B}_{S2,i}(t)-C_i(t)\right]q^{B}_{S2,i}(t)+\\ \mu^{R}_{S2,i}\left[(\lambda^{R}_{S2,i}(t)-C_i(t))\tau_i+\lambda^{B}_{S2,i}(t)(1-\tau_i)\right]q^{R}_{S2,i}(t)\end{array}\right\}, i\in N_P \quad (3.3)$$

s.t.

$$q_{S1,i}(t)\geq 0 \quad (3.3a)$$

$$q^{B}_{S2,i}(t)\geq 0 \quad (3.3b)$$

$$q^{R}_{S2,i}(t)\geq 0 \quad (3.3c)$$

$$q^{min}_{NG,i}\leq q_{S1,i}(t)+q^{B}_{S2,i}(t)+q^{R}_{S2,i}(t)\leq q^{max}_{NG,i} \quad (3.3d)$$

where $\lambda_{S1,i}(t)$, $\lambda^{B}_{S2,i}(t)$ and $\lambda^{R}_{S2,i}(t)$ are the capacity price offered by NG i in P2P bilateral market, balancing market and ancillary service market in period *t*, respectively; $C_i(t)$ is the cost function of the generation; $q_{S1,i}(t)$ is the trading capacity in the bilateral energy trading market, $q^{B}_{S2,i}(t)$ and $q^{R}_{S2,i}(t)$ are respectively, expected balancing capacity in the balancing market and regulation capacity in the ancillary service market in period *t*; $q^{min}_{NG,i}$ and $q^{max}_{NG,i}$ are the minimum and maximum capacity limit of NG i; $\mu_{S1,i}$, $\mu^{B}_{S2,i}$ and $\mu^{R}_{S2,i}$ denote the successful rate of bidding of producer NG i in each market, respectively. The successful rate of bidding indicates the expected ratio of actually allocated capacity and the submitted amount of capacity, which is a non-negative value in the range of [0,1]. It can be statistically determined based on the historical trading data and is stored in the database of MG.

The objective function (3.3) shows the expected maximal profit of a producer NG comprises three profitable transactions in different markets. The first and second item of (3.3) is the expected profit acquired in the bilateral market and balancing market, respectively. The third item, including two types of settlements, quantifies the expected profit acquired from the regulation service provision. τ_i in the third item

denotes the probability of the regulation capacity to be deployed by NG i, which can be extracted from the historical data that is also stored in the database. Its first part denotes the expected revenue of capacity to be actually deployed for frequency regulation service, in which the trading price of the ancillary market will be paid. The rest of the capacity that is not deployed will be remunerated for the trading price of the balancing market as compensation for the opportunity cost, which is shown in the second part of this item.

It should be noted that each operator of producer NG will determine the amount of traded capacity in three markets based on the above offering strategy once the market is open. Although three optimal solutions $q_{S1,i}$, $q_{S2,i}^{B}$ and $q_{S2,i}^{R}$ will be obtained by this strategy, only $q_{S1,i}$ as the devoted capacity for bilateral trading will be actually offered in Phase 1 in the P2P bilateral energy market. Once the optimal capacity for P2P trading is confirmed, the NG operator will submit this offer to BRP. Then BRP will conduct the matchmarking procedure to clear the market in Phase 2, as described in the following section. The tradeoff between devotion to energy balancing market and ancillary service market will be further tackled again after the information of demand being released by the BRP, i.e., at the beginning of the balancing market opening in Phase 3.

3.2.3 Matchmaking procedure in P2P Bilateral Energy Market

In Phase 1, NG operators will submit their available generation (producer NG) or demand (consumer NG) to BRP, who will thereafter examine the submission to avoid any violations. The producers and consumers will be sorted separately in the order of submitted offers (from the lowest to the highest) and bids (from the highest to the

lowest). For bids and offers with the same values, those with earlier submission time will be treated with priority. Once the 'queue' of producers and consumers is constructed, the BRP will serve as the coordinator to implement the matchmaking procedure in Phase 2, which can be described as follows:

- The producer with the lowest offers will be matched with the consumer with the highest bids.
- The producer with the second-lowest offers will be matched with the consumer with the second-highest bids.
- The rest matches can be made in the same manner, until the highest value of the rest bids is less than the lowest value of the rest offers.
- The final transaction price of each matched producer-consumer pair will be the average value of their offers and bids.
- Transactions with the amount of power exchange that exceeds the maximum capacity of tie-lines between the producer and the consumer will be suspended.

3.2.4 Mechanisms of Balancing and Ancillary Service Market

At the beginning of Phase 3, i.e., 10 minutes before the real-time operation, BRP will organize the coordinated clearing of balancing market and frequency regulation service market. In the balancing market, the amount of remaining power imbalance q_B of the entire MG will be broadcasted by BRP to each NG, while available NGs will submit their applicable amount of capacity and price to BRP. In this chapter, only the case of power deficiency is considered for the power imbalance in the balancing market, which requires the participation of producer NGs. The cost of purchasing energy from producer NGs in the balancing market should be paid by imbalanced

consumer NGs as they are responsible for the failure of matchmaking because of the overly high bidding price. In the ancillary service market, the amount of expected requirement capacity q_F for frequency regulation will be broadcasted to NGs while available NGs will also submit their applicable amount of capacity and price. The requirement of the regulation service is based on the net-load forecast, determined as $110^{\%}$ of the largest predicted net-load variation within a timeslot [128]. As the producer NG is the focus in this chapter, only up-regulation is considered. For the scenario of generation exceeding load demand, the additional unexpected renewable generation will be curtailed directly, as the cost of curtailment is much less than purchasing the down-regulation service [129].

The BRP will simultaneously clear the balancing and ancillary service market by minimizing the total cost, while the requirement of capacity to maintain network balancing and frequency regulation in real-time must be fulfilled. Three types of capacity remuneration mechanism (CRM) are considered for the payments of producers in the balancing and ancillary service market: marginal price (MP), 'pay-as-bid (PAB)' and 'pay as the opportunity cost (PAO)', which are introduced below.

- Marginal price (MP): The NGs with the winning bid after market clearing will be paid by the market marginal price. It is currently one of the most common CRMs.
- Pay-as-bid (PAB): The NGs with the winning bid after market clearing will be paid by the price they procure for the unit of capacity.
- Pay as the opportunity cost (PAO): For the remuneration of ancillary service deployment, the policy of PAO, in which the subsidy price is directly determined by the BRP according to the calculated opportunity cost for ancillary service

provision, is proposed and implemented in several existing markets to avoid possible strategic arbitrage of service providers [130]. In this work, by implementing PAO, the reserved capacity for ancillary service will be remunerated by the marginal price determined in the balancing energy market; while the capacity successfully traded in the balancing market is remunerated by the bidding price of the winning NG.

In the case study, how three types of CRM will impact the total producer profit will be discussed.

3.2.5 Optimal Offering Strategy in Balancing and Ancillary Service Market

In these two markets, producer NGs will tackle the tradeoff between devoting their available capacity to balancing market and ancillary service market to maximize their benefits. The optimal offering strategy for producers to allocate their available capacity to these two markets can be formulated as follows:

$$max \quad \begin{Bmatrix} \left[\lambda_{S2,i}^{B}(t) - C_i(t)\right] q_{S2,i}^{B^*}(t) + \\ \left[(\lambda_{S2,i}^{R}(t) - C_i(t))\tau_i + \lambda_{S2,i}^{B}(t)(1-\tau_i)\right] q_{S2,i}^{R^*}(t) - \\ C_{opp,i} \end{Bmatrix}, i \in N_P \tag{3.4}$$

$$C_{opp,i} = \underbrace{\left[\lambda_{S2,i}^{B}(t) - C_i(t)\right] q_{S2,i}^{B^*}(t)}_{\text{term 1}} - \underbrace{\left[(\lambda_{S2,i}^{R}(t) - C_i(t))\tau_i + \lambda_{S2,i}^{B}(t)(1-\tau_i)\right] q_{S2,i}^{R^*}(t)}_{\text{term 2}} \tag{3.4a}$$

s.t. $$q_{NG,i}^{min} - q_{S1,i} \le q_{S2,i}^{B^*} + q_{S2,i}^{R^*} \le q_{NG,i}^{max} - q_{S1,i} \tag{3.4b}$$

$$q_{S2,i}^{B^*} \ge q_B \tag{3.4c}$$

$$q_{S2,i}^{R^*} \ge q_F \tag{3.4d}$$

The first item in (3.4) represents the expected profit acquired in the balancing market. The second item describes how much profit can be gained by providing frequency regulation service. The third term $C_{opp,i}$ reflects the opportunity cost of reserved capacity for the provision of frequency regulation service instead of participating in the balancing market, which can be acquired by (3.4a). If the capacity reserved for the ancillary service is all traded in the balancing market, the profit would be represented by term 1 in (3.4a), while the actual profit of the ancillary service is described by term 2 in (3.4a). The opportunity cost can be represented by the difference between these two. Constraint (3.4b) declares that the total devoted capacity of each NG should be within the minimum and maximum value of availability. Constraint (3.4c) and (3.4d) indicate that the demand for energy balancing and frequency regulation requirements must be fulfilled.

In practice, in terms of various existing formations of the ancillary service market, most of them are specifically for transmission system which are organized and operated by the system operator or transmission organization [131]. For example, a web-based service so-called Frequency Response Price Submission that allows frequency response providers to submit holding prices on a monthly basis has been conducted by National Grid UK [28]. As the frequency regulation is the service that is more approaching real-time, our proposed paradigm provides opportunities for potential players to participate in the market with near to real-time procurements, which can encourage more prosumers to get involved in the market. As time goes by, the regulation service market would have a higher priority compared with other markets, which therefore leads to a higher price to reserve the capacity for the

regulation service. The price $\lambda_{S2,i}^{R}$ submitted by the producer NG for the ancillary service provision essentially must cover the holding cost and capacity cost. Holding cost is the expected payment made to producer NG by BRP to cover the cost when the NG chooses to provide the frequency regulation service, while the capacity cost is the payment by BRP to remunerate the producers the amount of capacity delivered after providing frequency regulation service.

3.3 Market-based Real-time Distributed Frequency Regulation

For the sake of secure operation of the MG, small frequency fluctuations due to the mismatch between supply and demand should be constantly balanced by controlling the real-time power dispatch of NGs. In the proposed NG energy and ancillary service trading paradigm, committed NGs for the frequency regulation service provision should follow the control signal from the distributed hierarchical control structure and adjust the power output accordingly. Given a certain limited capacity, how active a NG participates in the regulation service provision is closely related to how much capacity is devoted in the ancillary service market based on the optimal offering strategy and market clearing in the previous markets.

Therefore, to ensure the economic efficiency of real-time implementation, the devoted capacity for the ancillary service is incorporated into the control action for the participating NGs. Specifically, the NG with the largest reserved capacity has the highest incentive to provide the service. Here a parameter *engagement factor* φ_i is introduced to reveal the participation level of available NGs in the regulation. It is determined by the ratio between the devoted capacity of frequency regulation to the total rated capacity of the NG, which is defined as

$$\varphi_i = 1 + q_{S2,i}^{R^*}/q_{NG,i}^{max} \tag{3.5}$$

The *engagement factor* is embedded into (2) and a new droop characteristic indicating the priority of the participating NG can be reformulated as:

$$f_i = f^* - \varphi_i k_{eq,i} P_i + \Delta f_i \tag{3.6}$$

The frequency correction term Δf_i can be compensated by a secondary control structure. The pinning-based synchronization control protocols are developed for distributed secondary control. To achieve the frequency reference f^*, each participating NG needs to exchange the information with its neighboring NGs via the P2P communication. A parameter a is used to describe the on/off communication connection between any two NGs in the network: if NG i can receive the information from NG j then $a_{ij} = 1$, otherwise it is 0. Assuming the total number of participating NGs is n, the frequency disagreement dynamic between neighboring NGs via P2P information exchanging is shown as follows:

$$\dot{\Delta f_i} = -c\left[\sum_{j=1}^{n} \alpha_{ij}\left(f_i - f_j\right) + d(f_i - f^*)\right] - c\sum_{j=1}^{n} \alpha_{ij}\left(\varphi_i k_{eq,i} P_i - \varphi_j k_{eq,j} P_j\right) \tag{3.7}$$

where c is the control gain; α_{ij} indicates communication coupling defined by $\alpha_{ij} = a_{ij}$ if $i \neq j$, else $\alpha_{ij} = -\sum_j^n a_{ij}$; $d > 0$ is the pinning gain of the pinning NG which can access the reference frequency signal f^*, otherwise it is 0. By utilizing the control protocol (3.7), within certain iteration steps, pinning NG will regulate its output frequency to the reference value while non-pinning NG will minimize the disagreement with its neighbors until the frequency of all NGs achieves the reference state. Fig. 3.3 shows the real-time distributed frequency regulation procedure based on the previous market trading and clearing results. This control structure including the engagement factor is the feedback adaptive control with the parameter vary, where

the control loop adapts itself to changed reserved capacity. The reserved capacity is the signal fed back into the control.

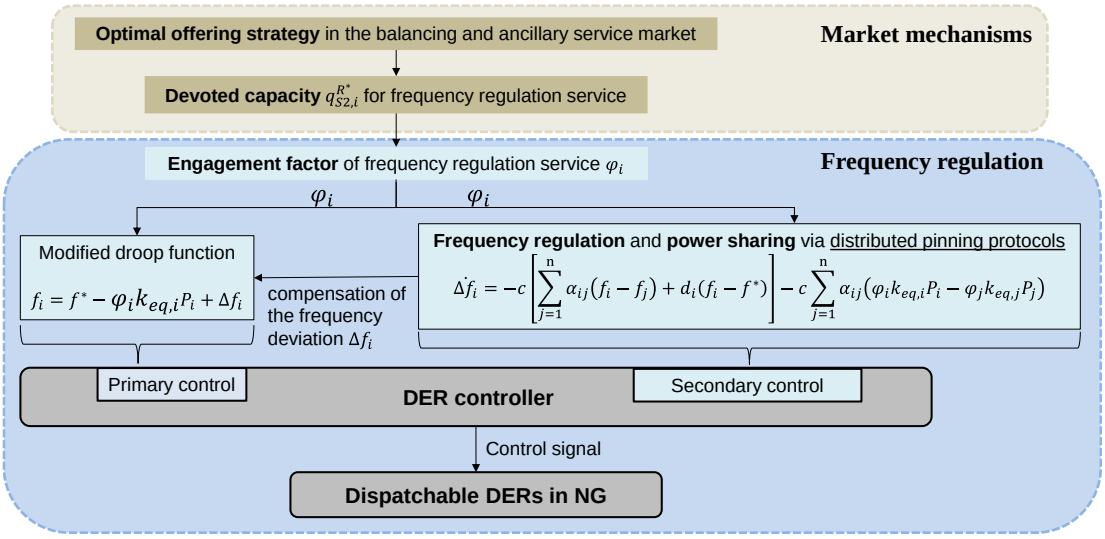

Fig. 3.3. Implementation of pinning-based distributed frequency regulation considering the engagement level of each NG

Next, the controllability of the proposed protocols is proved. Let $E_i = f_i - f^*$as the frequency regulation error, the error dynamics can be written as follows:

$$\dot{E}_\iota = \sum_{j=1}^{n} c\alpha_{ij}(E_j - E_i) - d_i E_i \tag{3.8}$$

The following Lyapunov candidate is used to derive the stability properties of the pinning-based control:

$$\mathrm{V} = \frac{1}{2}\sum_{i}^{n} {E_i}^T E_i \tag{3.9}$$

Then it follows that

$$\dot{V} = \sum_{i}^{n} {E_i}^T \dot{E}_\iota \tag{3.10}$$

$$= \sum_{i}^{n} {E_i}^T \{\sum_{j=1, j\neq i}^{N} c\alpha_{ij}(E_j - E_i) - dE_i\} \tag{3.10a}$$

$$\leq \sum_{i}^{n} {E_i}^T \sum_{j=1, j\neq i}^{N} c\alpha_{ij}(E_j - E_i) - \sum_{i}^{n} d_i \|E_i\|^2 \tag{3.10b}$$

$$\leq \sum_{i}^{n} \|{E_i}^T\| \sum_{j=1, j\neq i}^{N} c\alpha_{ij}\|E_j - E_i\| - \sum_{i}^{n} d_i \|E_i\|^2 \tag{3.10c}$$

$$\leq \sum_i^n \left\| E_i^T \right\| \sum_{j=1, j\neq i}^N c\alpha_{ij} (\left\| E_j \right\| + \| E_i \|) - \sum_i^n d_i \| E_i \|^2 \quad (3.10d)$$

$$= |\boldsymbol{E}|^T (\boldsymbol{B} - \boldsymbol{D}) |\boldsymbol{E}| \quad (3.11)$$

where $\boldsymbol{E} = [E_1, E_2, \dots, E_N]^T$ is the error vector; $\boldsymbol{B} = \left[c\alpha_{ij}\right]$ is the coupling configuration matrix of the communication network; $\boldsymbol{D} = diag(d_1, d_2, \dots, d_N)$ is the pinning gain matrix. Now it is observed that if $(\boldsymbol{B} - \boldsymbol{D})$ is a Hurwitz matrix, which means the real parts of all eigenvalues are strictly negative, then the asymptotic stability of the pinning-based secondary frequency control can be achieved, i.e., the frequency can be regulated to the reference state by given the proper pinning gain and communication connection.

Remark 1: By applying the above distributed secondary frequency regulation protocols, local control decisions can be made by each NG, which relies on a connected and distributed communication network. Considering the rapid development of ICT, P2P communication infrastructure can be established to enable the information exchange between each NG and its neighbors, i.e., each NG can communicate with at least one neighbor in the communication network via the communication router introduced in Section 2.1. The structure of P2P communication and the distributed control can nicely fit the wide scattering feature of DERs in the MG, which is advantageous in terms of scalability and flexibility. Moreover, the trading between NG and NG and the information sharing between NG and BRP can be realized based on P2P communication infrastructure.

Remark 2: Energy sharing and frequency regulation service provision is specifically designed for the islanded MG in this work, i.e., intra-microgrid trading and regulation. In fact, what we are addressing here is the worst case for a MG: how

an islanded grid can be self-sustained in case the support from the main grid is unavailable due to any operational issues. Besides, if the renewable generations are not taken into account, the wholesale spot market price, i.e., power supply purchased from the main grid, would be expensive in the real-time market. The proposed paradigm aims to investigate how to implement energy management in a self-sustained manner for the islanded MG with improved economic efficiency and guaranteed operation security.

3.4 Case Studies

In this section, three cases are designed to test and validate the proposed NG multi-market paradigm in terms of the market mechanisms and the real-time frequency regulation. The model of the MG and frequency regulation protocols are created in MATLAB/Simulink. The optimization programs for the optimal offering strategy are built in MATLAB and solved using YALMIP. For all cases, an islanded MG consisting of seven NGs are considered, and it is assumed that four of the NGs are producers while the rest NGs are consumers. The main objective of each case is shown as follows:

1) Case One: To demonstrate the sequential implementation procedure of market trading within a single timeslot.
2) Case Two: To verify the effectiveness of market-based real-time distributed frequency regulation.

3) Case Three: Based on the predicted net-load curve in eight timeslots, to demonstrate the amount of allocated capacity in three markets and to examine the total profit of the producer NG under three CRMs.

3.4.1 Case One

The trading parameters of each producer NG in different markets are illustrated in Table 3.1 for Case One. The cost function is unified as $C = 0.246P^2 + 0.0815P + 0.4333$ for all NGs in order to reflect the relationship between the price and the profit in the trading results. 15 minutes before the real-time operation, the P2P bilateral market is organized to enable prosumer NGs to trade their energy based on their requirements. According to the optimal solutions from the optimal sharing strategy elaborated in equation (3.3), each operator of the producer NG submits the amount of devoted capacity along with the selling price to the transactive platform managed by BRP. Meanwhile, each operator of the consumer NG submits its required amount of capacity along with the potential purchasing price. The matchmaking process is conducted by BRP as introduced in Section 3.2.3, where the lowest offer is matched with the highest bid in the first place. The submitted bids and offers and the determined P2P trading among NGs are demonstrated in Fig. 3.4. The total submitted energy of four producer NGs is 0.97MWh, which is less than the total consumer requirement of 1.4MWh. Therefore, all submitted offers are successful, while NG7 with the highest bidding price fails to be matched. The remaining imbalance of 0.43MWh will be addressed in the next phase with a potentially higher cost. In the P2P energy market, the final transaction price is the average value of offer and bid for the matched

producer-consumer pair. Then the potential profit (in $) obtained by each producer NG in one hour is calculated as 17.64, 25.81, 15.6, and 36.6, respectively.

Table 3.1. Trading parameters of producer NG in different markets

Case I	Rating (MW)	P2P bilateral market						Balancing and ancillary service market		
		Price ($/kWh)			Successful rate of bidding			Price ($/kWh)	Price ($/kW)	Probability
		$\lambda_{S1,i}$	$\lambda^{B}_{S2,i}$	$\lambda^{R}_{S2,i}$	$\mu_{S1,i}$	$\mu^{B}_{S2,i}$	$\mu^{R}_{S2,i}$	$\lambda^{B}_{S2,i}$	$\lambda^{R}_{S2,i}$	τ_i
NG1	0.8	0.095	0.099	0.105	0.80	0.72	0.64	0.099	0.111	0.82
NG2	1.0	0.098	0.102	0.111	0.82	0.66	0.52	0.104	0.117	0.79
NG3	1.0	0.100	0.108	0.110	0.75	0.62	0.58	0.112	0.116	0.81
NG4	1.2	0.103	0.098	0.114	0.78	0.65	0.53	0.102	0.119	0.82

Table 3.2. Trading results of producer NG in different markets

Case I	**P2P bilateral market**				**Balancing and ancillary service market**			
	Consumer requirement: 1.4MWh				Balancing requirement: 0.43MWh			
					Frequency regulation service requirement: 0.71MW			
	Devoted (MWh)	Allocated (MWh)	Remained (MW)	Profit ($)	Energy Devoted (MWh)	Ancillary Service Devoted (MW)	Energy Allocated (MWh)	Ancillary Service Allocated (MW)
NG1	0.18	0.18	0.62	17.64	0.21	0.41	0.21	0.41
NG2	0.26	0.26	0.74	25.81	0.3	0.44	0	0
NG3	0.16	0.16	0.84	15.6	0.41	0.43	0	0.3
NG4	0.37	0.37	0.83	36.66	0.39	0.44	0.22	0

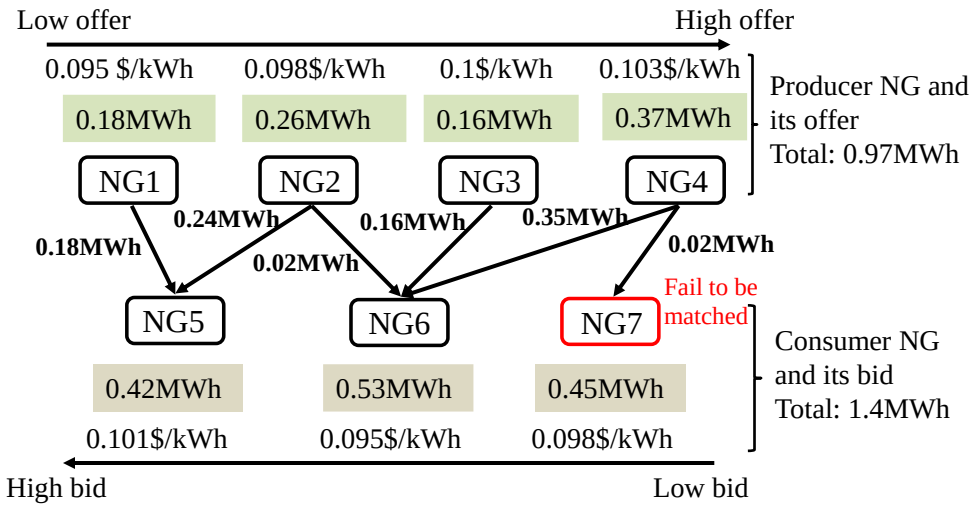

Fig. 3.4. P2P energy trading among NGs based on their offers and bids in the P2P bilateral energy market

In the subsequent balancing and ancillary service market, the producer NGs will devote their remained available quantities to the market, following the optimal allocation strategy elaborated in equation (3.4). Table 3.2 shows the trading results for each producer NG. The balancing requirement is the remaining 0.43MWh from the previous P2P energy market, and the frequency regulation requirement is 0.71MW. The BRP will then clear these two markets simultaneously based on the merit-order, while the bidding with a lower price will be accepted with priority, until the requirement is fulfilled. In this case, NG1 and NG4 are selected to provide energy balancing with the amount of 0.21 MWh and 0.22MWh, whilst NG1 and NG3 are selected to provide frequency regulation service with the amount of 0.41 MW and 0.3MW. In this regard, the engagement factor can be acquired for the following real-time operation, which is $\varphi_{NG1} = 1 + 0.41/0.8 = 1.51$ and $\varphi_{NG3} = 1 + 0.3/1 = 1.3$. In the real-time operation, such the engagement factor will be used to

formulate the primary and secondary control protocols (3.6) and (3.7) for the frequency regulation, which will be discussed in the next section.

3.4.2 Case Two

In Case Two, the effectiveness of market-based real-time distributed frequency regulation is verified. The deployment of the frequency regulation provision is based on the trading results in Case One. Fig. 3.5 shows the P2P communication link among NGs for the test islanded MG. The local information can be transmitted and received bidirectionally between neighboring NGs via the communication network.

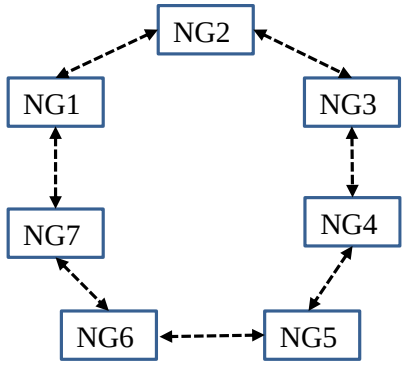

Fig. 3.5. Communication graph of NGs in the islanded MG

The coupling configuration matrix of the communication network is thus determined as below:

$$\boldsymbol{B} = \begin{bmatrix} -2 & 1 & 0 & 0 & 0 & 0 & 1 \\ 1 & -2 & 1 & 0 & 0 & 0 & 0 \\ 0 & 1 & -2 & 1 & 0 & 0 & 0 \\ 0 & 0 & 0 & -2 & 0 & 0 & 0 \\ 0 & 0 & 0 & 1 & -2 & 1 & 0 \\ 0 & 0 & 0 & 0 & 1 & -2 & 1 \\ 1 & 0 & 0 & 0 & 0 & 1 & -2 \end{bmatrix}$$

For the pinning-based secondary protocol, the control gain c is set to 100 and the pinning gain d is set to 10 which ensures the stability of the control protocol. The

frequency reference is set to 50Hz. The pre-defined droop gain k_{eq} of each producer NG (NG1-NG4) is set as 3.5×10^{-5}, 3×10^{-5}, 3×10^{-5}, 5.5×10^{-5}, respectively.

The worst scenario with the largest load variation ($\Delta P_{load} = 0.63$MW) at t = 2s in the real-time operation is investigated. Once the power imbalance occurs in the islanded MG, the frequency deviates from the reference value and consequently the frequency regulation will be automatically activated. For the proposed real-time frequency regulation, how much capacity will be provided, and which NG will participate in the regulation service provision is directly associated with the market clearing results. Fig. 3.6 shows the real-time power dispatch of each producer NG. During 0-2s, the entire network operates in the steady-state. The power output of each producer NG is approximately in a line with the sum of allocated capacity in the P2P bilateral energy market and balancing energy market shown in Table 3.2: NG1 (0.39MW), NG2 (0.26MW), NG3 (0.16MW) and NG4 (0.59MW). At t = 2s, in response to the frequency drop due to a sudden load increase of 0.63MW, NG1 and NG3 instantly adjust their power output to provide frequency regulation service as they are the committed NGs for the regulation service provision which is determined in the trading stage. The power sharing is conducted based on their engagement factors. It is observed that the power output of NG1 and NG3 is increased by 0.35MW and 0.28MW respectively, which is consistent with the allocated capacity for the ancillary service market. Fig. 3.7 shows the frequency response of each producer NG, where the frequency can be regulated fast to the reference value. By contrast, Fig. 3.8 shows the power sharing without the consideration of the market trading, where each

producer NG contributes to the regulation proportionally purely based on the pre-defined droop gain.

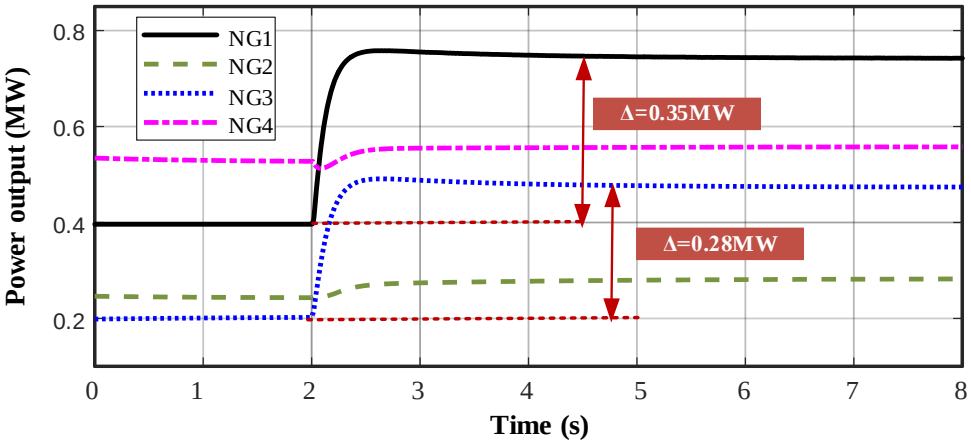

Fig. 3.6. Frequency regulation service provision by NG1 and NG3 considering the market trading

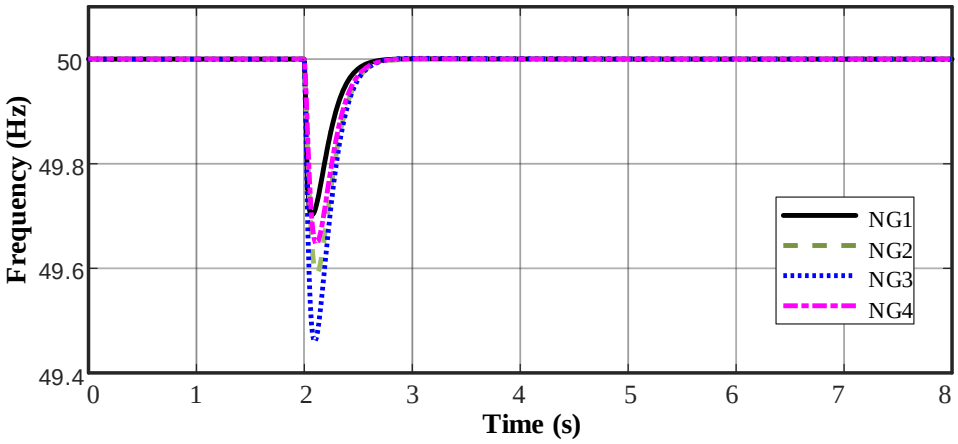

Fig. 3.7. Frequency response by implementing market-based distributed frequency regulation

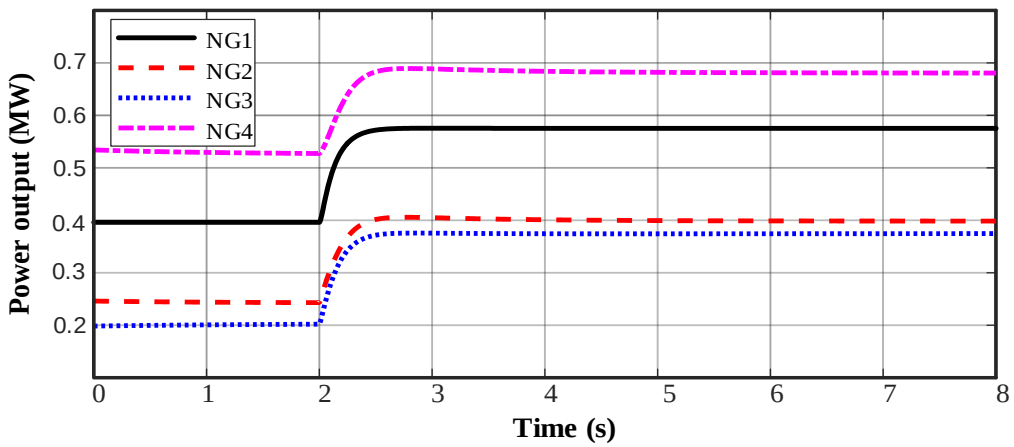

Fig. 3.8. Power sharing without the consideration of market trading

3.4.3 Case Three

In Case Three, the multi-market mechanisms are investigated in a longer period (eight timeslots). The expected capacity price and the total prosumers' requirement for each timeslot in Case Three are recorded in Table 3.3. Other parameters, such as the rating of NGs and the successful bidding rate, are the same as Case One. The optimal strategies are implemented to determine the devoted capacity for the producer NG. After the market is cleared, the allocated capacity of each producer NG in the P2P bilateral energy market, balancing energy market and ancillary service market is determined. Fig. 3.9 illustrates the predicted net load profile (total load consumption minus total generation) throughout eight timeslots.

Table 3.3. Consumer requirement in P2P market and expected capacity trading price (($/Unit)

T1		$\lambda_{S1,i}$	$\lambda^{B}_{S2,i}$	$\lambda^{R}_{S2,i}$	$\lambda^{B}_{S2,i}$	$\lambda^{R}_{S2,i}$
P2P market consumer requirement 1.4MWh	**NG1**	0.0945	0.099	0.105	0.099	0.111
	NG2	0.0975	0.102	0.111	0.1035	0.117
	NG3	0.1005	0.108	0.1095	0.1125	0.1155
	NG4	0.1035	0.0975	0.114	0.102	0.1185
T2		$\lambda_{S1,i}$	$\lambda^{B}_{S2,i}$	$\lambda^{R}_{S2,i}$	$\lambda^{B}_{S2,i}$	$\lambda^{R}_{S2,i}$
	NG1	0.0945	0.0975	0.1065	0.099	0.111

P2P market consumer requirement 1.6MWh	**NG2**	0.096	0.1035	0.111	0.0945	0.1095
	NG3	0.093	0.1095	0.108	0.096	0.1155
	NG4	0.1005	0.096	0.114	0.0975	0.1125
T3		$\lambda_{S1,i}$	$\lambda^{B}_{S2,i}$	$\lambda^{R}_{S2,i}$	$\lambda^{B}_{S2,i}$	$\lambda^{R}_{S2,i}$
P2P market consumer requirement 2.2MWh	**NG1**	0.0945	0.1005	0.1065	0.1005	0.1125
	NG2	0.096	0.1005	0.1095	0.0975	0.111
	NG3	0.102	0.105	0.111	0.096	0.114
	NG4	0.093	0.099	0.1125	0.0945	0.108
T4		$\lambda_{S1,i}$	$\lambda^{B}_{S2,i}$	$\lambda^{R}_{S2,i}$	$\lambda^{B}_{S2,i}$	$\lambda^{R}_{S2,i}$
P2P market consumer requirement 2.0MWh	**NG1**	0.0975	0.102	0.1035	0.093	0
	NG2	0.0945	0.1005	0.108	0.096	0
	NG3	0.099	0.1065	0.111	0.099	0
	NG4	0.096	0.099	0.1125	0.0975	0
T5		$\lambda_{S1,i}$	$\lambda^{B}_{S2,i}$	$\lambda^{R}_{S2,i}$	$\lambda^{B}_{S2,i}$	$\lambda^{R}_{S2,i}$
P2P market consumer requirement 2.4MWh	**NG1**	0.099	0.1035	0.1095	0.0975	0.111
	NG2	0.0975	0.102	0.108	0.0945	0.1125
	NG3	0.0945	0.105	0.1125	0.093	0.108
	NG4	0.096	0.1005	0.111	0.096	0.1095
T6		$\lambda_{S1,i}$	$\lambda^{B}_{S2,i}$	$\lambda^{R}_{S2,i}$	$\lambda^{B}_{S2,i}$	$\lambda^{R}_{S2,i}$
P2P market consumer requirement 1.8MWh	**NG1**	0.096	0.1005	0.1065	0.0975	0
	NG2	0.099	0.102	0.1095	0.102	0
	NG3	0.0975	0.108	0.1125	0.1005	0
	NG4	0.1005	0.1035	0.111	0.099	0
T7		$\lambda_{S1,i}$	$\lambda^{B}_{S2,i}$	$\lambda^{R}_{S2,i}$	$\lambda^{B}_{S2,i}$	$\lambda^{R}_{S2,i}$
P2P market consumer requirement 1.4MWh	**NG1**	0.093	0.0975	0.105	0.0975	0
	NG2	0.0975	0.1005	0.1065	0.102	0
	NG3	0.1005	0.1035	0.1095	0.1035	0
	NG4	0.096	0.102	0.108	0.096	0
T8		$\lambda_{S1,i}$	$\lambda^{B}_{S2,i}$	$\lambda^{R}_{S2,i}$	$\lambda^{B}_{S2,i}$	$\lambda^{R}_{S2,i}$
P2P market consumer requirement 1.8MWh	**NG1**	0.096	0.102	0.108	0.1005	0.114
	NG2	0.102	0.1035	0.1065	0.1035	0.111
	NG3	0.1005	0.1035	0.111	0.099	0.1125
	NG4	0.099	0.1005	0.1095	0.0975	0.114

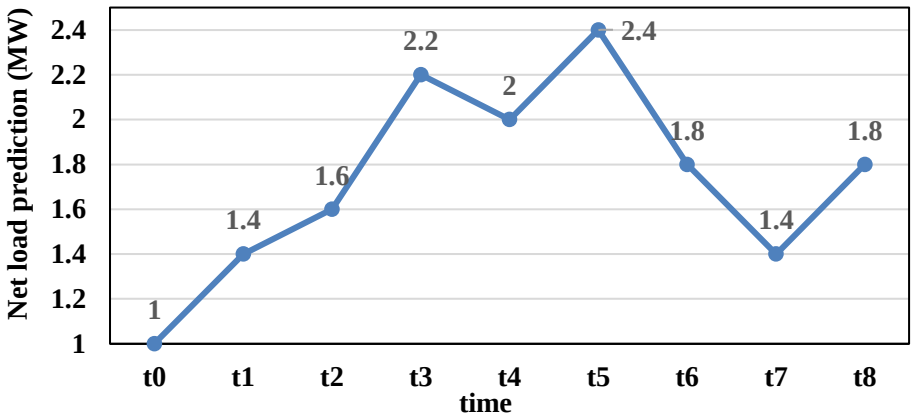

Fig. 3.9. Net load prediction in the eight timeslots

The frequency regulation service requirement for each timeslot is 110% of the net load fluctuation between the current timeslot and the next timeslot. As only up-regulation is considered, the frequency regulation requirement is zero if the net load is predicted to be reduced, i.e., the regulation requirement is zero in the 4^{th}, 6^{th} and 7^{th} timeslot. Fig. 3.10 shows how much capacity is allocated to each market in eight timeslots. It is observed that all producer NGs participate in the P2P energy trading market, while none of them allocate the capacity to the ancillary service market in the 4^{th}, 6^{th} and 7^{th} timeslot.

Then, total profit obtained by each producer NG in the balancing and ancillary service market through three different capacity remuneration mechanisms (CRMs) is examined respectively, shown in Fig. 3.11. It can be seen that more profit is acquired in the balancing market than that in the ancillary service market. The reason behind that is the ancillary service is not required in some timeslots, which directly causes zero revenue for the ancillary service. It is noticeable that different NGs receive different profits under the same approach of remuneration, which is due to their different bidding prices. Those who submit a lower price will be more likely to be selected as winning bids, and therefore their obtained profits are higher.

Next, the impact of CRMs is further discussed. Obviously, CRM will influence the total profits of producer NGs. If producer NGs are remunerated by the MP approach, they will receive more profits compared with the other two CRMs, which would potentially contribute to their willingness of devoting their capacity to facilitate real-time network operation. However, this also means BRP will pay more for the purchase of service procurement. In comparison, the PAB approach will lead to less financial cost in the perspective of BRP, and producer NGs will be fairly remunerated according to their willingness of bidding, so this is the most widely adopted method in existing markets. The main difference between PAB and PAO is the payment for ancillary service deployment. By adopting PAO, BRP could directly pay the producer NG with the actual opportunity cost instead of an overly high bidding price, which could effectively reduce the investment. However, the willingness of NGs' devotion would be affected as they can only receive the same payback as devoting the capacity to the energy market, which could result in a potential lack of capacity for frequency regulation in the real-time operation. Therefore, how to choose CRM for the balancing and ancillary service market should be determined carefully based on the practical considerations of different scenarios under different needs.

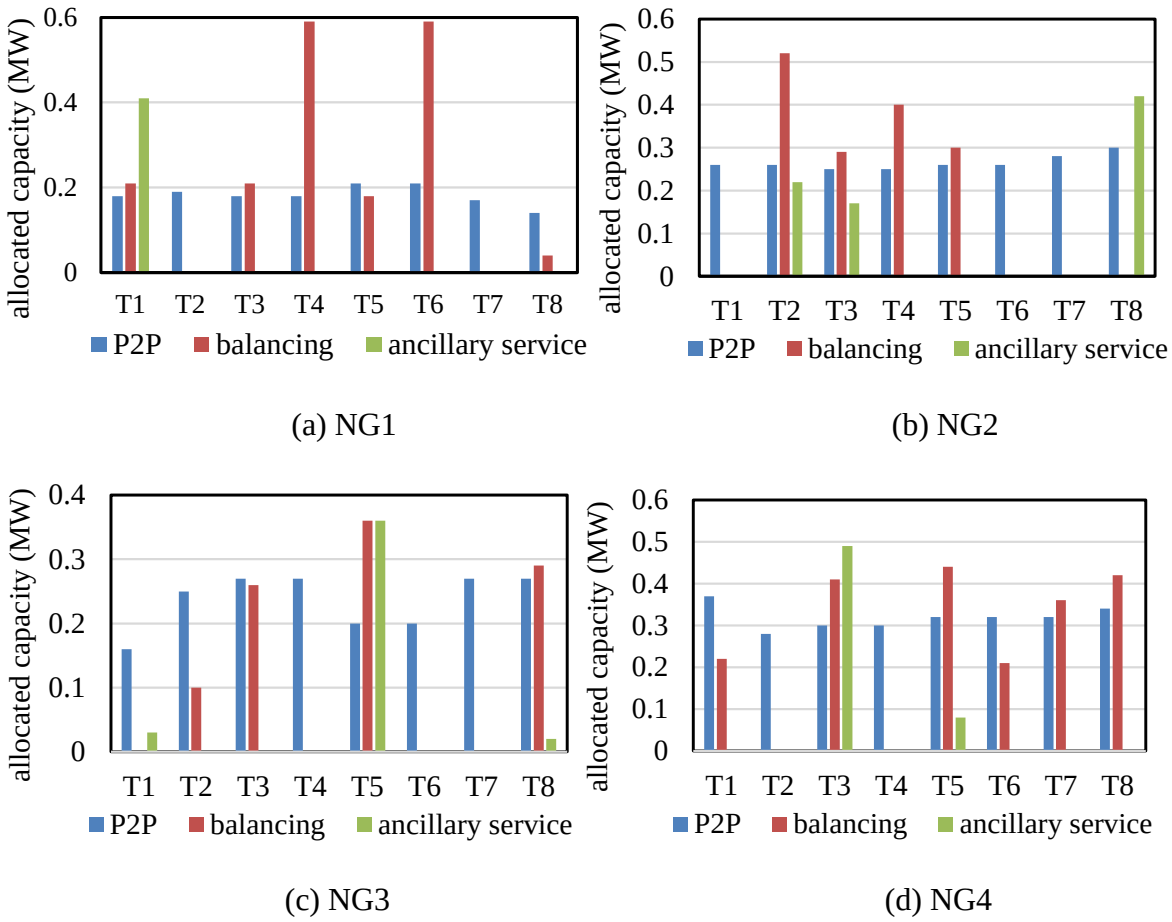

Fig. 3.10. Allocated capacity of each NG in three markets throughout eight timeslots

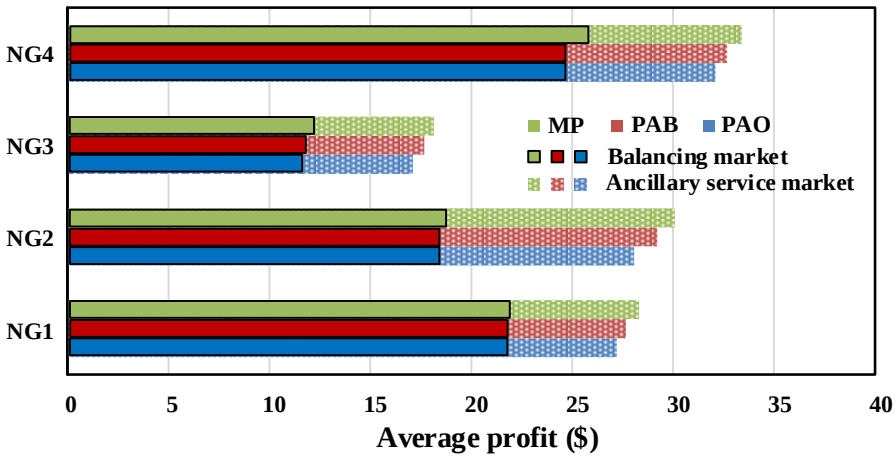

Fig. 3.11. Average profit within eight timeslots under different CRMs

3.5 Chapter Summary

In this chapter, a multi-market trading paradigm is proposed to achieve the goal of the maximal economic benefit of the producer NG, while the real-time frequency regulation service can be provided economically based on the market trading results. Specifically, in light of high-performing P2P communication infrastructures, NGs can be coordinated not only to trade energy with one another but to economically reserve the capacity for the regulation service to maintain the power balance and frequency within a MG in real-time. The entire paradigm is organized from the perspective of the potential producers in the market. P2P bilateral energy trading market, balancing market and ancillary service market is considered to facilitate the energy and capacity trading among NGs, where the market mechanisms and optimal offering strategies are designed carefully. In terms of the real-time implementation, the frequency regulation service can be provided by the committed NGs which are determined in the stage of market trading with the reserved capacity. Relying on P2P information sharing, the distributed control architecture including primary and pinning-based secondary control is implemented to enable the incentivized frequency regulation based on the engagement factor of each participated NG. Case studies verify the effectiveness of market trading mechanisms and market-based real-time frequency regulation.

Based on the simulation results, the key findings can be summarized: 1) All producer NGs participate in the P2P energy trading while their participation in the balancing market and ancillary service market are determined by the actual balancing requirement and the predicted frequency regulation requirement; 2) Compared with the frequency regulation without the consideration of market incentives, the proposed

market-based frequency regulation can achieve the same regulation effect and meanwhile enable an economically efficient power sharing; 3) MP is the capacity remuneration method which can positively contribute to the willingness of NGs' participation in the markets, while PAO is the capacity remuneration method which can effectively reduce the financial cost of BRP.

Chapter 4 Distributed *P* and *Q* Provision Based Voltage Regulation Scheme by Incentivized EV Fleet Charging for Resistive Distribution Networks

The capability of on-board bidirectional chargers to deliver both real and reactive power makes electric vehicles (EVs) become suitable candidates for the voltage regulation in the distribution network considering higher *R/X* ratio of distribution lines. This chapter proposes a distributed voltage regulation scheme for dominantly resistive distribution networks through coordinated EV charging/discharging. In the optimal planning stage, the maximal profit of each EV user for the regulation provision is guaranteed while the driving need can be satisfied. An optimal charging model is proposed to plan the total available *P* and *Q* and a parameter '*involvement level*' is introduced for the fair pricing of participating EV users. In the regulation stage, an adaptive voltage sensitivity coefficient is developed to estimate the amount of required power for voltage regulation. A novel parallel-consensus sharing strategy is designed so that the local power dispatch decision can be made by each EV through information sharing between neighboring buses. The back-up support from local energy storage system can be activated under the emergency scenario due to the communication failure and insufficient EV resources. Simulation results demonstrate that the proposed scheme can effectively and robustly regulate the voltage and is scalable to different network topologies.

4.1 Coordination of EVF Optimal Charging

In the context of this chapter, one EVF is a cluster of EVs charging/discharging in the same charging point comprising multiple smart chargers at a certain bus. EV users who are willing to participate into the regulation scheme could either be producers by discharging to the grid or be consumers by charging from the grid through the smart EV chargers. In this section, the working principle of reactive power provided by the smart charger is firstly presented. Then an optimal charging model is developed to plan the charging/discharging power and to guarantee the regulation service profit based on the involvement level of each EV user.

4.1.1 EV Smart Charger for Reactive Power Provision

Theoretically, by controlling the voltage and current of DC-link capacitor in the charger, the reactive power can be injected into, or absorbed from the grid. Such a process only takes place in power electronics interface between grid and charger without any involvement of the battery unit. Thus, there is no deterioration of the battery lifetime. Shadow area in Fig. 4.1 is the working region of a smart four-quadrant EV charger.

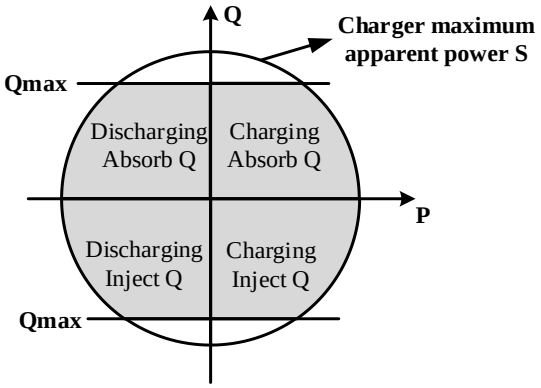

Fig. 4.1. Working region of a smart charger

Considering the ripple power inside the charger, the maximum reactive power (Q_{max}) provided/absorbed by an EV charger is related to charger capacity C, charger coupling inductor L_c, angular frequency ω and source voltage V_s, which can be calculated by (1) [133]. Smart chargers can interact with plugged-in EVs to capture the current percentage of charge remaining in the EV battery, i.e., state of charge (SOC) of the battery. The charging/discharging process can be controlled according to the commands obtained from the optimal charging program, which will be introduced in Section 4.1.3.

$$Q_{max} = \frac{\sqrt{1+4\frac{\omega L_c}{V_s^2}C}-1}{2\frac{\omega L_c}{V_s^2}} \tag{4.1}$$

4.1.2 Involvement Level Considering Users' Driving Needs

If the user of m^{th} idle EV ($m = 1,2,\dots,M$) wants to get involved in the regulation service during the regulation period T, target SOC, i.e., the percentage of battery capacity that the EV user wants to achieve after completing charging/discharging, will be estimated in advance. Considering the advances in intelligent battery management systems (BMS), the estimation can be done by the intelligent BMS of the smart EV. The EV user only needs input the destination and BMS will give an estimation on the target SOC based on the real-time traffic conditions and the user's driving behaviour. With the target SOC, the needed battery energy E_{need}^m through the charging/discharging process can be determined by

$$E_{need}^m = \begin{cases} E_m(SOC_{end}^m - SOC_{now}^m), \text{charging} \\ E_m(SOC_{now}^m - SOC_{end}^m), \text{discharging} \end{cases} \tag{4.2}$$

where E_m denotes the rated battery capacity of m^{th} EV; SOC_{end}^m is the target SOC and SOC_{now}^m is the current SOC of the battery. A parameter so called *involvement level* is then defined to indicate how active the engagement of an EV user will be in the regulation scheme:

$$\beta_m(\tau) = 1 - E_{reg}^m(\tau)/E_{need}^m \tag{4.3}$$

where $E_{reg}^m(\tau)$ characterizes the amount of battery energy being charged or discharged of m^{th}EV from initial plug-in time τ_{ini} to current timeslot τ, which is

$$E_{reg}^m(\tau) = \begin{cases} \int_{\tau_{ini}}^{\tau} \eta P_c^m(\tau)\, d\tau, \text{charging} \\ \int_{\tau_{ini}}^{\tau} \frac{P_d^m(\tau)}{\eta}\, d\tau, \text{discharging} \end{cases} \tag{4.4}$$

where η denotes charging (discharging) efficiency,$P_c^m(\tau)$ and $P_d^m(\tau)$ denote power rate of charging and discharging of the charger at timeslot τ respectively. It is obvious that E_{need}^m is a constant once the EV user fixes the target SOC. Therefore, involvement level $\beta_m(\tau)$ is a non-negative time-varying parameter whose value solely depends on $E_{reg}^m(\tau)$. Consequently, higher charging/discharging rate would contribute to a larger involvement level. As time elapses, $\beta_m(\tau)$ is decreasing since less energy is required. Once the battery reaches the SOC target, $\beta_m(\tau)$ will be equal to 0, which means this EV will leave the scheme.

4.1.3 Formulation of EVF Optimal Charging Based on Involvement Level

To encourage EV users to participate in the regulation whilst achieving the fair pricing, the profit that m^{th} EV generated is closely related to its individual involvement level. EV users with larger involvement level would have higher payback

during the regulation period T. Thus, the unit profit of real power P acquired by m^{th} EV is defined by:

$$\pi_p^m(\tau) = (\beta_m(\tau) + 1)a \tag{4.5}$$

where a represents the incentive dynamic tariff in the electricity market. To create a reasonable EVF charging model, the following assumptions have been made: 1) To adapt to the typical PV generation in the midday as well as the peak demand in the evening, 10:00-14:00 and 19:00-23:00 are set to be two regulation periods; 2) The unit profit $\pi_q^m(\tau)$ of Q provision is 50% of the unit profit $\pi_p^m(\tau)$ of P provision; 3) The charging/discharging process will not cause overloading and feeder thermal capacity is not considered in the model as the focus of this chapter is to regulate voltage.

Under the above assumptions, the optimal charging model of m^{th} EV is developed consisting of four parts, as shown in (4.6): 1) the profit generated from the regulation service by providing *P*; 2) the similar profit by providing *Q*; 3) normal charging fee; 4) the battery degradation cost (unit degradation cost b is only considered when the battery is discharging).

$$\max \sum_{\tau_0}^{T} \Delta\tau \begin{bmatrix} \frac{\pi_p^m(\tau) P_d^m(\tau)}{\eta} + \pi_q^m(\tau) Q_m(\tau) \\ -aP_c^m(\tau)\eta - \frac{bP_d^m(\tau)}{\eta} \end{bmatrix},\ m = 1,2,\dots,M \tag{4.6}$$

s.t

$$0 \le P_c^m(\tau) \le S \tag{4.7}$$

$$0 \le P_d^m(\tau) \le S \tag{4.8}$$

$$(P_c^m(\tau) + P_d^m(\tau))^2 + Q_m(\tau)^2 \le S^2 \tag{4.9}$$

$$Q_m(\tau) = \begin{cases} 0, if\ P_c^m(\tau) + P_d^m(\tau) = 0 \\ 0 < Q_m(\tau) < Q_{max}, others \end{cases} \tag{4.10}$$

$$P_c^m(\tau) \times u = 0 \tag{4.11}$$

$$P_d^m(\tau) \times v = 0 \tag{4.12}$$

$$u + v \leq 1 \tag{4.13}$$

$$0 \leq \beta_m(\tau) \leq 1 \tag{4.14}$$

$$\sum_m^M (P_c^m(\tau) + P_d^m(\tau)) < \bar{P} \tag{4.15}$$

$$\sum_m^M Q_m(\tau) < \bar{Q} \tag{4.16}$$

Decision variables in the model above are charging/discharging power $P_c^m(\tau)/P_d^m(\tau)$ and reactive power $Q_m(\tau)$ for m^{th} EV in different timeslots. Constraints (4.7) - (4.10) define the normal working region of a smart charger, which is the shadow area in Fig. 1. Constraints (4.11) - (4.13) stipulate that charging and discharging for an EV cannot occur simultaneously, where u and v are binary variables, either 0 or 1. Constraint (4.15) and (4.16) indicate that the total allowable charging/discharging power of participating EVs is limited by the maximum power $\bar{P}$ and $\bar{Q}$, which ensures the distribution line capacity will not be violated. Due to the nonlinearities in both objective function and constraints, the proposed model is the problem of mixed integer nonlinear programming (MINLP). Such a problem can be solved effectively using nonlinear branch-and-bound methods if it is the convex problem, while more works need to be done for the nonconvex MINLP, such as piecewise linear approximation and generic relaxation strategies [134]. The optimization process of the problem will be discussed in Section IV. Donating the total regulation period as T and $\tau = \tau_0, \tau_0 + \Delta\tau, \tau_0 + 2\Delta\tau \ldots, T$ with $\Delta\tau = 15$mins, the total amount of optimal real and reactive power provided by i^{th} EVF (charging point) at a specific timeslot τ is

$$r_p^i = \sum_m^M [P_c^m(\tau) + P_d^m(\tau)] \tag{4.17}$$

$$r_q^i = \sum_m^M Q_m(\tau) \tag{4.18}$$

And $r^i = [r_p^i, r_q^i]$ represents the total amount of optimal power of i^{th} EVF hereafter.

Remark: The proposed model maximizes the financial benefit for an individual EV user participating in the regulation service and meanwhile ensures its driving need can be satisfied. The incentives offered to the individual EV for providing real and reactive power are considered in the model. In particular, the provision of reactive power can earn the revenue for the EV user without the adverse impact on the battery lifetime. Overall, EV users would obtain the profit by providing the voltage regulation during the charging/discharging process. the consistent promotion of ancillary service markets by the government and grid operators in many countries and regions will achieve a healthy and normalized market-driven participation, which would be more attractive to EV users. Consequently, the market-driven scheme will gradually replace the existing financial incentives and encourage the EV users to get involved into the service provision. It is believed that without affecting the travel plan, many of them would like to contribute to the power system operation with a cheaper electricity price and a certain payback. It should be noted that charging/discharging power of the participating EV user will be coordinated to provide the voltage regulation support by connecting with the smart charger. The advantage of this process is that the available EV battery capacity can be effectively utilized for the voltage regulation and meanwhile corresponding profit can be secured by the participating EV users even without the knowledge of the network side.

4.2 Proposed Distributed Voltage Regulation Scheme

The schematic diagram of the proposed regulation scheme is shown in Fig. 4.2, which takes bus i as an example. In the optimal charging planning stage, available P and Q of each EVF is planned before the regulation starts. In the distributed regulation stage, once the voltage deviation is detected at a certain bus, the required P and Q for the voltage recovery of this bus is estimated by the local processor based on the adaptive local voltage sensitivity. The available power that can be provided by each EVF and the required power for the voltage regulation will then be shared among buses over the communication network based on the developed parallel-consensus sharing strategy. Power-sharing ratio can be acquired for the local power dispatch of each EVF and the violated voltage therefore can be regulated by collectively providing incentivized P and Q from all EVFs in the network. However, if the collective support from EVFs cannot successfully regulate the voltage due to a communication failure or insufficient number of participating EVs, the back-up support from the local energy storage system (ESS) will be activated. This is displayed as the *emergency scenario* in the diagram. It should be noted that all operations are conducted at a local bus level, so that the regulation is fully distributed. Details in terms of the distributed regulation stage are introduced in the following.

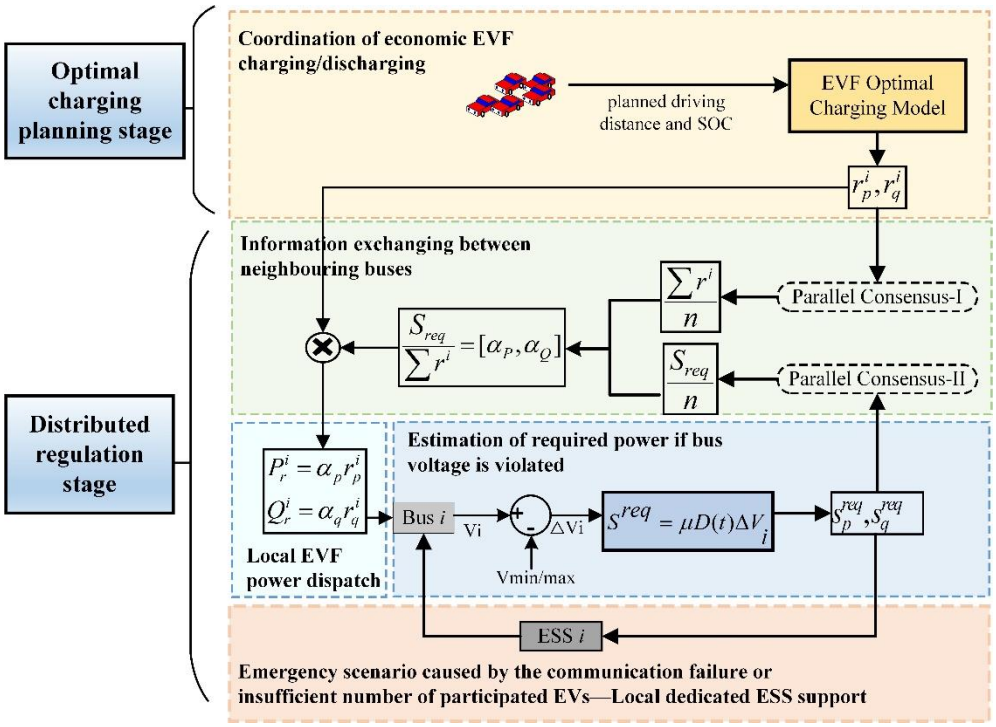

Fig. 4.2. Schematic diagram of proposed voltage regulation scheme

During the regulation period, the local bus monitor takes the measurement of bus voltage $V_i[t]$. If $V_i[t]$ is detected to be out of the prescribed steady-state voltage limit $[V_{min}, V_{max}]$, required real power $S_p^i[t]$ and reactive power $S_q^i[t]$ for voltage recovery will be estimated by the local processor. In this chapter, we adopt a time-varying adaptive coefficient to describe the local voltage sensitivity. The instants of sensitivity, *V-Q* and *V-P*, can be estimated by only taking the difference of bus voltage and local net power injections between consecutive time slots, as follows:

$$D_p^i[t] = \frac{P_{net}^i[t] - P_{net}^i[t-1]}{V_i[t] - V_i[t-1]} \tag{4.19}$$

$$D_q^i[t] = \frac{Q_{net}^i[t] - Q_{net}^i[t-1]}{V_i[t] - V_i[t-1]} \tag{4.20}$$

where $P_{net}^{i}[t]$ and $Q_{net}^{i}[t]$ denote net real and reactive power injections into bus i at time instant t respectively. Let $\mathcal{D}[t] = [D_p^i[t], D_q^i[t]]$, the required power can be calculated by

$$\mathcal{S}[t] = \begin{cases} \mu\mathcal{D}[t](V_i[t] - V_{max}), V_i[t] > V_{max} \\ 0, \qquad\qquad V_{min} < V_i[t] < V_{max} \\ \mu\mathcal{D}[t](V_{min} - V_i[t]), V_{min} > V_i[t] \end{cases} \tag{4.21}$$

where $\mathcal{S}[t] = [S_p^i[t], S_q^i[t]]$. μ is the constant gain which influences the control efficiency as well as the solution convergence. Such power estimation process has high adaptability to the topology-changing network and makes the control fully distributed due to the adoption of local voltage sensitivity coefficient $\mathcal{D}[t]$. The data received from the monitors are a mixture of the original data and the device noise. Here we consider the measurement error ε as the unbiased error, which can be usually regarded as a normal distribution probability function with a standard deviation σ. Weighted least squares method can be applied to utilize the inaccurate measurements to get the best estimation of collected variables. The monitor measurement accuracy is assumed to be ±3%, corresponding to a standard deviation of 3σ, which means the monitor will give a reading within ±3% of the true value for approximately 99% of the time.

The time-varying sensitivity coefficient developed above aims to describe the real-time voltage sensitivity in a model-free manner. Due to frequent changes of network topology and operational states of renewables, fixed sensitivity calculation methods are no more accurate. The proposed sensitivity calculation enables fairly precise control actions in real-time if the time step is small enough and the calculations are

frequent, so that the continuous update of the sensitivity can correct any potential adverse control action during the regulation.

4.2.1 Information Sharing for Local Power Support

1) Communication Graph and Discrete-time Consensus

The communication network topology together with the information exchange link of a distribution network can be described by a graph G, which consists of a pair of sets $\{V, E\}$. $V = \{1,2, \dots, n\}$ is the finite vertex set of all buses in a network and $E \subseteq V \times V$ is the set of edges connecting any distinct pair of them. If bus j can receive the information from bus i, we say bus j is a neighboring bus of bus i. The set including all neighboring buses of bus i is donated by $\mathcal{N}_i$. The number of neighboring buses of bus i is called in-degree of i, donated by $\mathcal{D}_i^-$. Similarly, out-degree of i represents the number of buses that have bus i as a neighbor, denoted by $\mathcal{D}_i^+$. If the information can be sent and received bi-directionally between neighboring buses, graph G is undirected, i.e., $\mathcal{D}_i^- = \mathcal{D}_i^+ := \mathcal{D}_i, \forall\, i = 1, \dots, n$. In this chapter, the undirected graph is used for the communication network. The discrete-time consensus algorithm is chosen to develop a sharing strategy:

$$x_i[k+1] = \left(1 - \frac{\mathcal{N}_i}{1+\mathcal{D}}\right) x_i[k] + \sum_{j \in \mathcal{N}_i} \frac{1}{1+\mathcal{D}} x_j[k] \tag{4.22}$$

where $\mathcal{D}$ is the maximum degree in the network, defined as $\mathcal{D} = \max\{\mathcal{D}_i\}$. The certain state x_i of bus i at the next time-step is updated by a linear combination of its own state and the state of its neighboring buses at current time step k. Based on stability analysis in [65], the converged solution of (4.22) is given as follows, where an agreement can be reached depending on the initial states of each bus.

$$\lim_{k\to\infty} x_i[k] = \frac{1}{n}\sum_{i=1}^{n} x_i[0] \tag{4.23}$$

2) Development of parallel-consensus sharing strategy

If the voltage deviation is detected in a certain bus, it will become the violated bus and immediately activate the information sharing process. $\mathcal{S}[t]$ will be shared with the neighboring buses of the violated bus. We use $\boldsymbol{S^{req}} = [S_p^{req}, S_q^{req}]$ to represent the initial condition of a violated bus hereafter. At time t, required power $\boldsymbol{S^{req}}$ is only known by the violated bus while available power for the regulation service $r^i = [r_p^i, r_q^i]$ is only known by EVF i itself. The total available P and Q from EVFs in the network can be expressed as

$$R_p := \sum_{i=1}^{n} r_p^i \tag{4.24}$$

$$R_q := \sum_{i=1}^{n} r_q^i \tag{4.25}$$

where n is the total number of buses. Let $\boldsymbol{R} = [R_p, R_q]$ and it is assumed that $\boldsymbol{S^{req}} \leq \boldsymbol{R}$, i.e., total available power provided collectively by EVFs is sufficient for the required power of the violated bus. If each bus knows both $\boldsymbol{S^{req}}$ and $\boldsymbol{R}$, the proportional P and Q dispatched by EVF i can be calculated by (4.26) and (4.27) respectively, given that k is the step that the solution has converged.

$$\lim_{k\to\infty} P_r^i[k] = \frac{S_p^{req}}{R_p} r_p^i \tag{4.26}$$

$$\lim_{k\to\infty} Q_r^i[k] = \frac{S_q^{req}}{R_q} r_q^i \tag{4.27}$$

We define $\alpha_P = \frac{S_p^{req}}{R_p}$ and $\alpha_Q = \frac{S_q^{req}}{R_q}$ as the P and Q allocation ratio respectively. However, such results can only be acquired based on the prerequisite that each bus is

able to know the global information on $\boldsymbol{S^{req}}$ and $\boldsymbol{R}$. It cannot be realized in a fully distributed communication network without a central controller. To address this problem, a parallel-consensus sharing strategy is developed in this chapter to efficiently calculate the power allocation ratio α_P and α_Q.

Given the undirected communication topology, consensus algorithm shown in (4.22) can be conducted simultaneously twice with distinct purposes. For ***Consensus process-I***, required power $\boldsymbol{S^{req}}$ is shared among buses by

$$S^i[k+1] = \left(1 - \frac{\mathcal{N}_i}{1+\mathcal{D}}\right) S^i[k] + \sum_{j\in\mathcal{N}_i} \frac{1}{1+\mathcal{D}} S^j[k] \tag{4.28}$$

The initial condition of each bus is set to $\frac{\boldsymbol{S^{req}}}{\mathcal{D}}$ if the bus is one of the neighbors of the violated bus, otherwise it is zero. As expressed by (4.23), after enough times of iterations, the solution will converge to a steady-state value, which is accessible for all buses in the network.

$$\lim_{k\to\infty} S^i[k] = \frac{1}{n}\sum_{i=1}^{n} S^i[0] = \frac{\boldsymbol{S^{req}}}{\boldsymbol{n}}, \forall\, i = 1, \dots, n. \tag{4.29}$$

Similarly, for ***Consensus process-II***, available power of each EVF is updated by

$$r^i[k+1] = \left(1 - \frac{\mathcal{N}_i}{1+\mathcal{D}}\right) r^i[k] + \sum_{j\in\mathcal{N}_i} \frac{1}{1+\mathcal{D}} r^j[k] \tag{4.30}$$

The steady-state solution shared by all buses is $\frac{\boldsymbol{R}}{n}$, shown as:

$$\lim_{k\to\infty} r^i[k] = \frac{1}{n}\sum_{i=1}^{n} r^i[0] = \frac{\boldsymbol{R}}{\boldsymbol{n}}, \forall\, i = 1, \dots, n. \tag{4.31}$$

Therefore, power-sharing ratio α_P and α_Q can be acquired by each controllable bus locally through the ratio of solutions from two consensus processes:

$$\frac{\boldsymbol{S^{req}}}{n} \Big/ \frac{\boldsymbol{R}}{n} = \frac{\boldsymbol{S^{req}}}{\boldsymbol{R}} = \left[\frac{S_p^{req}}{R_p}, \frac{S_q^{req}}{R_q}\right] \tag{4.32}$$

Two consensus processes are completely independent of one another and can be performed simultaneously without mutual disturbance. Based on above descriptions, the flowchart of the proposed voltage regulation scheme is shown in Fig. 4.3.

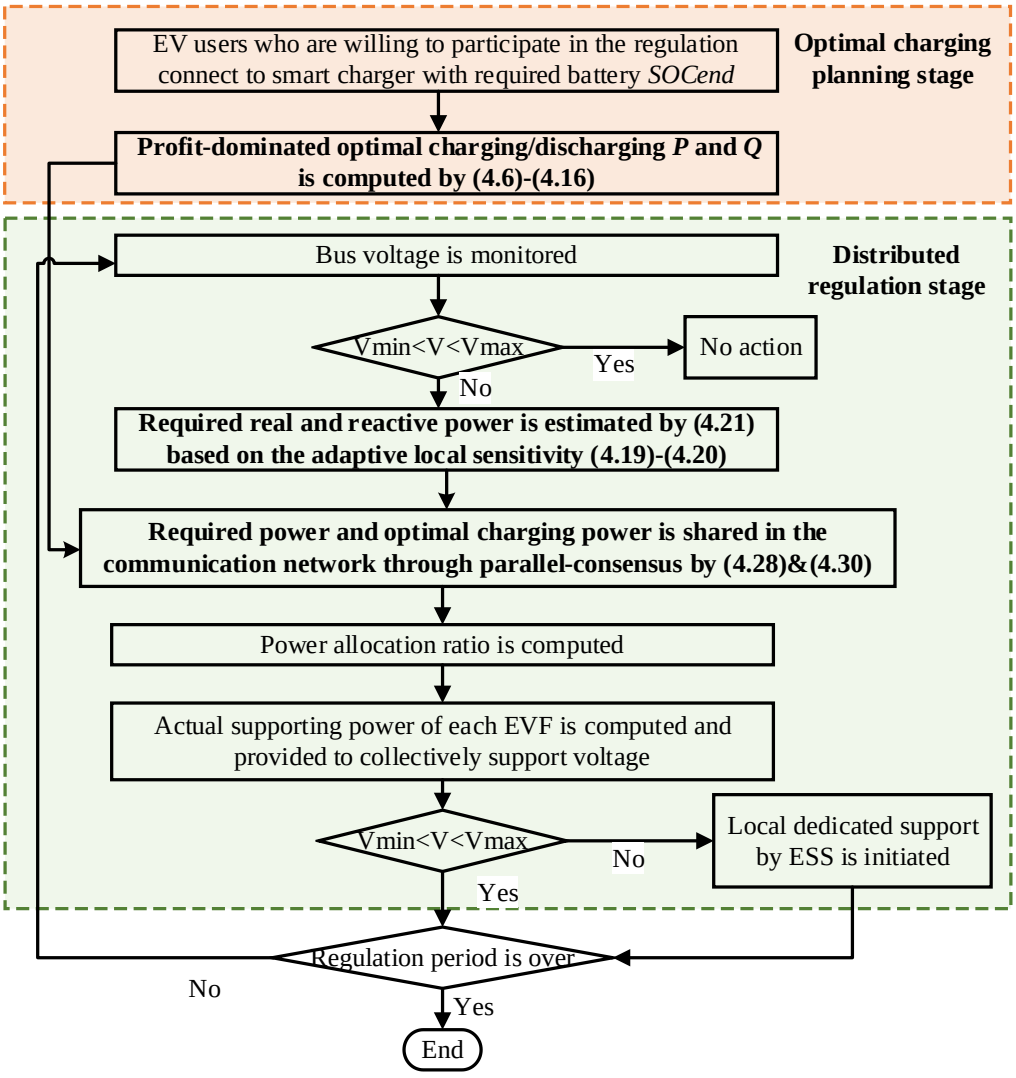

Fig. 4.3. Flowchart of the proposed voltage regulation scheme

Remarks:

1) Usually, there is a bus assigned as the virtual leader, which is responsible for sending the first signal to its neighbors so that the consensus can be activated. One of the characteristics of parallel-consensus sharing strategy is that there is no need to

specify the leader, i.e., leader-free. The bus which is detected with voltage violations will activate the consensus processes automatically.

2) The proposed scheme by involving the participation of EV fleet aims to provide a cost-effective option for the voltage regulation without a need of further investment in the distribution network. It is a supplement to conventional voltage control solutions relying on the expensive regulation devices and not intended to replace them. By means of the regulation provided by EVF with incentives, the operation time of conventional regulation devices can be significantly reduced and thus the capital cost and maintenance cost can be saved. In this connection, the proposed scheme benefits both parties of utilities and EV users.

3) Comparing to the centralized control, the proposed distributed regulation structure is more advantageous in terms of the scalability and flexibility, which can nicely fit the wide scattering feature of EVFs and renewables in the distribution network and enhance the regulation reliability [23].

4.2.2 Discussion on the Hardware Requirement

Considering the development of information and communication technology (ICT), the concept of the intelligent bus terminal (IBT) is introduced to facilitate the implementation of the proposed voltage regulation framework. IBT, which is constructed of advanced IoT devices, has the following three major functions: monitoring, computing and communication, as shown in Fig. 4.4. Sensors and metering facilities are responsible for collecting real-time measurements of the voltage and the power. Once a voltage deviation is detected, local bus processors run computations according to the prior software instruction. To achieve the local control

decision, communication infrastructure enables the information exchange of each IBT with its neighboring IBTs via the communication network.

Under the consideration of capital and maintenance cost, it is impractical that all buses in a distribution network are equipped with an IBT. Therefore, only two types of buses with high importance are IBT-enabled in the network: critical bus and controllable bus. The buses that are integrated with renewables (e.g., solar PVs) are considered to be the critical buses since they are more likely to suffer from voltage violations. EV charging points equipped with multiple smart chargers are located at the buses along the distribution feeder. Such buses are considered as the controllable buses.

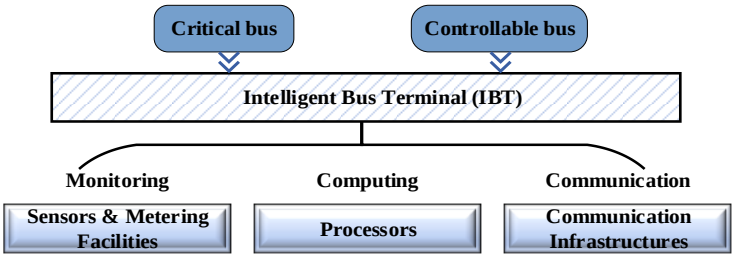

Fig. 4.4. Three functions of IBT and two types of IBT-enabled buses

The stable communication among buses and EVFs is the foundation to a reliable distributed voltage control. The estimated bandwidth of the proposed distributed regulation is around 100kbps-2Mbps such that the current communication technologies can meet the communication requirement [135]. Current deployed communication technologies can be categorized into two types: wired and wireless. Wired technologies (e.g., fiber optic communication and power line communication) have high data transfer rate from hundred megabits per second up to several gigabits per second with high coverage range (up to 100km). Yet it is costly to implement wired technologies to meet the requirement of distributed monitoring and control of

wide-scale networks. Wireless technologies (e.g., Wi-Fi and ZigBee) are preferable options to be utilized for the distributed control structure. ZigBee supports low date rate from 20kbps to 250kbps. The date rate of Wi-Fi (IEEE802.11) ranges from 1Mbps to 100Mbps. However, the small coverage range (up to 100m) makes them more suitable for communications in the small-scale network [135].

With the tremendous increase in both dimension and complexity of distribution networks, it is crucial to have massive communication connections and sufficient bandwidth to support the real-time sophisticated monitoring and control of critical components in the network. The data to be shared for the distributed voltage regulation in wide-scale distribution networks require that the corresponding communication technology supports high data rate (up to 10Mbps), large coverage distance (up to 10km) and low latency (25 -100ms) [136]. Notably, the fifth generation of mobile networks (5G), as the most advanced cellular wireless communication technology, is built for diverse applications based on the machine-to-machine communication and operations of critical infrastructures, such as smart grid [137]. It can achieve high data transfer rate up to 10Gbps and low latency time of 1ms. The potential communication burden can be dealt with efficiently. In addition, 5G allows massive connections (10 million connections/km^2), which enables the interconnection of huge number of components [138]. Therefore, the wide deployment of mature 5G technology could allow 5G to become a strong candidate to speed up the communication among scattered DERs. Moreover, it could provide a more compatible option to support the expansion of the distributed network which requires sophisticated control and communication in the near future.

4.3 Case Studies

A seven-bus feeder with R/X = 3.11, which is a part of the IEEE-13 bus distribution network, is used as the test network to demonstrate the effectiveness of the proposed voltage regulation scheme on a resistive distribution network. As shown in Fig. 4.5 (left diagram), bus 1, 6 and 7 are the buses with PV installed. Bus 1, 3, 5 and 7 are the buses where EVFs are integrated. All these buses are IBT-enabled which are of the main investigation in the following cases as the voltage of these buses tend to be more fragile due to the integration of PVs. The communication network of IBT-enabled buses is shown in Fig. 4.5 (right diagram). The circle communication topology is used as this topology can simply satisfies N-1 rule, which means there will be no isolated node even if any single communication link is disabled. Hence, if only one link is broken, the information can be still shared among buses via the rest of connected links and the power support can be collectively provided by all EVFs.

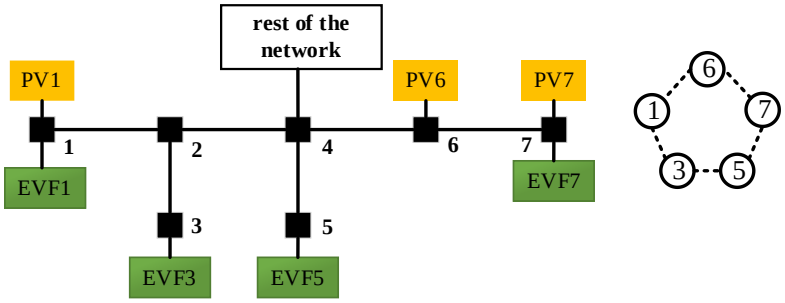

Fig. 4.5. Schematic diagram of test network (left) and its communication topology (right)

4.3.1 Demonstration of Optimal EVF Charging Model

The key capability of the EVF optimal charging model is first examined. To obtain the optimal available charging/discharging power, the proposed MINLP model (4.6) - (4.16) is solved by BARON through YALMIP interface in MATLAB running on an

Intel Core i5 CPU at 3.5GHZ with 16GB RAM computer. BARON is a robust solver which is specifically for global optimization of nonconvex optimization problems. Deterministic global optimization algorithms of the brand-and-bound type are implemented by BARON to guarantee the global optimal solution [28].

The typical peak demand period from 19:00-21:00 is adopted to simulate the undervoltage regulation period. For demonstration purpose, total 80 EVS are classified into 16 groups with different randomly generated SOC_{now} and SOC_{end}, and EV users in the same group has the same discharging pattern, shown in Table 4.1. To avoid deep discharge and to increase battery life, the minimum SOC_{end} is set to 0.3. Each EVF comprises four EV groups and M is the total number of EV users in one EVF. Parameters used for the optimal charging modeling are shown in Table 4.2 and only 3.3 kVA chargers are considered in this case. Each optimal planning timeslot is 15 minutes.

Table 4.1. Initial and target SOC of participating EV users

EVF		SOC_{now}	SOC_{end}	ΔSOC	**EVF**		SOC_{now}	SOC_{end}	ΔSOC
	EV1	0.70	0.56	0.14		EV9	0.72	0.30	0.42
EVF1	EV2	0.64	0.30	0.34	**EVF5**	EV10	0.47	0.36	0.11
M=25	EV3	0.69	0.38	0.31	M=10	EV11	0.59	0.36	0.23
	EV4	0.88	0.68	0.20		EV12	0.69	0.40	0.29
	EV5	0.51	0.30	0.21		EV13	0.44	0.33	0.11
EVF3	EV6	0.63	0.48	0.15	**EVF7**	EV14	0.78	0.36	0.42
M=20	EV7	0.72	0.36	0.36	M=25	EV15	0.53	0.30	0.23
	EV8	0.83	0.64	0.19		EV16	0.47	0.30	0.17

Table 4.2. Parameters of EV optimal charging model

Symbol	**Parameter**	**Value**
a	Daily tariff of EV charging	Taken from reference [29]
b	Battery degradation cost	0.042 $/kWh
η	Charging efficiency	92.5%
S	Charger apparent power	3.3 / 5.5 / 7.0 kVA
E	Battery rated capacity	50 kWh

L_C	Coupling inductor	0.002 H
V_s	System voltage	240 V
f	System frequency	50 Hz

The discharging power and related reactive power of participating EVs in one EVF are coordinately planned considering their individual involvement levels. By comparing four types of EV groups (EV1-EV4), it can be known that EV2 and EV1 can provide the most and least of discharging energy as the difference between their initial and target SOC is the largest and smallest, respectively. Fig. 4.6 shows the involvement level of these four types of EVs in EVF1. It is observed that EV2 and EV1 have the largest and least involvement level respectively, which is consistent with their driving needs demonstrated in Table 4.1.

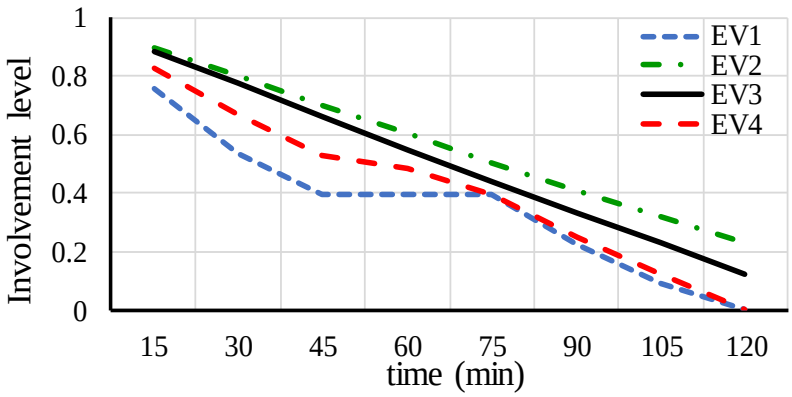

Fig. 4.6. Involvement level of four types of EV in EVF1

To demonstrate the financial benefit for EV users who participate in the scheme, the profit obtained by four different EV users is recorded and illustrated in Table 4.3. Four users are from EV group 1, 2, 3 and 4, respectively (regarded as Table 4.1). The revenue earned by providing power and reactive power as well as the battery degradation cost due to the discharging are taken into account for the net profit for each EV user. Involvement level is a factor that influences the profit earned through the discharging/charging process of the participating EV user. The participant with a

higher involvement level will contribute more to the voltage regulation with the higher charging/discharging rate, which certainly will have a higher payback. The results in Table 4.3 reveal that the profit acquired by each user is gradually decreased in the consecutive timeslots. This is because the EV user indicates higher involvement level in the earlier stage of the entire regulation period. Besides, the results indicate that the EV user 2 from group 2 gains the most profit and then followed by the user from group 3, 4 and 1. This also verifies that the EV user with higher involvement level gets more total profit for the entire regulation period. Such the results are consistent with their involvement levels shown in Fig. 4.6.

Table 4.3. Profit obtained by the individual EV user in the regulation period

	T1	**T2**	**T3**	**T4**	**T5**	**T6**	**T7**	**T8**	**Total profit ($)**
EV 1	0.587	0.579	0.577	0.559	0.502	0.435	0.368	0.297	3.904
EV 2	0.928	0.886	0.724	0.674	0.585	0.536	0.391	0.386	5.110
EV 3	0.787	0.784	0.748	0.705	0.566	0.463	0.453	0.385	4.891
EV 4	0.767	0.764	0.739	0.707	0.564	0.432	0.436	0.336	4.745

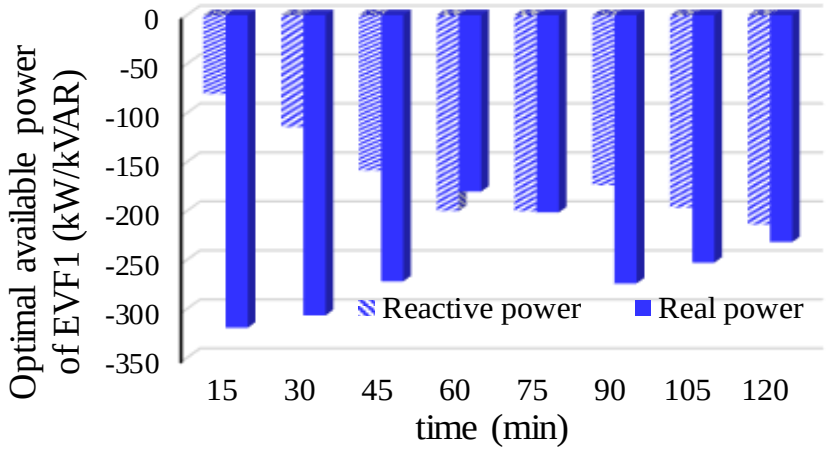

Fig. 4.7. Available power of EVF1 in 2-h regulation period

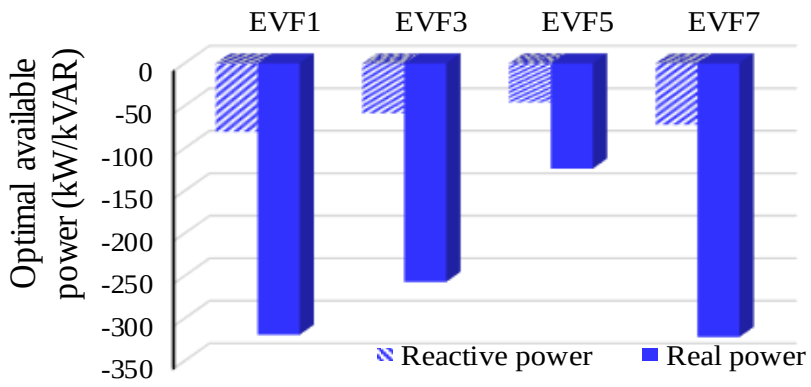

Fig. 4.8. Available power of each EVF in 15-min regulation timeslot

Fig. 4.7 shows the total amount of available power provided by all EVs to achieve the maximal profit from EVF1's point of view during the entire two-hour regulation period. Fig. 4.8 shows the total amount of available power provided by each EVF in the first 15-min regulation timeslot. To be noted, the information regarding the available power of each EVF at every timeslot is only known by EVF itself. The information will be shared among buses via communication network once the parallel-consensus is activated under the requirement.

4.3.2 Demonstration of Regulation Performance without PV

In this case, the period between 19:00-21:00 is still adopted. The impact of PV systems is not considered here as it is usually the low PV generation period. Bus monitor works every 30 seconds to monitor the bus voltage and update the required power. During the first 240s of 19:00-21:00, uncontrollable loads in the network are consecutively increased by 20%, 8% and 6% uniformly at 5s, 60s and 120s. As shown in Fig. 4.9, without any regulation, the voltage of bus 7 drops below the minimum limitation at 60s and drops further when the load is increased again at 120s. The voltage of critical bus 6 stays within the normal range.

Under the regulation, the estimation process is first activated after detecting the voltage deviation signal ΔV at bus 7. The local processor estimates the required power to recover the voltage based on the local instant voltage sensitivity. The control constant gain μ is chosen as 1.35, which ensures a less oscillated and faster response. Fig. 4.10 shows the estimated required power by the processor without the consideration of measurement noise. As the voltage violation occurs at bus 7, it automatically becomes the violated bus with power estimation $S^{req} = [113.1,46.2]$ and [408.9,94.7] to activate parallel consensus sharing. To investigate how the regulation responses to the measurement noise, random noise following normal probability density function with a standard deviation 3σ=3% is applied to the monitor reading value. The green line in Fig. 4.9 demonstrates that the regulation is robust to the measurement noise.

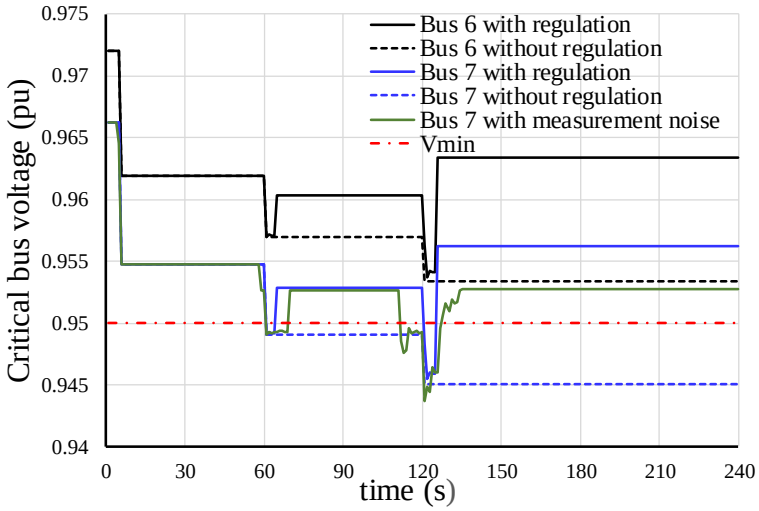

Fig. 4.9. Critical bus voltage with and without regulation

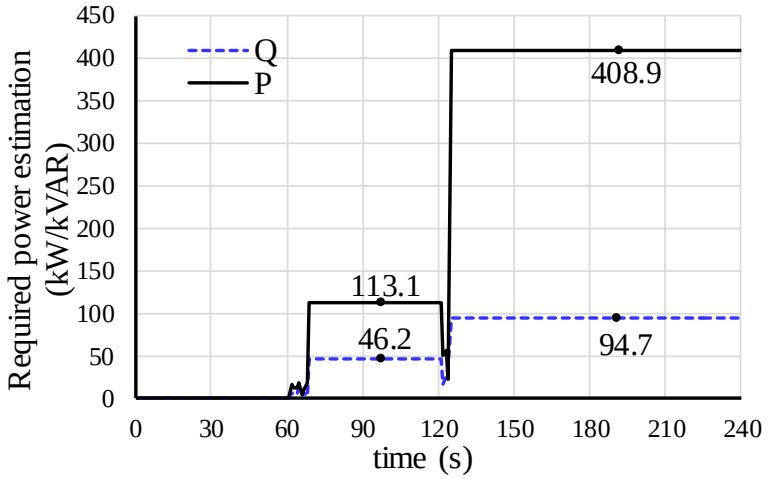

Fig. 4.10. Required power estimation once voltage deviation is detected

Fig. 4.11 illustrates the evolution of averaging consensus algorithm and verify the convergence of the proposed parallel-consensus strategy. For the parallel consensus process-I, initial states of bus 5 and bus 6 are $S^5[0] = S^6[0] = S^{req}/3$ as bus 7 has communication links with these two buses, while initial values for bus 1 and bus 3 are zero. Following (4.28), each bus keeps updating its value until a common steady-state solution is reached. The amount of shared power iteratively converges to the same value, which is approximately equal to [22.6,9.2] and [81.78,18.94] respectively, as shown in Fig. 4.11 (a). This is consistent with the solution $\frac{S^{req}}{n}$ in (4.29).

For the parallel consensus process-II, the information on the amount of available power of each EVF in the first 15-minute timeslot is exchanged within the communication network based on (4.30). The average value of the total available power is achieved within 40 iterations by every bus, as shown in Fig. 4.11 (b). After steady-state solutions in the parallel-consensus processes are acquired, the power allocation ratio and the amount of provided power from each bus can be further determined. Fig. 4.12 shows the amount of dispatched power of each EVF to support

the voltage. It can be seen the supporting power is dispatched based on the allocation ratio, where the bus with larger power capability injects more power. In this case, EVF1 at bus 1 contributes most to the voltage regulation.

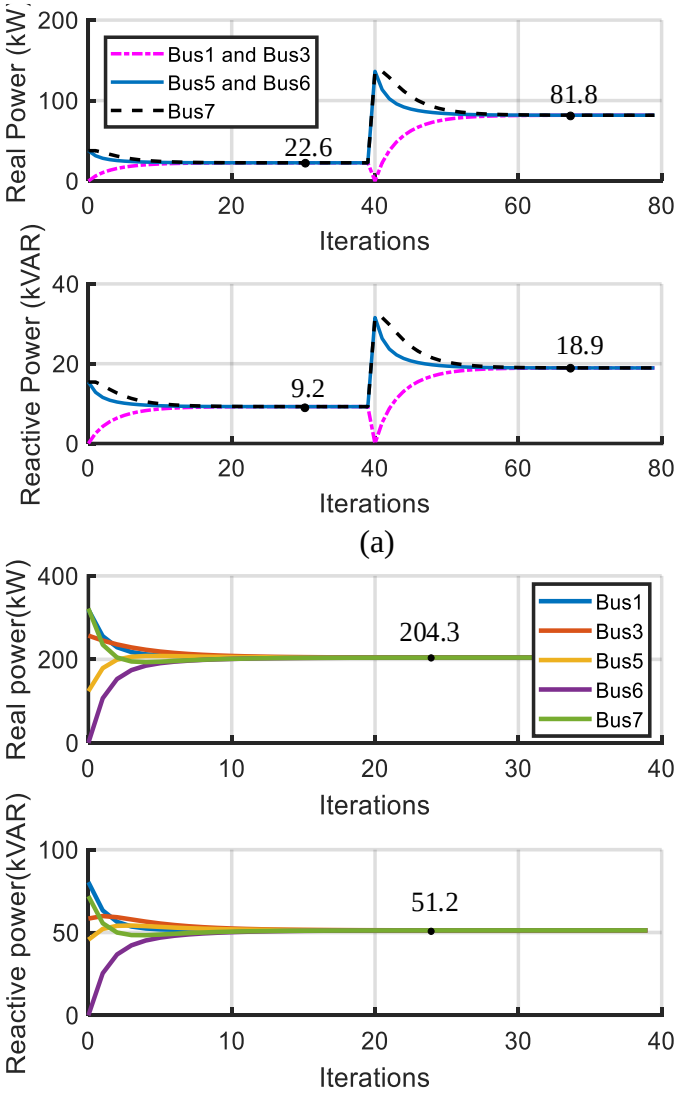

Fig. 4.11. Evolution of the averaging consensus algorithm: (a). Consensus process-I: required real and reactive power sharing among buses. (b). Consensus process-II: available optimal power sharing among buses.

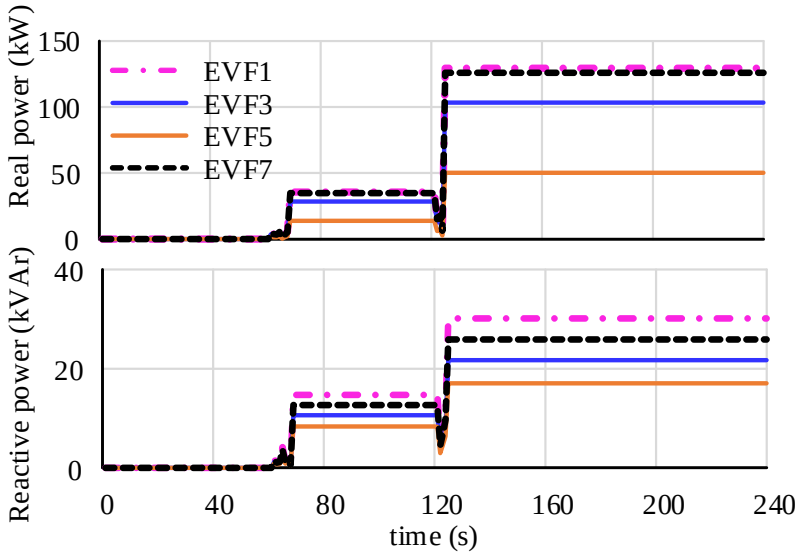

Fig. 4.12. Supporting discharging real and reactive power of each EVF

4.3.3 Demonstration of Regulation Performance under an Emergency Scenario - Inadequate EVs

An emergency scenario is examined where the collective power support from all EVFs cannot successfully regulate the voltage due to insufficient EV resources. As presented previously, the local ESS installed at the critical bus will respond as the back-up support if the voltage cannot be recovered solely through the support from EVFs. In this case, uncontrollable loads in the network are consecutively increased by 26% and 6% uniformly at 60s and 120s. It is assumed that 3/4 EV users quit the regulation scheme at 125s. As shown in Fig. 4.13, the massive leaving causes total available power from EVF reduced by 300kW compared to the original EVF power in Case B. Fig. 4.14 plots the voltage of critical bus 7. It can be seen the voltage drops at 60s and increases to the normal value immediately. However, the voltage regulation is not successful after 120s due to the inadequate EVF power. The local ESS is then

activated at this point and the rest of required power is provided by the ESS to ensure the voltage rises again above the minimum limitation.

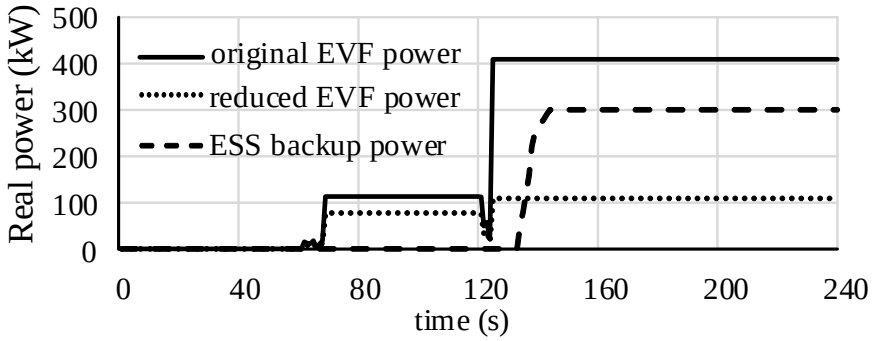

Fig. 4.13. Total available power of EVF and ESS

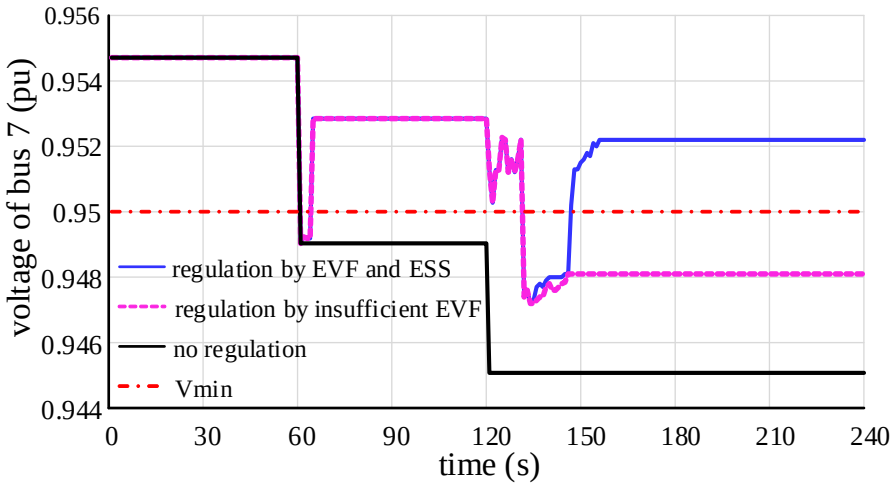

Fig. 4.14. Voltage regulation under the scenario with insufficient EV support

4.3.4 Demonstration of Regulation Performance Under an Emergency Scenario - Communication failure

In this case, an emergency scenario considering a sudden communication failure, i.e., more than one link of the circle communication topology shown in Fig. 4.5 (left) are broken, is examined to show how the regulation performance can be maintained by the back-up support from the local ESS. Fig. 4.15 plots the voltage profile of critical bus 7 in a 40-minute (2400s) regulation period, considering the midday PV power generation. At 1000s, two communication links connecting critical bus 7 are

simultaneously disconnected which causes the isolation of bus 7 from the scheme, and the collective voltage support from other controllable buses (EVFs) no longer respond. It is evident that the voltage violates the maximum constraint again due to the loss of power support from EVFs at around 1100s. The regulation failure is detected by the IBT when information from the neighboring buses cannot be received within 30 seconds of the voltage violation. At this point, the dedicated voltage support by local ESS is activated and the local ESS starts to charge with the power rate estimated by the local processor. The voltage is restored to the normal value at approximately 1300s.

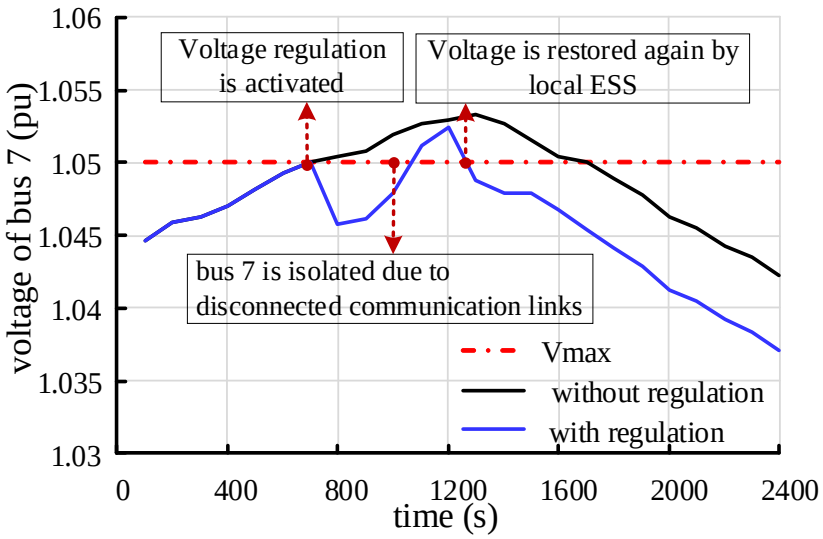

Fig. 4.15. Voltage regulation under the scenario with a sudden communication failure

4.3.5 Demonstration of Regulation Performance Under Different Line Lengths

In the low-voltage distribution network, the changes in the critical bus voltages can be instantly reflected in other buses due to relatively shorter feeder and higher *R/X* ratio. In this regard, the electrical distance is an important factor that impacts the voltage profile. In this case, to verify the effectiveness of the proposed scheme, the regulation performances under different electrical distances between critical buses and their adjacent buses are investigated. The average length *d* of lines 1-2, 2-3, 4-6 and

6-7 is set to 457.2m, 533.4m, 608m and 685.8m, respectively. Other configurations are the same as section 4.3.2. Fig. 4.16 illustrates the voltage profile of bus 7 with and without regulation under various line lengths. It can be seen the voltage is violated at 60s with d = 457.2m while it is violated at 5s under other scenarios with longer line lengths. Once ΔV is detected, the required power is immediately estimated. As shown in Fig. 4.17, more power is required for the voltage recovery in the network with the longer line. The supporting power of each EVF is allocated through parallel-consensus sharing strategy. The voltage deviations can be effectively mitigated by injecting corresponding discharging power from each EVF locally for all scenarios with different line lengths, as shown in the lower diagram in Fig. 4.16.

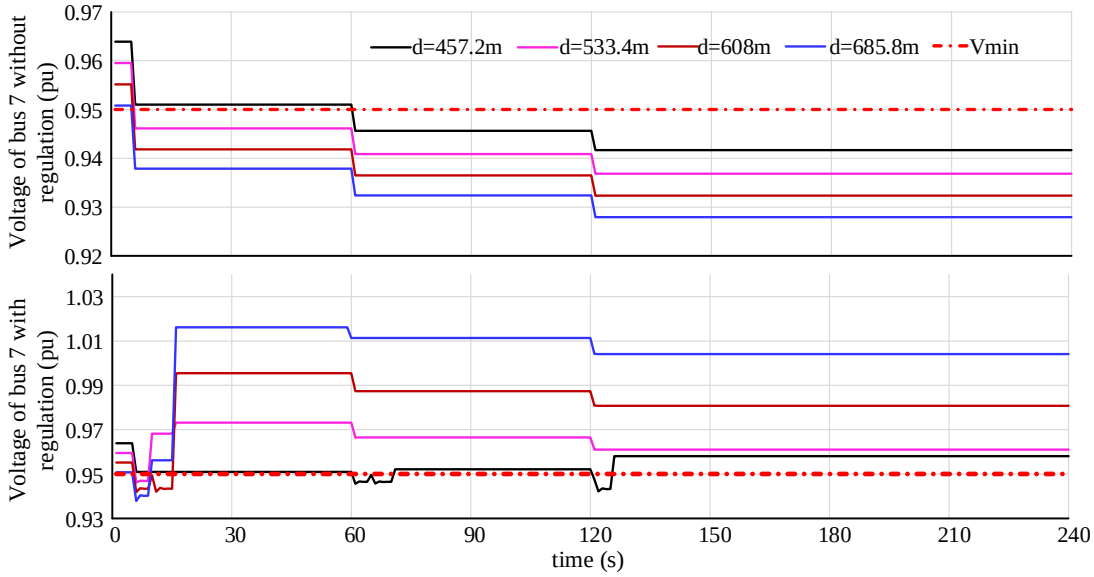

Fig. 4.16. Voltage of bus 7 under different line lengths with/without regulation

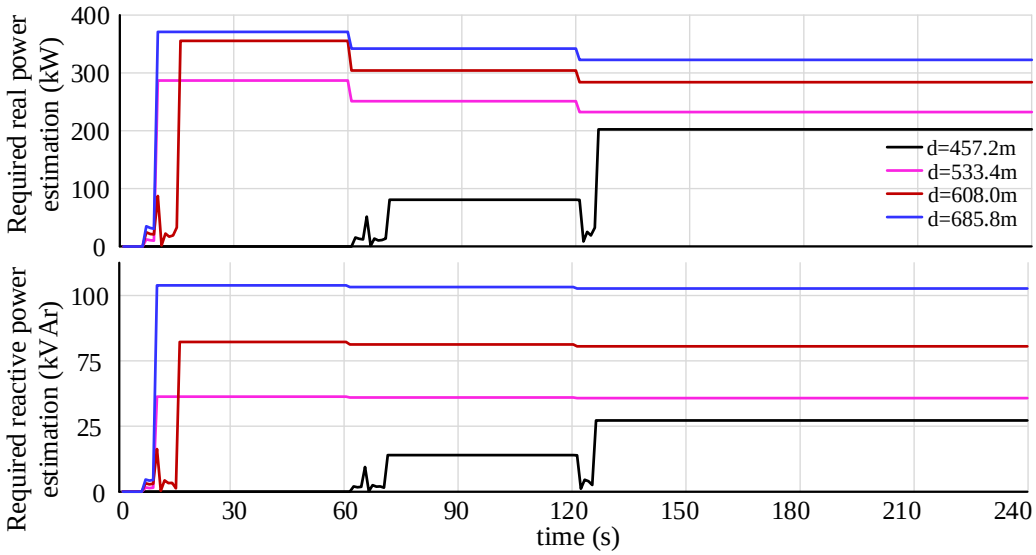

Fig. 4.17. Required real and reactive power estimation for the voltage recovery under different line lengths

4.3.6 Demonstration of Regulation Performance Considering PV Variations and Random Load Changes

To verify the effectiveness of the proposed regulation scheme, random PV variations and different uncontrollable load patterns are considered in this case. Different irradiance profiles are designed for each PV system ($P_{mpp1} = 1.2\text{GW}, P_{mpp6} = 1.3\text{GW}$ and $P_{mpp7} = 1.0\text{GW}$) to model PV output due to the random factors such as cloud cover. Fig. 4.18 shows the profiles of three PV systems during the period of 10:00-14:00 when the PV generation is relatively high. Uncontrollable loads in the network are randomly assigned with two loadshapes, shown in Fig. 4.19, so that loads are increased or decreased by various percentages at different timeslots.

The simulation results are demonstrated in Figs. 4.20 - 4.21. As shown in Fig. 4.20, critical bus 1 and bus 7 both experience voltage rising issue and the proposed regulation scheme can effectively deal with it. Once the voltage is over the maximum limitation at around 10:50, required power absorption for the voltage recovery is

estimated and then shared among EVFs in through parallel-consensus sharing strategy. The available EV users participate into the regulation scheme by charging the cars. Fig. 4.21 shows the amount of power that is absorbed by charging EVs by each EVF for the overvoltage regulation.

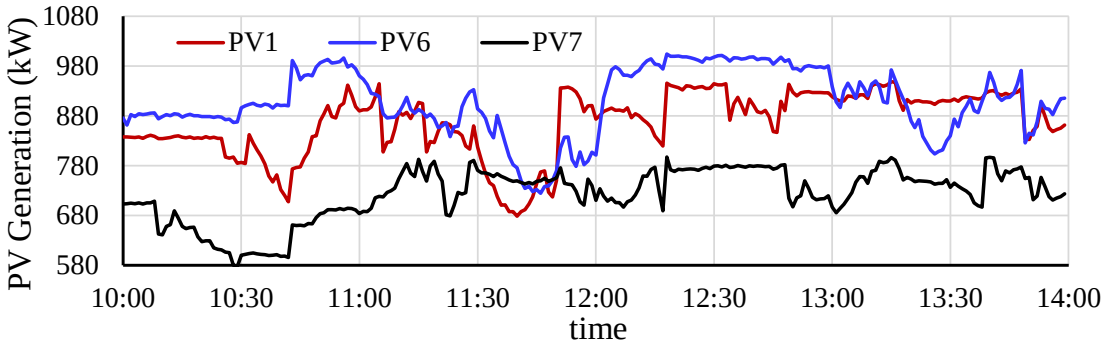

Fig. 4.18. PV generation of three PV systems with different irradiance profiles

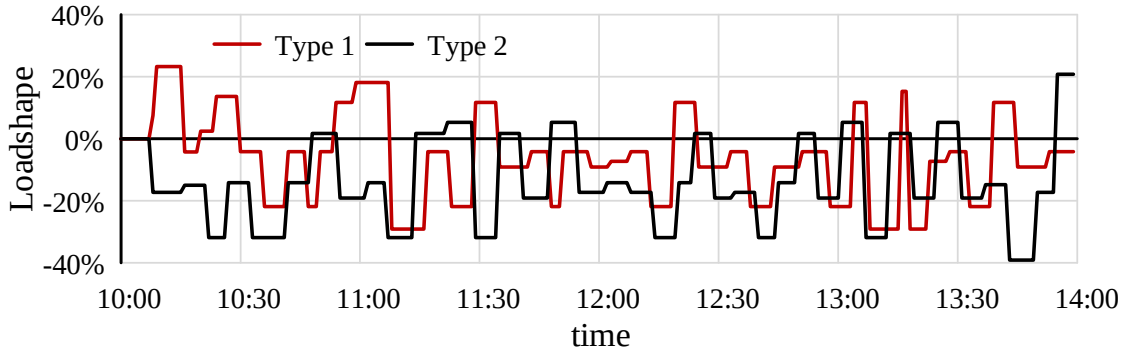

Fig. 4.19. Two types of loadshape assigned to the uncontrollable loads

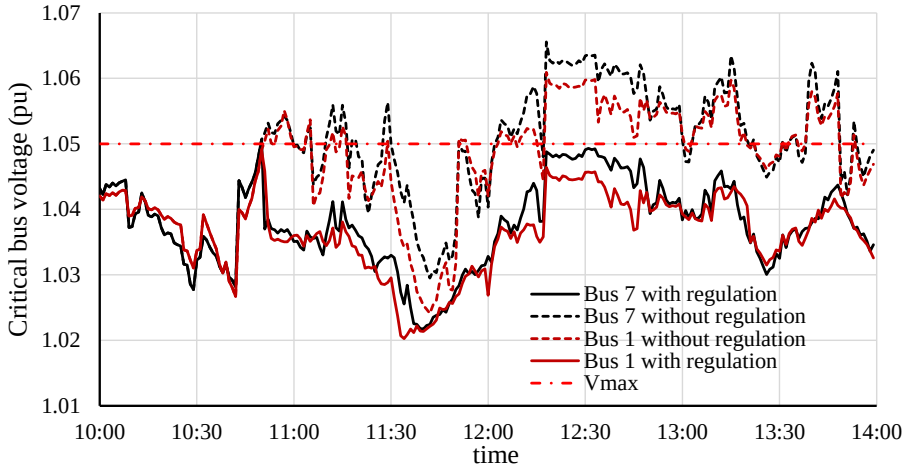

Fig. 4.20. Critical bus voltage with and without regulation

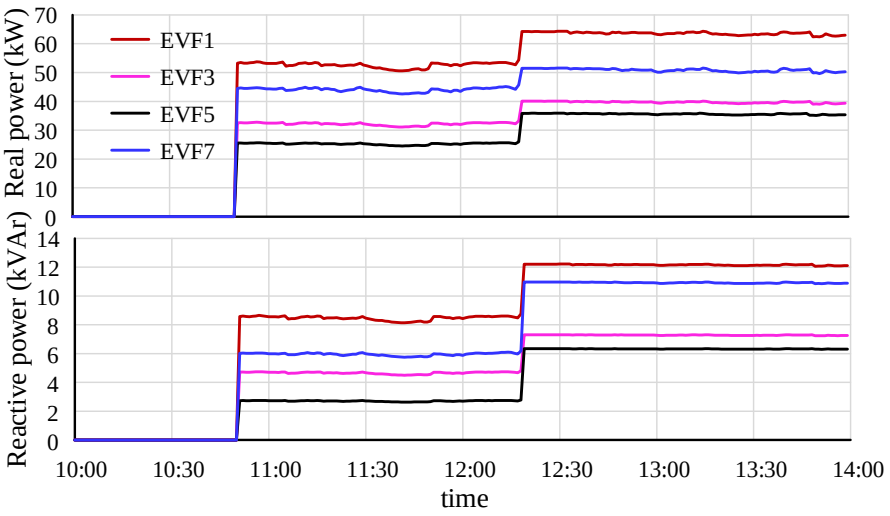

Fig. 4.21. Supporting charging real and reactive power of each EVF

4.3.7 Extension Study on a Larger-scale Network

The proposed regulation strategy is scalable and can be applied to any resistive distribution network. To validate the scalability of the proposed voltage regulation strategy and demonstrate the effectiveness of the proposed strategy on a larger-scale network, IEEE 37 bus distribution system integrated with EV charging points and solar PVs is used. The schematic diagram of the physical network and the communication topology of IBT-enabled buses is shown in Fig. 4.22. The average *R/X* of distribution lines is 1.94. In this case, the total number of participating EVs is expanded to 300, which are distributed at seven charging points in the network, where EVF 3 and EVF 1 has the largest and the least number of EVs. The initial SOC and target SOC for each EV is randomly generated within the range of [0.5, 1] and [0.2, 0.6], respectively. Three power ratings, 3.3 kVA, 5.5 kVA and 7 kVA, are randomly assigned to the smart charger and other parameters used for the optimal charging model are the same as Table 4.2. For this network, the control constant gain μ is chosen as 1.3 based on the trial-and-error method.

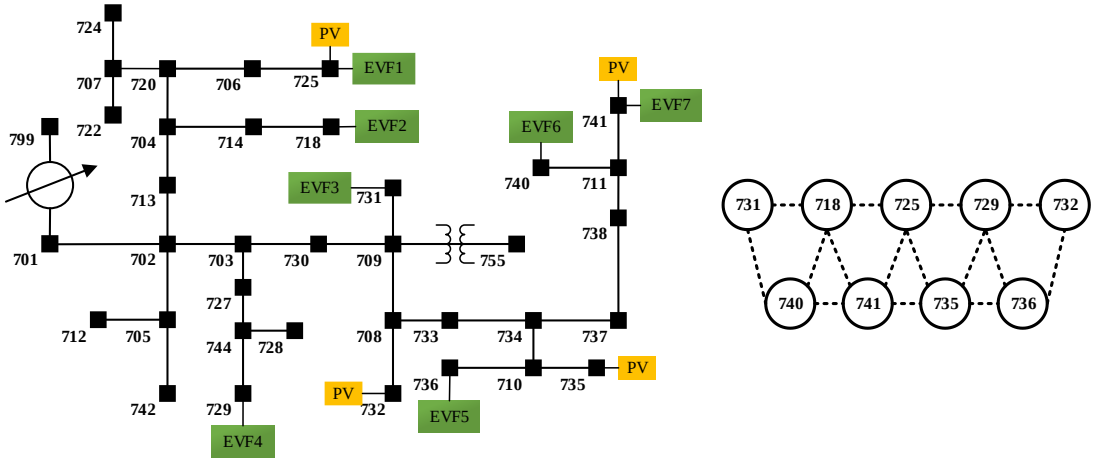

Fig. 4.22. Schematic diagram of IEEE-37 bus distribution network (left) and communication topology (right)

The critical bus voltage in the undervoltage regulation period 19:00-23:00 is plotted in Fig. 4.23, where the voltage violates the minimal limitation at around 20:00 due to the increased peak load demand if there is no regulation action, as shown in the upper diagram. With the collective support from different EVFs, the voltage can be successfully adjusted back to the normal range, shown in the lower diagram in Fig. 4.23. Fig. 4.24 demonstrates the supporting real and reactive power of each EVF. Most EV users discharge at EVF 3 and therefore EVF 3 can provide most power for the voltage regulation. In terms of the solution time, the difference between the simple test network in previous cases and the network applied here is marginal.

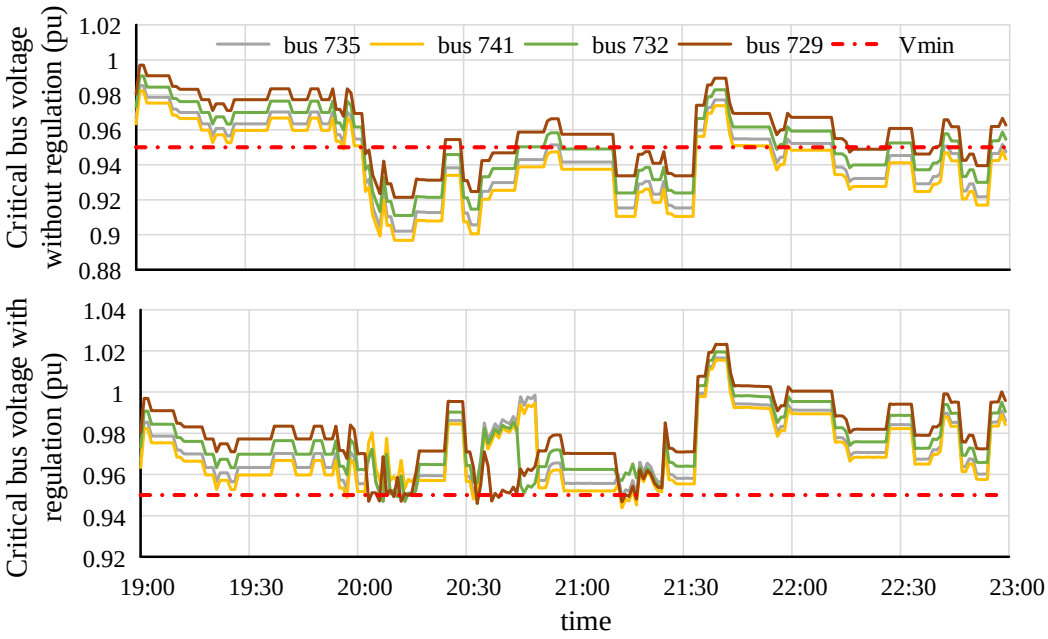

Fig. 4.23. Critical bus voltage with and without regulation

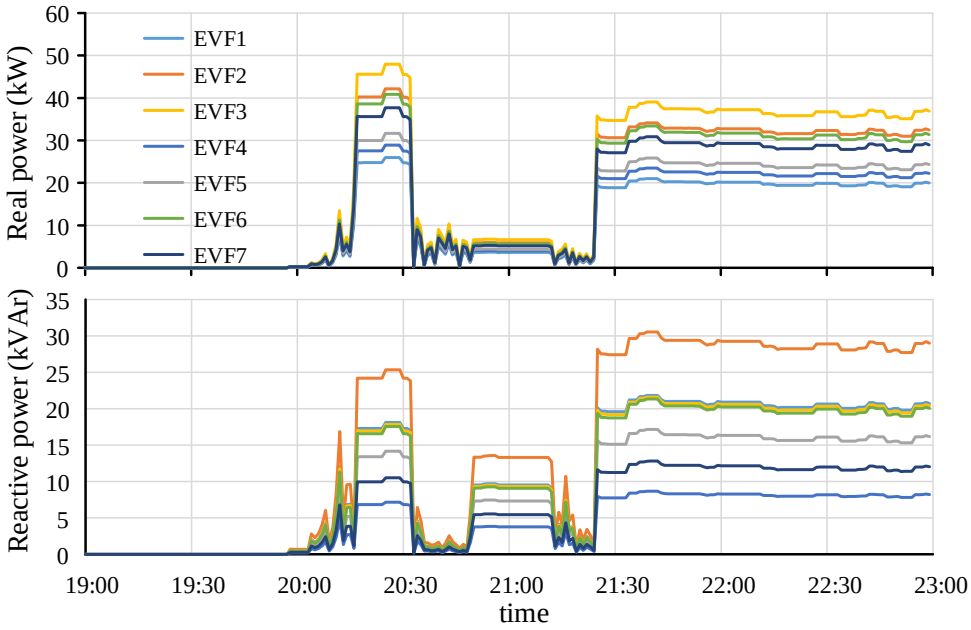

Fig. 4.24. Supporting discharging real and reactive power of each EVF

Moreover, in order to further validate the effectiveness regarding the voltage regulation performance, the proposed regulation scheme is compared with a generic droop-based reactive injection technique mentioned in [30]. The critical bus 741 with the worst voltage profile is chosen as an example to examine. In Fig. 4.25, the voltage

profile is flattened above 0.95 pu under the droop-based regulation, where the local shunt capacitor is utilized to provide the reactive power. By contrast, the voltage regulated by the collective EVF power is higher than the one regulated by the local droop-based technique. Hence, it is revealed that the proposed scheme utilizing both real and reactive power for the voltage support can enhance the regulation performance for the resistive distribution network compared with the regulation technique only with the reactive power compensation.

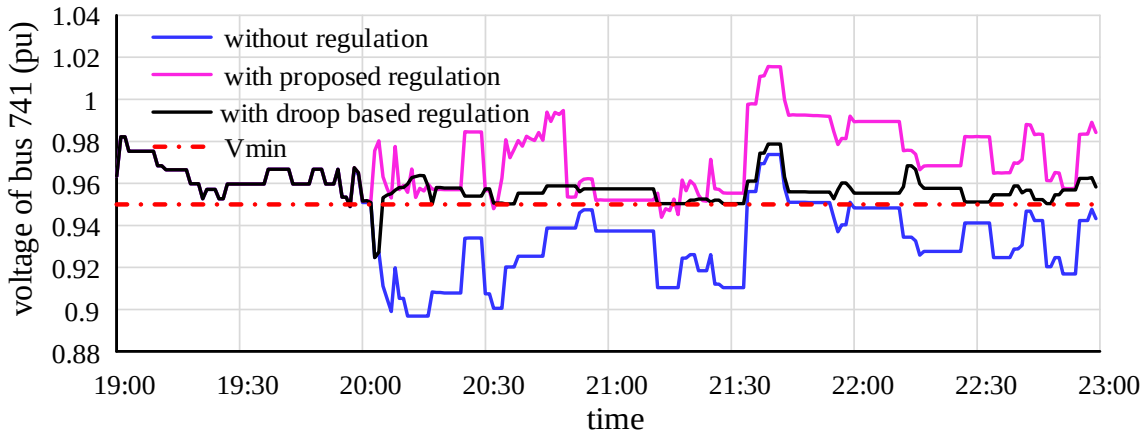

Fig. 4.25. Voltage of bus 741 with and without regulation

4.4 Chapter Summary

Considering the increasing integration of EVs and the capability of EV chargers for both real and reactive power support, a voltage regulation scheme is developed for the resistive distribution network through coordinated EVF charging/discharging process. Due to high *R/X* ratio in the distribution network, the proposed scheme investigates the possibility of utilizing both *P* and *Q* to support the voltage via bi-directional smart chargers with the consideration of financial incentives of participating EV users. The results of case studies have demonstrated that the proposed scheme can achieve the satisfactory voltage regulation performance, whilst

robust to the measurement noise, inadequate EV resources and communication failure. It is expected that the scheme with good scalability could provide more regulation options for different *R/X* ratio scenarios in the future active distribution network, with the existence of a large number of EVs and renewables. Under the incentivized charging coordination, more EV users would be encouraged to participate in the regulation service which could consequently facilitate the transportation electrification.

Chapter 5 Privacy-preserving Distributed Energy Management System for Active Distribution Network under Eavesdropping Attacks

Active distribution network (ADN) as a typically cyber-physical system is vulnerable to cybersecurity threats under the extensive application of information and communication technologies and dominated implementation of distributed operational schemes. In this chapter, the eavesdropping attacks that lead to privacy breaches by stealing power usage and price information are mainly addressed in order to cope with the increasing demand for privacy preservation. A privacy-preserving energy management system (EMS) for ADNs is proposed by incorporating homomorphic cryptosystem techniques and secure exchange protocols are developed to prevent information disclosure against internal or external eavesdropping attacks during the iterative communications when conducting distributed consensus-based EMS algorithms. Two objectives can be realized through two-level homomorphically encrypted EMS: economic coordination among virtual power plants (VPPs) and load customers, cooperative power sharing among distributed generators (DGs) within a VPP. The private information of VPPs and customers, e.g., price information and local power generation/demand, can be effectively protected. The correctness of the final solutions, e.g., optimal market clearing price and unified DG power utilization ratio, can be deterministically guaranteed. The simulation results demonstrate the

effectiveness and the computational efficiency of the proposed homomorphically encrypted EMS.

5.1 Distributed Energy Management System and Its Associated Information Privacy Concerns

In this section, a two-level active distribution network EMS is firstly proposed with two objectives: social welfare maximization and cooperative power sharing. To realize two objectives in a distributed way, distributed consensus-based solutions are then presented. The privacy concerns and potential risks due to the direct data flow between communicating neighbors are discussed.

5.1.1 Two-level EMS for ADN

A group of DGs can be aggregated as a VPP connected to the ADN to provide flexible power generation. Multiple VPPs work cooperatively as power suppliers to quickly respond to changing power demand in the network. To improve social welfare and to achieve efficient cooperative control, a two-level EMS is proposed, involving three types of entities in the network: VPPs and DGs (suppliers) and loads (customers). The economic dispatch of different VPPs, demand response of customers, and the cooperative control of DGs can be realized through the proposed two-level EMS, as illustrated in Fig. 5.1. Dashed lines indicate the information exchange via communication links.

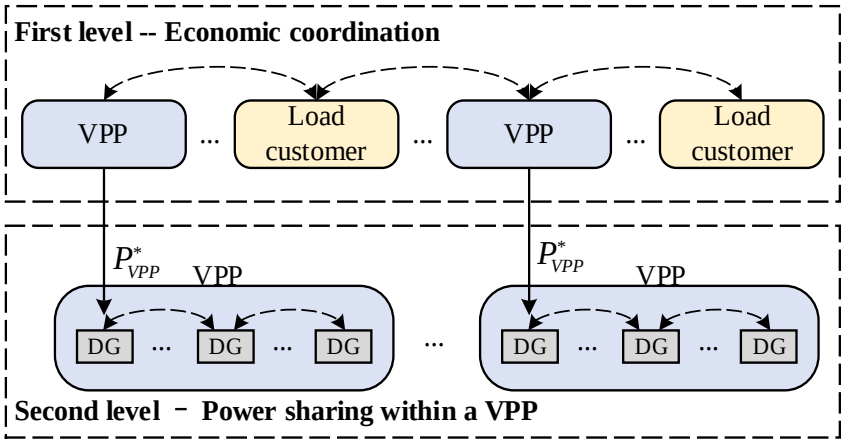

Fig. 5.1. Schematic diagram of the proposed two-level EMS for the ADN

Economic operation of a distribution network should involve active participation of both supply and demand sides in the energy market. In a deregulated energy market, both parties are supposed to be self-interested and have optimal strategies to participate in the market. The self-interested market model describes the essential objectives of suppliers and customers, which are discussed below. Let us consider VPPs belonging to the set $\mathcal{V}_{vpp} = \{1,2,\dots,N_s\}$ and load customers belonging to the set $\mathcal{V}_c = \{1,2,\dots,N_c\}$. The active power loss is incorporated into the market model. For each VPP operator $i \in \mathcal{V}_{vpp}$ and each customer $j \in \mathcal{V}_c$, the energy selling price and bidding price is denoted by $\lambda_{s,i}$ and $\lambda_{b,j}$, respectively, and the objective of the self-interested market model is to maximize VPP profit and customer utility, respectively, formulated as follows:

$$\max_{P_{VPP}} \left(\lambda_{s,i} P_{VPP,i}(1-\gamma_i) - C_i\left(P_{VPP,i}\right)\right) \tag{5.1}$$

$$\max_{P_D} \left(U_j\left(P_{D,j}\right) - \lambda_{b,i} P_{D,j}\left(1+\gamma_j\right)\right) \tag{5.2}$$

where the power generation of the VPP and the power demand of the customer is denoted by $P_{VPP,i}$ and $P_{D,i}$, respectively. γ_i and γ_j are loss coefficients corresponding

to i^{th} VPP and j^{th} customer in the range of [0,1]; $C_i = \frac{1}{2}a_i P_{VPP,i}^2 + b_i P_{VPP,i} + c_i$ is the cost function of the VPP and $U_j = \frac{1}{2}\alpha_j P_{D,j}^2 + \beta_j P_{D,j}$ is the utility function of the customer [111]. The marginal cost function $R_{c,i}$ for i^{th} VPP and the marginal utility function $R_{u,j}$ for j^{th} customer is defined as (5.3) and (5.4), respectively.

$$R_{c,i}(P_{VPP,i}) = \frac{\partial C_i(P_{VPP,i})}{\partial P_{VPP,i}} = a_i P_{VPP,i} + b_i \tag{5.3}$$

$$R_{u,j}(P_{D,j}) = \frac{\partial U_j(P_{D,j})}{\partial P_{D,j}} = \alpha_j P_{D,j} + \beta_j \tag{5.4}$$

In the first level of the EMS, to maximize social welfare and to reduce energy costs from the perspective of the entire ADN, based on (5.1) and (5.2), the economic coordination problem can be formulated as follows:

$$\max\left(\sum_{j\in\mathcal{V}_c} U_j\left(P_{D,j}\right) - \sum_{i\in\mathcal{V}_{vpp}} C_i\left(P_{VPP,i}\right)\right) \tag{5.5}$$

s.t.
$$\sum_{i=1}^{N_s} P_{VPP,i} = \sum_{j=1}^{N_c} P_{D,j} + P_{LOSS} \tag{5.5a}$$

$$P_{VPP,i}^{min} \le P_{VPP,i} \le P_{VPP,i}^{max} \tag{5.5b}$$

$$P_{D,j}^{min} \le P_{D,j} \le P_{D,j}^{max} \tag{5.5c}$$

$P_{VPP,i}^{min}\left(P_{D,j}^{min}\right)$ and $P_{VPP,i}^{max}(P_{D,j}^{max})$ is the lower and upper limit of the VPP generation (load demand), respectively. P_{LOSS} denotes the total active power loss, which can be written as

$$P_{LOSS} = \gamma_i \sum_{i=1}^{N_s} P_{VPP,i} + \gamma_j \sum_{j=1}^{N_c} P_{D,j} \tag{5.6}$$

where $\gamma_i = \frac{\partial P_{LOSS}}{\partial P_{VPP,i}}$ and $\gamma_j = \frac{\partial P_{LOSS}}{\partial P_{D,j}}$ is the incremental loss for i^{th} VPP and j^{th} customer, respectively [139]. Through the self-interested model, each VPP operator

will find an optimal power generation $P^*_{VPP,i}$ such that the marginal cost equals to the energy selling price λ_s. The optimal solution of (5.1) therefore can be found by

$$\lambda_{s,i}(1-\gamma_i) - R_{c,i}(P_{VPP,i}) = 0 \tag{5.7}$$

Similarly, the customer will find the optimal solution $P^*_{D,j}$ of (5.2) by equating the marginal utility to its bidding price:

$$\lambda_{b,i}\big(1+\gamma_j\big) - R_{u,j}(P_{D,j}) = 0 \tag{5.8}$$

Considering constraint (5.5b) and (5.5c), the generation of the VPP and consumption of the customer can be determined based on (5.7) and (5.8), as follows

$$P_{VPP,i} = \begin{cases} P^{min}_{VPP,i}, & \lambda_{s,i} < \frac{R^{min}_{c,i}}{1-\gamma_i} \\ P^{max}_{VPP,i}, & \lambda_{s,i} > \frac{R^{max}_{c,i}}{1-\gamma_i} \\ \frac{\lambda_{s,i}(1-\gamma_i)-b_i}{a_i}, & \text{otherwise} \end{cases} \tag{5.9}$$

$$P_{D,j} = \begin{cases} P^{min}_{D,j}, & \lambda_{b,i} < \frac{R^{min}_{u,j}}{1+\gamma_j} \\ P^{max}_{D,j}, & \lambda_{b,i} > \frac{R^{max}_{u,j}}{1+\gamma_j} \\ \frac{\lambda_{b,i}(1+\gamma_j)-\beta_j}{\alpha_j}, & \text{otherwise} \end{cases} \tag{5.10}$$

where $R^{min}_{c,i}$(or $R^{min}_{u,j}$) and $R^{max}_{c,i}$(or $R^{max}_{u,j}$) is the lower and upper bound of the marginal cost (or utility), respectively. They can be known from (5.3) and (5.4) by giving $P^{min}_{VPP,i}\big(\text{or } P^{min}_{D,j}\big)$ and $P^{max}_{VPP,i}\big(\text{or } P^{max}_{D,j}\big)$. Social welfare is maximized at the equilibrium of the market, i.e., the selling price $\lambda_{s,i}$ and the bidding price $\lambda_{b,j}$ both settle at a unique price denoted by λ^*. This optimum will also result in an identical marginal cost and utility for all participants.

In the second level of the proposed EMS, a cooperative power sharing strategy will be subsequently conducted for all DGs in each VPP once the optimal power generation P_{VPP}^{*} is determined. Consider DGs belonging to the set $\mathcal{V}_{DG} = \{1,2,\dots,N_d\}$. For each DG $m \in \mathcal{V}_{DG}$, the following problem is formulated to satisfy the power generation requirement and meanwhile to ensure accurate power sharing among DGs

$$\min_{P_{DG}} \frac{1}{2}(P^{total} - P_{VPP}^{*})^2 \tag{5.13}$$

s.t.

$$P^{total} = \sum_{m}^{N_d} \delta_m P_{DG,m}^{max} \tag{5.13a}$$

$$0 \le \delta_1 = \cdots = \delta_m = \frac{P_{DG,m}}{P_{DG,m}^{max}} \le 1 \tag{5.13b}$$

$$0 \le P_{DG,m} \le P_{DG,m}^{max} \tag{5.13c}$$

where $P_{DG,m}$ and $P_{DG,m}^{max}$ is the power output and upper power output limit, respectively; $\delta_m \in [0,1]$ is defined as the power utilization ratio.

5.1.2 Preliminaries on Communication Graph

A graph $\mathcal{G} = (\mathcal{V}, \mathcal{E})$ is used to capture the communication network consisting of multiple nodes belonging to the set $\mathcal{V} = \{\mathcal{V}_1, \dots, \mathcal{V}_N\}$. A finite edge set $\mathcal{E} = \{(p,q)\} \in \mathcal{V} \times \mathcal{V}$ consists of the communication links where node $\mathcal{V}_q$ can receive the information from node $\mathcal{V}_p$. For any node $\mathcal{V}_p \in \mathcal{G}$, the nodes that can directly receive information from it are defined as its out-neighbors, denoted by $N_p^{\text{out}} = \{\mathcal{V}_q | (p,q) \in \mathcal{E}\}$. The cardinality of N_p^{out} is called the out-degree and denoted by $\mathcal{D}_p^{\text{out}}$. The nodes that can directly send information to node $\mathcal{V}_p \in \mathcal{G}$ are defined as its in-neighbors, denoted by $N_p^{\text{in}} = \{\mathcal{V}_q | (p,q) \in \mathcal{E}\}$. The cardinality of N_p^{in} is called the in-degree and denoted by $\mathcal{D}_p^{\text{in}}$. The graph is strongly connected if there exists a directed path for any pair of

nodes $\mathcal{V}_p$ and $\mathcal{V}_q$, $p \neq q$. Note that $\mathcal{D}_p^{\text{in}} \neq 0$ and $\mathcal{D}_q^{\text{out}} \neq 0$ in a strongly connected graph.

5.1.3 Consensus-based Distributed Solutions for the EMS

In the first level of the EMS, a strongly connected graph $\mathcal{G}_{ADN} = (\mathcal{V}_{ADN}, \mathcal{E}_{ADN})$ is introduced to describe the communication network of the ADN and $\mathcal{V}_{ADN} = \{\mathcal{V}_{vpp} \cup \mathcal{V}_c\}$. For any $i, j \in \mathcal{V}_{ADN}$, the associated weighting factors for the communication link between a pair of communicating neighbors are defined as follows [110]

$$\phi_{ij} = \begin{cases} \frac{1}{\mathcal{D}_i^{\text{in}}}, \text{if } j \in N_i^{in} \\ 0, \text{otherwise} \end{cases} \tag{5.14a}$$

$$\omega_{ij} = \begin{cases} \frac{1}{\mathcal{D}_j^{\text{out}}}, \text{if } i \in N_j^{out} \\ 0, \text{otherwise} \end{cases} \tag{5.14b}$$

Notice that i and j represent here either a VPP or a load customer. An operator $[]_-$ is used to define the mathematical operation as follows:

$$[a]_- = \begin{cases} a, a \geq 0 \\ 0, a < 0 \end{cases} \tag{5.15}$$

Based on the weighting factor, the economic coordination for the VPPs and load customers in the first level of the proposed EMS is solved by a consensus-based distributed algorithm, formulated as follows:

$$\lambda_i(k+1) = \lambda_i(k) + \left[\sum_{j \in N_i^+} \phi_{ij} \left(\lambda_j(k) - \lambda_i(k)\right)\right]_- + \sigma y_i(k) \tag{5.16a}$$

$$y_i(k+1) = \sum_{j \in N_i^+} \omega_{ij} y_j(k) - \left(P_i(k+1) - P_i(k)\right) \tag{5.16b}$$

where $\lambda_i(k) = [\lambda_{s,i}(k), \lambda_{b,i}(k)]^T$ is a compact set of the energy selling price and energy bidding price for the VPP and the load customer. By introducing (5.15),

$\sum_{j\in N_i^+}\phi_{ij}(k)\left(\lambda_j(k)-\lambda_i(k)\right)$ in (5.16a) is guaranteed to be nonnegative, which ensures the convergence. $y_i(k)$ is the local estimation of the power imbalance, which is the feedback item driving $\lambda_i(k)$ to the optimal value. $P_i(k)$ is updated by (5.9) if $i \in \mathcal{V}_{vpp}$ and by (5.10) if $i \in \mathcal{V}_c$ at every step *k*.

From (5.14), it is not difficult to find that $\sum_{j\in N_i^{\text{in}}}\phi_{ij}=1$ and $\sum_{i\in N_j^{\text{out}}}\omega_{ij}=1$, which is the sufficient condition for convergence. And the following theorem holds.

Theorem 1[140]: Considering the algorithm (16) with the weighting factors in (5.14), the algorithm achieves an optimal global solution $\lim_{k\to\infty}\lambda_i(k)=\lambda^*$ and $\lim_{k\to\infty}y_i(k)=0$, provided that the communication graph is strongly connected and there exists a sufficiently small gain σ.

In the second level of the EMS, a strongly connected graph $\mathcal{G}_{DG}=(\mathcal{V}_{DG},\mathcal{E}_{DG})$ is adopted to describe the communication network for a single VPP consisting of multiple DGs. For any $m,n\in\mathcal{V}_{DG}$, the weighted adjacency matrix D can be defined as

$$[D]_{mn}=\begin{cases} d_{mn}, \text{ if } n\in N_m^{in} \text{ and } m\neq n \\ 1-\sum_{n\in N_m^{\text{in}}} d_{mn}, \text{ if } m=n \\ 0, \text{ otherwise} \end{cases} \tag{5.17}$$

Obviously, D is a row-stochastic matrix, i.e., $\sum_{n\in N_m^{\text{in}}}d_{mn}=1$. All entries should be positive and satisfy $\varepsilon\le d_{mn}\le 1$ for all $n\in N_m^{\text{in}}$, where $0<\varepsilon\le\min_m\left\{\frac{1}{D_m^{in}}\right\}$. A leader-follower consensus algorithm is used to solve the self-organizing power sharing problem (5.13) in the VPP. Without loss of generality, DG1 is assigned as the leader that has access to the reference P_{VPP}^* as well as a global variable P^{total}. Denote

t as the iteration step of the second-level cooperative control in the EMS. The utilization ratio of leader DG is updated by

$$\delta_1(t+1) = \delta_1(k) + \rho(P^*_{VPP} - P^{total}(t)) \tag{5.18a}$$

where $\rho > 0$ is the control gain. To achieve a unified power utilization ratio for each DG in the VPP, the utilization ratio of the follower DG, is updated by

$$\delta_m(t+1) = \sum_{n \in N_m^{\text{in}}} d_{mn}\delta_n(t)\,,\ m,n \neq 1 \tag{5.18b}$$

The convergence of the cooperative power sharing problem is guaranteed with a sufficiently small gain ρ, as stated in the following theorem.

Theorem 2[141]: The cooperative control (5.13) solved by the leader-follower consensus (5.18) guarantees that all DGs asymptotically converge to the optimal solution, $\lim_{t\to\infty} \delta_m(t) = \delta^*$ and $\lim_{t\to\infty} P^{total}(t) = P^*_{VPP}$, provided that the communication graph is strongly connected and there exists a sufficiently small gain ρ.

The solution of (5.5) and (5.13) in a privacy-preserving manner and against eavesdropping attacks is our main focus, so that detailed convergence analysis is not provided here.

5.1.4 Privacy Concerns and Risks

As the ADN is a typical multi-agent CPS, significant concerns are raised that the privacy of individual participants can be leaked during the information sharing in the EMS under eavesdropping attacks. Note that the eavesdropping attack can be launched not only by an extraneous observer but also a corrupted entity in the cyber

network. Curious and adversarial attackers can collect private data or sensitive information for illegal purposes.

In particular, the consensus-based distributed algorithms discussed above relying on the information exchange among different entities through iterative communications will pose the risk of unintentional information disclosure. In the first level of the EMS, the initial price $\lambda_i(0)$ and the initial load demand/power supply $y_i(0)$ is regarded as the privacy of the participating VPP and customer. It cannot be revealed to others during the distributed decision-making process in the communication network. In fact, it is crucial to keep participants' parameters (e.g., coefficients of the cost/utility function) private to unauthorized parties by protecting the information of initial bidding/selling price and the power demand/supply. Besides, load demand and power supply should be maintained at a high-security level as the exposure of such information may reveal much about the personal preference of the load customer and the business secret of the VPP [99]. Therefore, necessary measures for privacy preservation should be taken in the EMS to prevent the curious entity from gathering the personal information of others during the information exchange.

5.2 Preliminaries on Homomorphic Cryptosystem

The homomorphic cryptosystem, as one of the cryptographic techniques, empowers a distinguished feature to maintain data confidentiality during both information transmission and processing. In particular, the homomorphic Paillier cryptosystem permits agents to perform computations on encrypted data without first decrypting it. Compared with the method of differential privacy, the correctness of the results and the privacy of agents can be both ensured by applying a homomorphic cryptosystem.

Such functionalities make it a suitable candidate to be implemented in the distributed EMS to prevent agents' private information from being eavesdropped.

A homomorphic cryptosystem typically comprises three main functions to prevent data leakage during the entire process of data transmission and processing: a) key generation *K*, b) data encryption *E*, and c) data decryption *D*. A public key Key^{pub} and a private key Key^{pri} are generated through the key generation process. Based on the public key, an original message α can be turned into a ciphertext β by encryption function *E*. Oppositely, the ciphertext β can be decrypted by decryption function *D* to the original message α based on the private key. It should be noted that the public key generated by an agent can be shared with others for encryption, but its private key should be kept secret. In other words, any agent can use the same public key to encrypt original messages to cipher ones while only the trustworthy entity with the corresponding private key can decrypt the ciphertext.

The Paillier cryptosystem, as one of popular homomorphic cryptosystems, is implemented to this work. It enables certain types of data processing without necessarily having direct access to them. The functions of the Paillier cryptosystem are introduced below to facilitate development of the proposed homomorphically encrypted EMS in the next section.

Notations. Denote the set of positive real numbers in the format of floating-point and integer as $\mathbb{R}_F$ and $\mathbb{R}_I$, respectively. $gcd\,(a,b)$ and $lcm\,(a,b)$ denotes the greatest common divisor and the least common multiple of integers a and b, respectively; mod denotes the modular operation; $\lfloor a \rfloor$ denotes the floor of a real number a, i.e., largest integer smaller or equal to a.

Key generation: Randomly select two large prime numbers *c* and *v* and calculate $h = cv$ and $\varphi = lcm(c-1, v-1)$; A random integer g is chosen such that $gcd\ (Z\ (g^{\varphi} \bmod h^2), h) = 1$, where $Z(t) = \left\lfloor \frac{t-1}{h} \right\rfloor$. The public key is denoted $Key^{pub}\ (g, h)$ and the private key is $Key^{pri}\ (\varphi)$.

Encryption: A natural integer number $\alpha \in \mathbb{R}_I$ can be encrypted using the public key

$$E(\alpha) = g^{\alpha} r^{h} \bmod h^2 \tag{5.19}$$

where $r \in \mathbb{R}_I$ is a random positive integer.

Decryption: The ciphertext βcan be decrypted using the private key

$$D(\beta) = \frac{Z(\beta^{\varphi} \bmod h^2)}{Z(g^{\varphi} \bmod h^2)} \bmod h \tag{5.20}$$

The correctness, semantic security, and homomorphic property of the Paillier cryptosystem are demonstrated as follows [142]:

1) Correctness: For any nonnegative integer $\alpha \in \mathbb{R}_I$, the following holds

$$D\big(E(\alpha)\big) = \alpha \tag{5.21}$$

2) Semantic security: If the decisional composite residuosity assumption (DCRA[1]) holds, then the Paillier cryptosystem is semantically secure.

3) Homomorphic properties: Define any $\alpha_1, \ldots, \alpha_n \in \mathbb{R}_I$, then

a. Additively homomorphic property:

$$D(\prod_{i=1}^{n} E(\alpha_i)) = \sum_{i=1}^{n} \alpha_i \tag{5.22}$$

b. Multiplicatively semi-homomorphic property:

DCRA[1]: Given a composite *C* and an integer *z*, it is computationally intractable to decide whether *z* is a C-residue modulo C^2 or not, i.e., whether there exists *y* such that $z = y^C \bmod C^2$. It is widely believed that the DCRA is true.

$$D(E(\alpha_1)^{\alpha_2}) = \alpha_1\alpha_2 \tag{5.23}$$

The homomorphic properties allow in-network algebraic operations on encrypted values without the need for decryption, which is vital for developing the proposed homomorphically encrypted EMS in the next section.

5.3 Homomorphically Encrypted EMS Based on Secure Exchange Protocols

This section presents a detailed design and practical deployment for the privacy-preserving EMS. The Paillier cryptosystem is implemented to construct the secure information exchange protocol to maintain confidentiality for each participant during the information exchange. It is fully distributed and without adding noise to the state variables. The proposed protocol can prevent the information leakage to the eavesdropping attacker while achieving the deterministic convergence to the optimal solution of (5.16) and (5.18). The objective of the secure exchange protocol is twofold:

- Privacy preservation: For each participant (can be either VPP $i \in \mathcal{V}_{vpp}$ or a load customer $i \in \mathcal{V}_c$ or a DG $m \in \mathcal{V}_c$), its information $\lambda_i(k)$, $y_i(k)$ and $\delta_m(t)$ cannot be inferred by any semi-honest eavesdropping attacker in each iteration during data exchange.
- Correctness: In the first level of EMS, when $k \to \infty$, the energy selling price $\lambda_{s,i}(k)$ and energy bidding price $\lambda_{b,i}(k)$ can settle at an optimal solution λ^* for each VPP and load customer. In the second level of EMS, when $t \to \infty$, the power utilization ratio $\delta_m(t)$ can converge to a unified ratio for each DG.

In the following design and analysis, the semi-honest eavesdropping attacks are considered, i.e., any adversary follows the proposed algorithm correctly but attempts to use its received information to infer private data of other entities.

5.3.1 Random Weight Reconstruction

As shown in (5.16), a participant i needs information of the weighted difference $\phi_{ij}\left(\lambda_j(k)-\lambda_i(k)\right)$ for the local update. To ensure that any participant obtains the weighted difference between itself and any of its neighbors without revealing each other's information, the state information can be encrypted and broadcast to neighbors at every iteration step. However, without a third party secretly distributing ϕ_{ij}, the privacy of both interacting participants cannot be protected even with the state encryption. For example, participant j's state $\lambda_j(k)$ can be still inferred through $\lambda_j(k)=\frac{\phi_{ij}\left(\lambda_j(k)-\lambda_i(k)\right)}{\phi_{ij}}+\lambda_i(k)$ by its communicating neighbor i as the weight ϕ_{ij} is constant and available to participant i. To address this issue, a random weight construction method [107] is extended to the homomorphically encrypted EMS, preventing a pair of communicating participants from inferring each other's states through the information exchange. The weight can be represented by the product of two random numbers as follows:

$$\phi_{ij}=\phi_{i\to j}\phi_{j\to i} \tag{5.24a}$$

$$\omega_{ij}=\omega_{i\to j}\omega_{j\to i} \tag{5.24b}$$

where $\phi_{i\to j}(\omega_{i\to j})$ is the random weight generated by and only known to participant i and $\phi_{j\to i}(\omega_{j\to i})$ is the random weight generated by and only known to participant j. As defined in [143], the random weight $\phi_{i\to j}(\phi_{j\to i})$ and $\omega_{i\to j}(\omega_{j\to i})$ should be selected in the feasible range of $\left[\epsilon_1, \frac{1}{\mathcal{D}_i^{\text{in}}} - \epsilon_2\right]$ and $\left[\epsilon_1, \frac{1}{\mathcal{D}_j^{\text{out}}} - \epsilon_2\right]$, respectively, where ϵ_1 and ϵ_2 are positive numbers that satisfy $\epsilon_1 + \epsilon_2 < 1/\max_i\{D_i^{in}\}$. Similarly, for the weight (17), one can have

$$d_{mn} = d_{m\to n} d_{n\to m} \tag{5.24c}$$

The random weight should be selected in the feasible range of $[\underline{d}, \bar{d}]$ and according to [107], to ensure the convergence, the feasible range must satisfy $0 < \underline{d} < \bar{d} < 1/\sqrt{\rho \max_m\{D_m^{in}\}}$.

5.3.2 Transformation between Floating Numbers and Integers

The Paillier cryptosystem relying on certain modular operations only works for integers. However, the state values of electrical variables are primarily in the form of floating-point numbers [144]. Thus, the transformation between the floating-point number and the integer is necessary before the encryption. According to floating-point arithmetic, a floating-point number $x_F \in \mathbb{R}_F$ can be simply transformed to an integer $x_I \in \mathbb{R}_I$ by $x_I = 10^{\tau} x_F$, where τ denotes the preserved decimal fraction digits. After the decryption, the following functions can be applied to convert an integer x_I to a signed real number x_F with τ decimal fraction digits, where $\mu \in \mathbb{R}_I$ is a positive odd integer [98]:

$$x_F = \begin{cases} x_I/10^{\tau}, & if\ 0 \le x_I \le \frac{\mu-1}{2} \\ (x_I - \mu)/10^{\tau}, & if\ \frac{\mu+1}{2} \le x_I < \mu \end{cases} \tag{5.25}$$

5.3.3 Secure Exchange Protocols

Next, without loss of generality, a pair of communicating participants $(\mathcal{V}_1, \mathcal{V}_2)$ is used to illustrate the design process of the secure exchange protocol for the first level of EMS, shown in Fig. 5.2. Solid arrows imply the computation flow and dashed arrows imply the information exchange in the communication link. $\mathcal{V}_1$ and $\mathcal{V}_2$ can represent either the VPP or load customer. The subscript k is omitted next for the sake of clear demonstration. The step-by-step details of Fig. 5.2 are explained next. Note that the operation at k^{th} iteration is described.

Pre-processing: Key generation

Before conducting the privacy-preserving interaction protocol, $\mathcal{V}_1(\mathcal{V}_2)$ generates a public key $Key_1^{pub}(Key_2^{pub})$ and a private key $Key_1^{pri}(Key_2^{pri})$.

Step 1: Initialization

Integer transformation: state variables of $\mathcal{V}_1$ and $\mathcal{V}_2$ are transformed to integers by multiplying 10^{τ}, denoted by $\lambda_1^I, \lambda_2^I, y_1^I, y_2^I \in \mathbb{R}_I$, where τ is preserved decimal fraction digits.

Random weight selection: $\mathcal{V}_1$ randomly selects weight $\phi_{1\to2}$ and $\omega_{1\to2}$; $\mathcal{V}_2$ randomly selects weight $\phi_{2\to1}$and $\omega_{2\to1}$;

Step 2: Encryption using own public key

$\mathcal{V}_1$ uses public key Key_1^{pub} to encrypt $-\lambda_1^I$ to $E_1(-\lambda_1^I)$; $\mathcal{V}_2$ uses public key Key_2^{pub} to encrypt $-\lambda_2^I$ to $E_1(-\lambda_2^I)$.

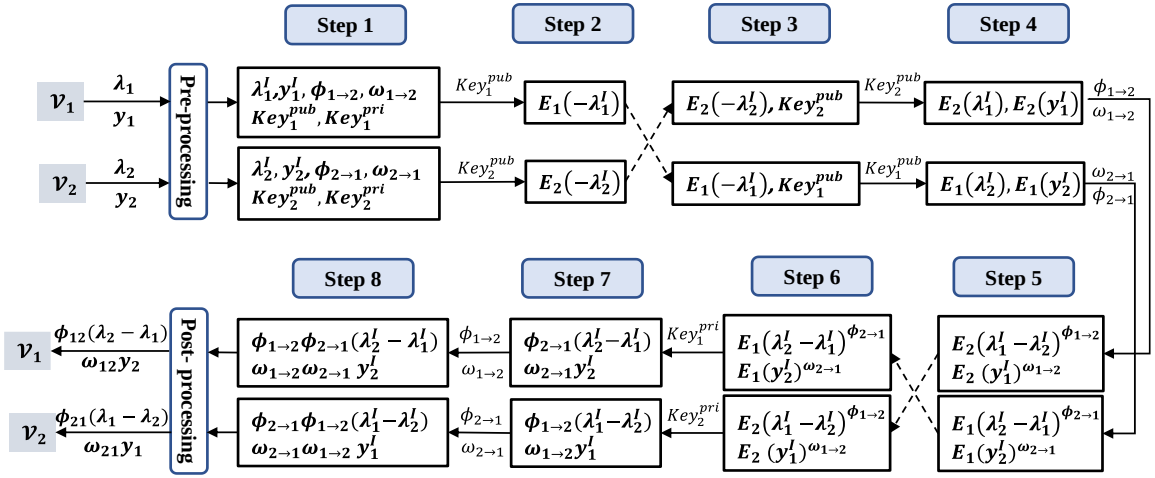

Fig. 5.2. Illustration of the secure exchange protocol based on the homomorphic Paillier cryptosystem for the first level of the EMS.

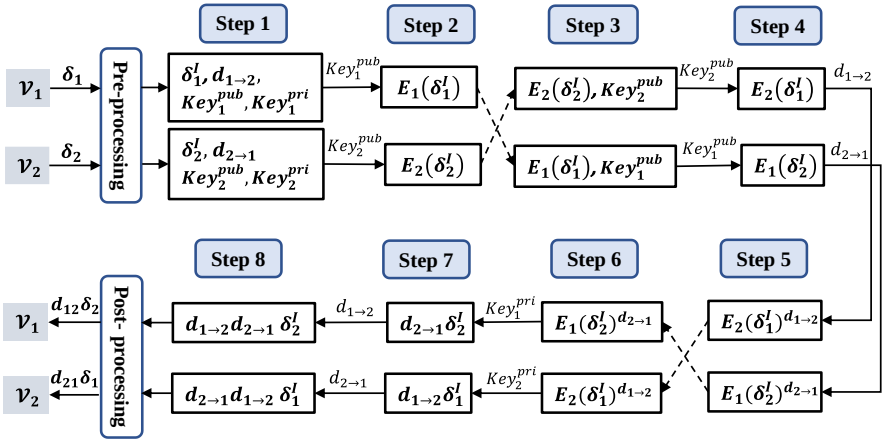

Fig. 5.3. Illustration of the secure exchange protocol based on the homomorphic Paillier cryptosystem for the second level of the EMS.

Step 3: Transmission of encrypted states and public key

$\mathcal{V}_1$ sends $E_1(-\lambda_1^I)$ and Key_1^{pub} to $\mathcal{V}_2$; $\mathcal{V}_2$ sends $E_2(-\lambda_2^I)$ and Key_2^{pub} to $\mathcal{V}_1$ (private keys are kept as secret on their own and do not share with others).

Step 4: Encryption using neighbor's public key

$\mathcal{V}_1$ uses public key Key_2^{pub} to encrypt λ_1^I and y_1^I to $E_2(\lambda_1^I)$ and $E_2(y_1^I)$, respectively; $\mathcal{V}_2$ uses public key Key_1^{pub} to encrypt λ_2^I and y_2^I to $E_1(\lambda_2^I)$ and $E_1(y_2^I)$, respectively.

Step 5: Computation on encrypted states

According to additively homomorphic property (22) and multiplicatively semi-homomorphic property (23), $\mathcal{V}_1$ computes the encrypted difference as$E_2(\lambda_1^I-\lambda_2^I) = E_2(\lambda_1^I)E_2(-\lambda_2^I)$, then multiplying the weight to acquire $E_2(\lambda_1^I-\lambda_2^I)^{\phi_{1\to2}}$ and $E_2(y_1^I)^{\omega_{1\to2}}$.Similarly, $E_1(\lambda_2^I-\lambda_1^I)^{\phi_{2\to1}}$ and $E_1(y_2^I)^{\omega_{2\to1}}$ are acquired by $\mathcal{V}_2$.

Step 6: Transmission of processed encrypted results

$\mathcal{V}_1$ returns $E_2(\lambda_1^I-\lambda_2^I)^{\phi_{1\to2}}$ and $E_2(y_1^I)^{\omega_{1\to2}}$ to $\mathcal{V}_2$; $\mathcal{V}_2$ returns $E_1(\lambda_2^I-\lambda_1^I)^{\phi_{2\to1}}$ and $E_1(y_2^I)^{\omega_{2\to1}}$ to $\mathcal{V}_1$;

Step 7: Decryption using own private key

$\mathcal{V}_1$ uses private key Key_1^{pri} to decrypt $D\left(E_1(\lambda_2^I-\lambda_1^I)^{\phi_{2\to1}}\right) = \phi_{2\to1}(\lambda_2^I-\lambda_1^I)$ and $D(E_1(y_2^I)^{\omega_{2\to1}}) = \omega_{2\to1}y_2^I$; $\mathcal{V}_2$ uses private key Key_2^{pri} to decrypt $D\left(E_2(\lambda_1^I-\lambda_2^I)^{\phi_{1\to2}}\right) = \phi_{1\to2}(\lambda_1^I-\lambda_2^I)$ and $D(E_2(y_1^I)^{\omega_{1\to2}}) = \omega_{1\to2}y_1^I$.

Step 8: Weight multiplication

$\mathcal{V}_1$ multiplies the decrypted result with its own generated weight to get: $\phi_{21}(\lambda_2^I-\lambda_1^I) = \phi_{2\to1}\phi_{1\to2}(\lambda_2^I-\lambda_1^I)$ and $\omega_{21}y_2^I = \omega_{2\to1}\omega_{1\to2}y_2^I$; $\mathcal{V}_2$ multiplies the

decrypted result with its own generated weight to get: $\phi_{12}(\lambda_1^I - \lambda_2^I) = \phi_{1\to2}\phi_{2\to1}(\lambda_1^I - \lambda_2^I)$ and $\omega_{12}y_1^I = \omega_{1\to2}\omega_{2\to1}y_1^I$.

Post-processing: **Floating-point number transmission**

The states are converted to floating-point numbers using (5.25).

Similarly, a secure exchange protocol is designed to find a unified power utilization ratio for all DGs in the VPP to prevent information disclosure, which is shown in Fig. 5.3. $\mathcal{V}_1$ and $\mathcal{V}_2$ represent DG agents accordingly. The subscript t is also omitted for the sake of clear demonstration.

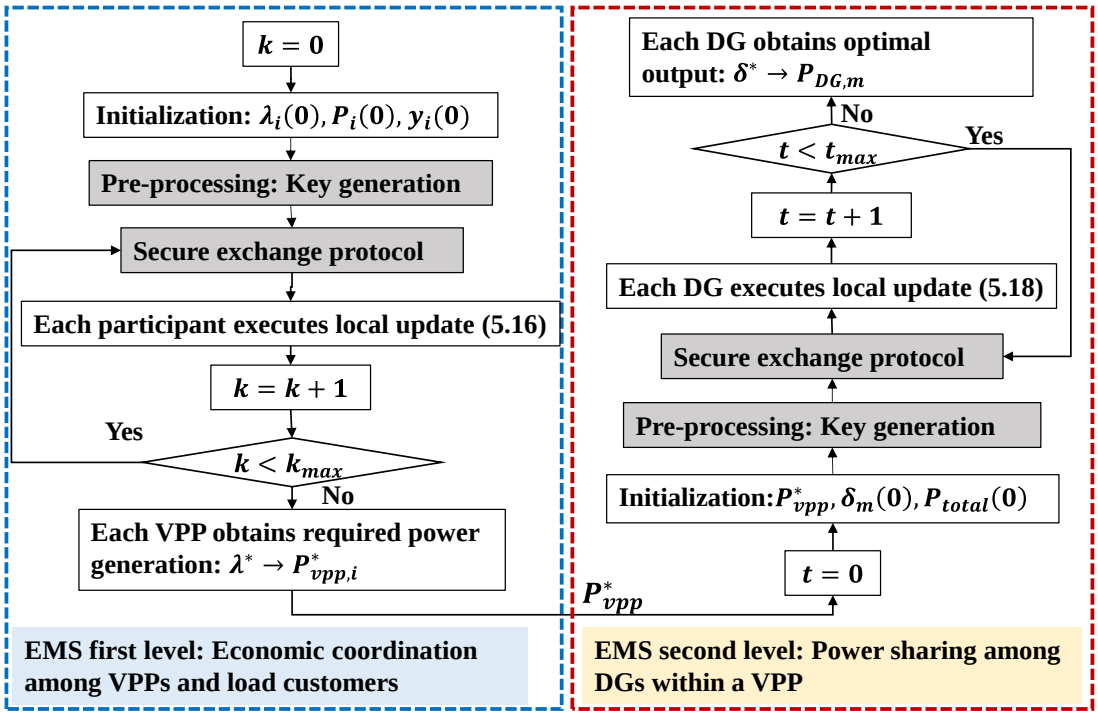

Fig. 5.4. Flowchart of the execution process of the homomorphically encrypted two-level EMS based on the secure exchange protocols.

In summary, Fig. 5.4 illustrates the execution process of the homomorphically encrypted EMS through the secure exchange protocols to achieve different objectives at each level. It should be noted that: 1) The key generation process is only required once at the beginning of the iteration. The generated public and private keys are reused

in the subsequent iterations till the convergence. 2) The conversion between floating numbers and integers is performed at each iteration. 3) The topology of the communication network is the backbone of the stable distributed optimization as it supports the information sharing and data flowing among different agents. The secure data exchange protocol is used to encrypt the data flowing in the communication network, which prevents the data from the leakage.

5.4 Discussions on Secure Exchange Protocols

5.4.1 Privacy Preservation and Correctness

The proposed secure exchange protocol has two main properties: privacy preservation and correctness. The property of privacy preservation follows the semantic security of the Paillier cryptosystem. If DCRA holds, the proposed protocol provides protection against the honest-but-curious eavesdropping attack [98]. We take λ_i^I as an example to explain the privacy preservation between two communicating participants at each iteration step. For agent $\mathcal{V}_1$, after receiving encrypted information $E_1(\lambda_2^I - \lambda_1^I)^{\phi_{2\to1}}$ from $\mathcal{V}_2$, $\mathcal{V}_1$ decrypts it with Key_1^{pri} so that decrypted information $\phi_{2\to1}(\lambda_2^I - \lambda_1^I)$ is obtained. Nevertheless, $\mathcal{V}_1$ cannot infer λ_2^I through $\phi_{2\to1}(\lambda_2^I - \lambda_1^I)$ as $\phi_{2\to1}$ is only known to $\mathcal{V}_1$. For agent $\mathcal{V}_2$, after receiving encrypted information $E_1(-\lambda_1^I)$ from $\mathcal{V}_1$, it cannot see λ_1^I as it does not have the private key Key_1^{pri} to decrypt it. For an extraneous eavesdropper that eavesdrops the communication link between participants, it cannot infer λ_i^I as the information is encrypted to $E_i(-\lambda_i^I)$ by the corresponding agent itself, and then transmitted over the communication link. The information privacy on y_i^I and δ_i^I is protected in the same way by conducting the

secure exchange protocol. Therefore, it can be concluded that the privacy of all participants is preserved against internal or external eavesdropping attacks.

The correctness property follows the homomorphic property of the Paillier cryptosystem. For any $i \in \mathcal{V}_{vpp}$ or $i \in \mathcal{V}_c$, the following equalities hold:

$$D_i\left(E_i\left(\lim_{k\to\infty} y_i^I(k)\right)\right) = \lim_{k\to\infty} y_i^I(k) \tag{5.26a}$$

$$D_i\left(E_i\left(\lim_{k\to\infty} \lambda_i^I(k)\right)\right) = \lim_{k\to\infty} \lambda_i^I(k) \tag{5.26b}$$

For any $m \in \mathcal{V}_{DG}$, the following holds:

$$D_m\left(E_m\left(\lim_{t\to\infty} \delta_m^I(t)\right)\right) = \lim_{t\to\infty} \delta_m^I(t) \tag{5.26c}$$

5.4.2 Practical Implementation Considerations

The conversion between the floating and the integer number will bring unavoidable quantization error Δ, as follows:

$$\Delta = |x_F - x_I| = x_F|(1 - 10^{\tau})| \tag{5.27}$$

Such quantization error can be neglected if we choose a sufficiently large preserved digital number τ.

The computation overhead, i.e., the algorithmic complexity, indicates how the computation complexity depends on the input size, which is specified using the Big O notation. The bit length of the key is denoted by l. Under the proposed secure exchange protocol, for an agent i, the total computation overhead of each iteration is $O(\mathcal{D}_i^{\text{in}} l)$ [107]. The computational complexity of the secure protocol based on the Paillier cryptosystem is increased with the number of in-neighbors of a certain agent

rather than network size. Hence, the homomorphically encrypted EMS can be applied on large networks with moderate connections.

5.5 Case Studies

In this section, the effectiveness and the efficiency of the proposed homomorphically encrypted exchange protocols for the two-level EMS are verified using two test networks. The functions of the Paillier cryptosystem and the proposed privacy-preserving protocols are developed and implemented in MATLAB. The first 5-bus network, as shown in Fig. 5.5(a), consists of two VPPs and three load customers. Dashed lines represent the information exchange among VPPs and loads. Corresponding parameter settings are shown in Table 5.1. The ring-circle with undirected links is used as the communication topology for the VPPs and loads. The communications among DGs in the VPP2 are illustrated in Fig. 5.5(b) and DG1 is set as leader DG which can access the power reference P^*_{VPP}. Solid lines represent the information exchange among DGs.

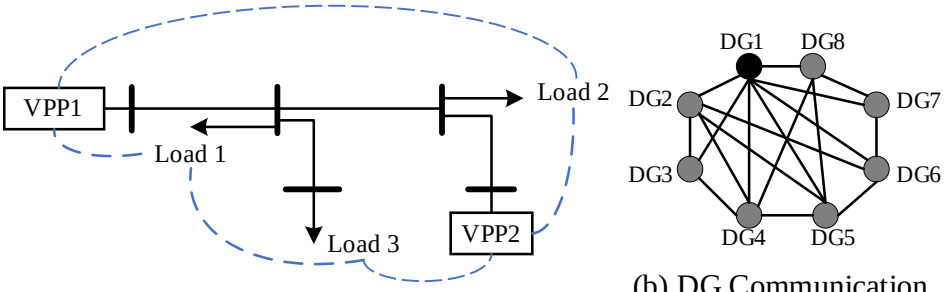

(a) Five-bus distribution network

(b) DG Communication within a VPP

Fig. 5.5. (a) Schematic diagram of five-bus distribution network. (b) Communication configuration for DGs in the VPP1.

Table 5.1. Parameter configuration for the first test network

VPP	a_i	b_i	c_i	$P^{min}_{VPP,i}$(kW)	$P^{max}_{VPP,i}$(kW)	$P_i(0)$(kW)	γ_i

1	0.0016	4.26	40	180	255	220	-0.025
2	0.0017	4.54	60	150	355	206	0.016

Load	α_j	β_j	$P_{D,j}^{min}$(kW)	$P_{D,j}^{max}$(kW)	$P_i(0)$(kW)	γ_i
1	-0.065	15.86	100	160	160	0.017
2	-0.061	17.45	150	200	180	0.022
3	-0.056	19.35	180	250	230	0.013

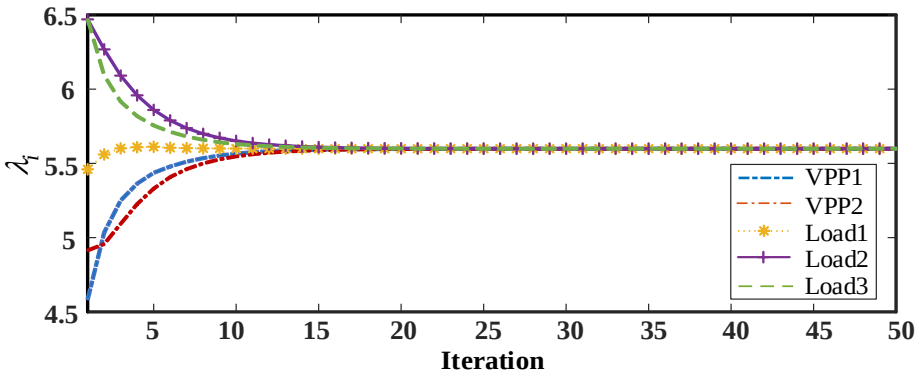

Fig. 5.6. Convergence to the optimal market-clearing price.

The effectiveness of homomorphically encrypted economic coordination under the secure exchange protocols is firstly evaluated. Set preserved decimal fraction digit $\tau = 5$. The bit length of public and private keys is set as 256. Variable states in the format of the floating number are converted to 64-bit integers before the encryption. The feedback gain σ is set to 0.5×10^{-3} for the algorithm (5.16). The weight $\phi_{i\to j}$ and $\omega_{i\to j}$ are also scaled up and represented by 64-bit integers. The obtained results are shown in Figs. 5.6 – 5.7.

The optimal value of λ_i is found to be 5.6 and the power balance between generation and demand approaches zero when the algorithm converges. In Fig. 5.7, upper and lower diagram illustrate local power mismatch update and generation/demand adjustment in response to price update, respectively. The generation output and

demand output are limited by the constraints within the constraints given in Table 5.1. Fig. 5.8 visualizes and demonstrates the privacy preservation of the transmitting states. At each iteration, the encrypted weighted difference $E_i\left(\lambda_j^l - \lambda_i^l\right)^{\phi_{j\to i}}$ is exchanged as a random big integer between a pair of communicating participants (i, j). It should be underlined that the convergence is still achieved although the encrypted messages appear to be random, verifying that an eavesdropping attacker cannot infer any information during the entire distributed operation.

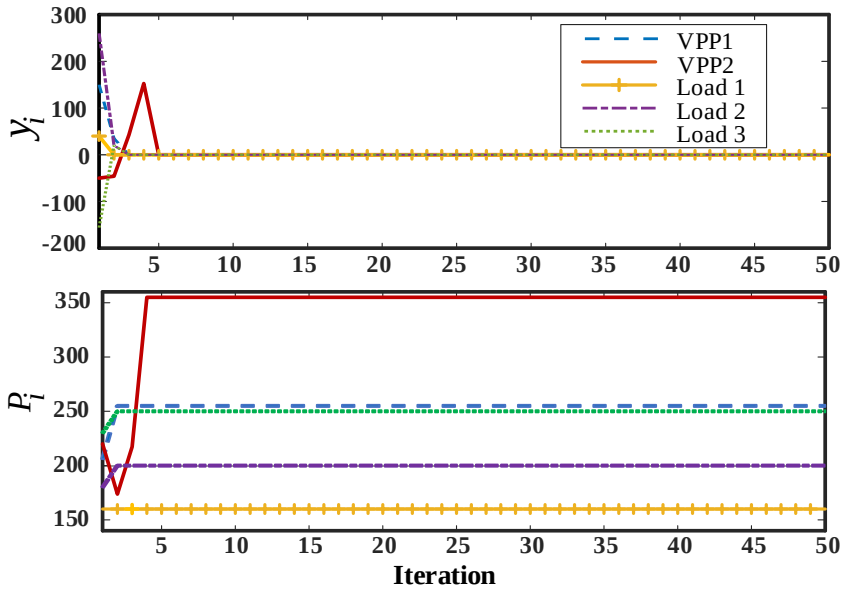

Fig. 5.7. Updates of local power mismatch and generation/demand in the first level of EMS.

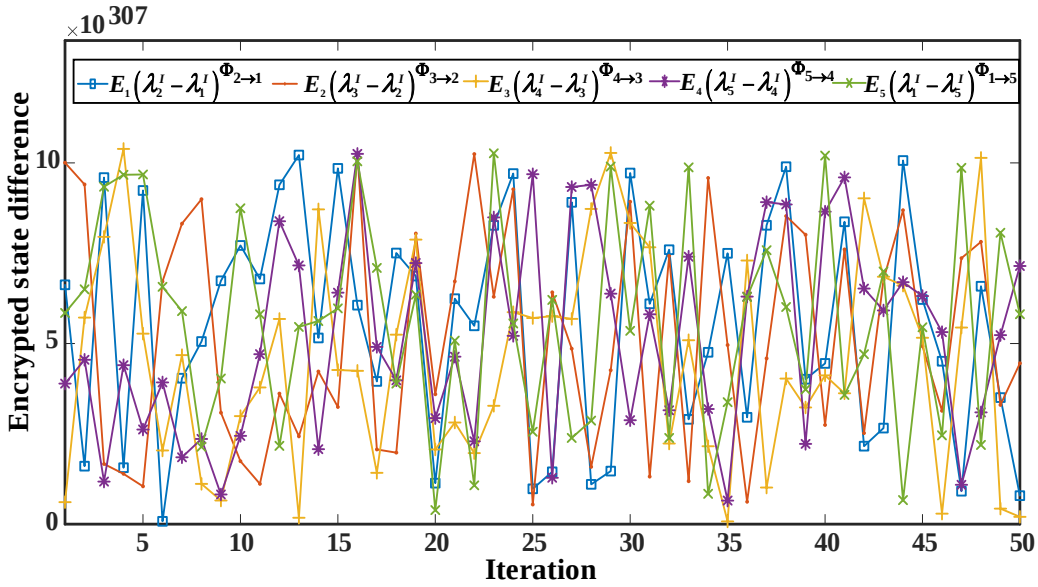

Fig. 5.8. Encrypted state difference transmitted to communicating neighbors.

Once the optimal power generation of the VPP, i.e., $P_{VPP1}^{*} = 255\text{kW}, P_{VPP2}^{*} = 350\text{kW}$, is determined in the first level of EMS, the second level of the EMS is activated within a VPP. Here VPP2 is taken as an example to demonstrate the process of cooperative power sharing. Choose the control gain $\rho = 0.004$ for the algorithm (5.18). As shown in Fig. 5.5 (b), DG1 has the most communicating neighbors, which led to $\max_i\{D_i^{in}\} = 7$. Hence, $0 < \underline{d} < \bar{d} < 1/\sqrt{\rho \max_i\{D_i^{in}\}} = \sqrt{0.004 * 7} = 0.167$ and the permissible range for the weight $d_{i\to j}$ is set as $[\underline{d}, \bar{d}] = [0.01, 0.16]$. The objective is to meet the generation requirement $P_{VPP2}^{*} = 350\text{kW}$ and to ensure the unified power utilization ratio is achieved. Fig. 5.9 shows the obtained results. Upper and lower diagram illustrate the update of the total amount of DG power output and power utilization ratio for each DG, respectively. Each DG approaches a unified power utilization ratio $\delta_i = 0.8$ while the total power output of all DGs satisfies the required power reference when the algorithm converges. DG2 is taken as an example

to examine its received encrypted states from communicating neighbors, shown in Fig. 5.10. The disorderliness verifies that privacy is protected.

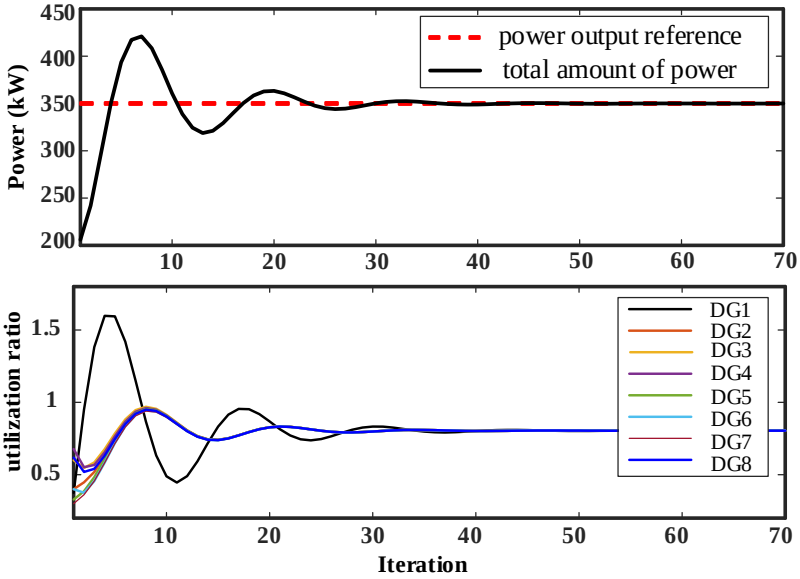

Fig. 5.9. Cooperative power sharing among DGs in the second level of EMS within VPP2.

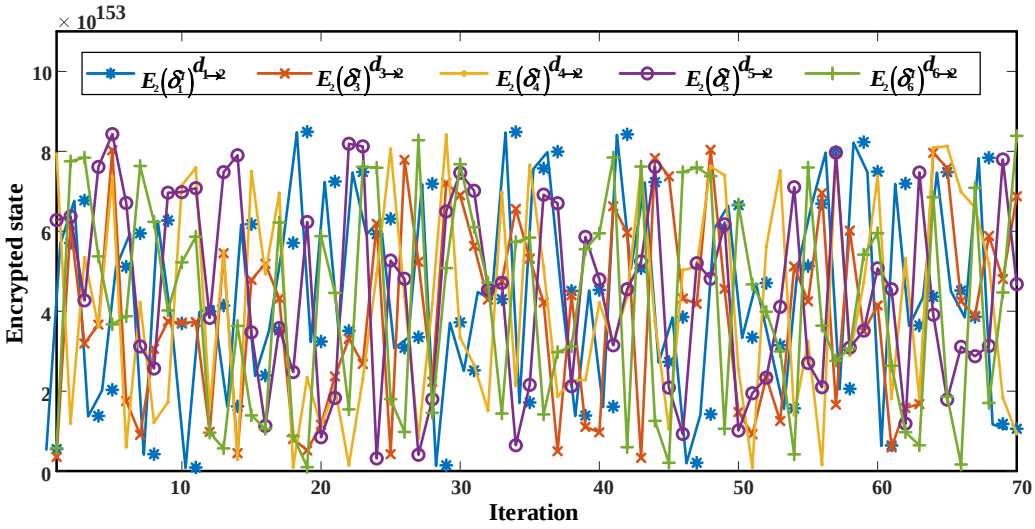

Fig. 5.10. Encrypted states received by DG2 from communicating neighbors.

IEEE 34-bus test network is used as the second test distribution network, including ten VPPs and nineteen load customers, as shown in Fig. 5.11. The corresponding parameter settings are recorded in Table 5.2. The maximum and minimum power

constraint for each VPP and load is set as $+2.5P_i(t)$ and $-2.5P_i(t)$, respectively. The graph of the communication network is shown in Fig. 5.12.

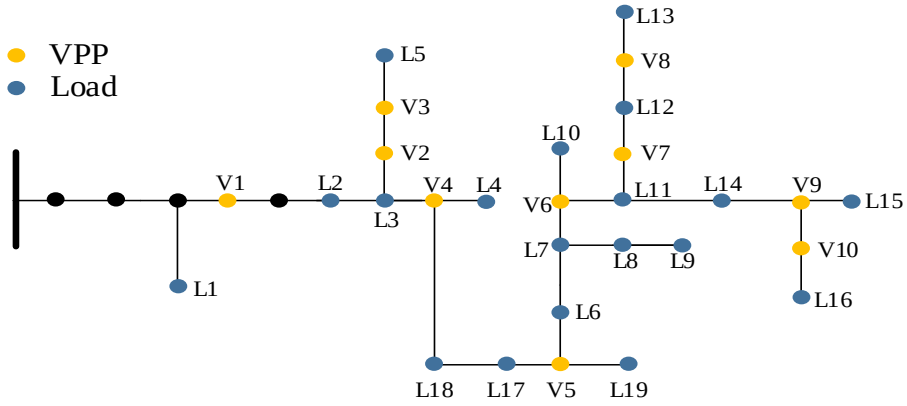

Fig. 5.11. Schematic diagram of IEEE 34-bus distribution network.

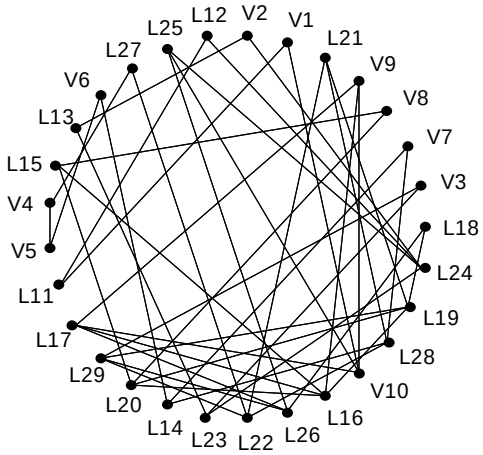

Fig. 5.12. Communication configuration for 29 participants in the network.

Table 5.2. Parameter configuration for the second test network

VPP	a_i	b_i	$P_i(0)$ (kW)	**Load**	α_j	β_j	$P_i(0)$ (kW)
1	0.0046	13.06	135.88	1	-0.140	25.75	110.15
2	0.0111	5.295	214.92	2	-0.062	18.42	176.75
3	0.0099	11.37	108.04	3	-0.151	27.63	109.69
4	0.0095	3.36	127.69	4	-0.084	10.59	75.55
5	0.0104	12.79	232.56	5	-0.081	16.275	120.64
6	0.0029	11.75	240	6	-0.212	28.365	80.26
7	0.0021	3.375	44.628	7	-0.119	28.14	142.02
8	0.0062	9.435	234.48	8	-0.159	23.55	88.57
9	0.0077	6.45	74.6	9	-0.127	21.42	100.8
10	0.0048	12.39	172.09	10	-0.069	15.225	132.38
				11	-0.097	28.56	175.75

12	-0.082	10.305	75.13
13	-0.092	23.94	154.69
14	-0.094	22.05	139.3
15	-0.091	26.25	172.85
16	-0.340	16.455	28.98
17	-0.183	24.375	79.67
18	-0.132	26.295	127.37
19	-0.130	14.76	67.92

The performance of the first-level economic coordination under a secure exchange protocol is investigated. In the simulation, the bit length of the key is set as 256. The feedback gain σ is set to 0.1×10^{-4} for the algorithm (5.16). The results are shown in Fig. 5.13, revealing that the consensus on λ^* is achieved within 150 iterations and the generation and load demand is adjusted in response to the price. The encrypted weighted state difference $E_i\left(\lambda_j^I - \lambda_i^I\right)^{\phi_{j\to i}}$ is shown in Fig. 5.14. The random big integers verify that the privacy of each agent is adequately protected as it is difficult for the attackers to obtain or infer any useful information from such unreadable patterns.

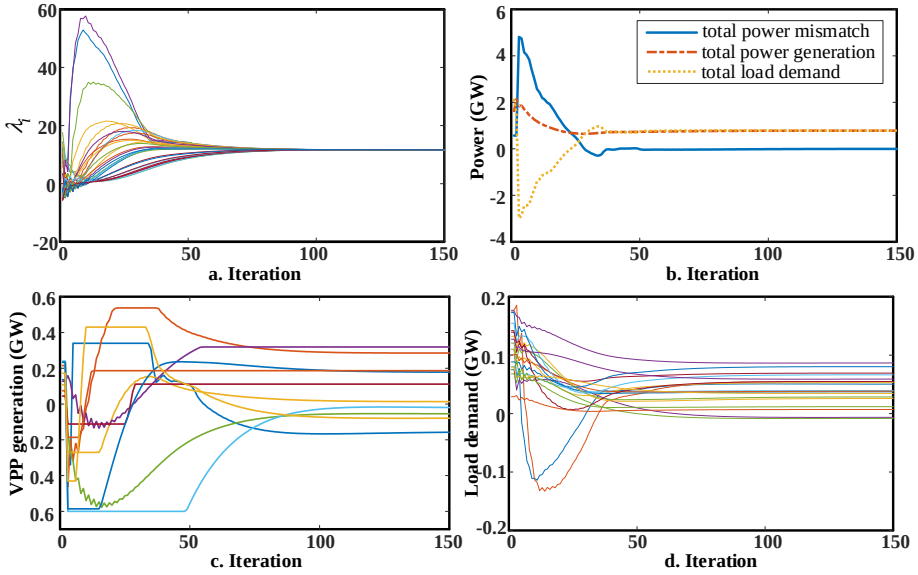

Fig. 5.13. State Evolution. (a) Update of prices (all VPPs and loads) (b) Power mismatch (c) Generation adjustment in response to price update (10 VPPs) (d) Demand adjustment in response to price update (19 loads)

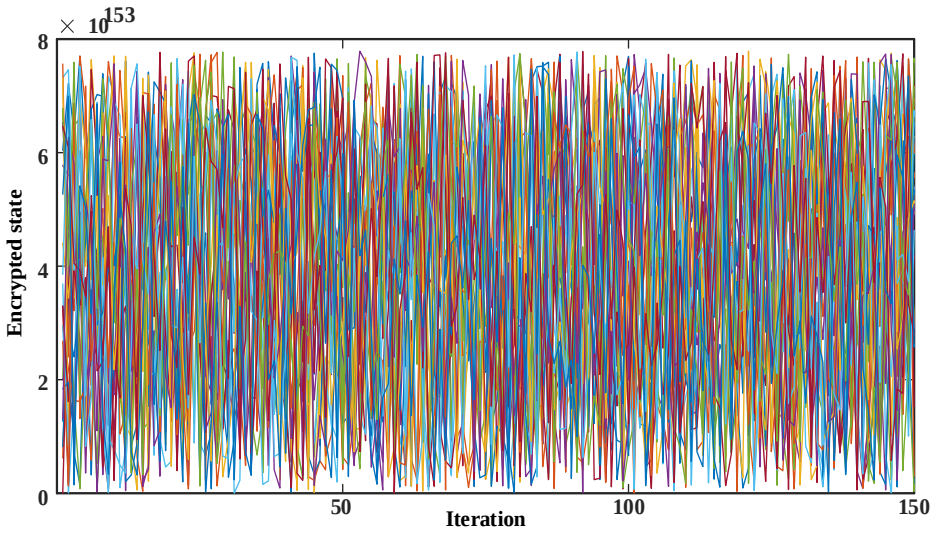

Fig. 5.14. Encrypted state difference transmitted to communicating neighbors (total 29 encrypted state differences).

The computational efficiency under different key lengths is compared, shown in Table 5.3. It takes a longer total simulation time to run homomorphic cryptosystem-based algorithm (5.16) with a longer key length. Overall, the simulation time is still acceptable and efficient enough for the EMS operation even under the longer key length.

Table 5.3. Computational efficiency under different key lengths

Key length (bit)	64	128	256	512	1024	Unencrypted
Total simulation time (s)	6.12	8.48	10.86	14.65	17.21	4.56
Computation time / agent (s)	0.21	0.29	0.27	0.51	0.59	0.15

5.6 Chapter Summary

In this chapter, a homomorphically encrypted two-level energy management system for the economic coordination and power sharing in the active distribution network is

developed to guarantee each agent's data security and privacy during the information exchange. As a typical implementation system for homomorphic cryptosystem, the Paillier cryptosystem is applied to develop secure exchange protocols by encoding randomness into the system dynamics such that enhanced privacy security and deterministic convergence of the consensus-based algorithms can be achieved. The private information, such as price information, load demand, and power utilization, are successfully protected against internal and external eavesdropping attackers. The effectiveness and the computational efficiency of the proposed encrypted approach are verified by two test networks.

Chapter 6 Conclusions and Future work

In this thesis, several distributed control and operational schemes are proposed to address challenges in different aspects in the future decarbonized and informatized low voltage network for a reliable, economical, and secure operation. The research methodology predominantly relies on the control strategy development and the formulation and solution of optimization problems. The core throughout the thesis is the application of the distributed scheme based on neighboring information sharing. Various issues and concerns resulted from the distributed operation in different scenarios are addressed accordingly. From the network planning perspective, guidance is provided for the network operator to properly design the communication network of the MG to save the potential cost. From the electricity market perspective, a future P2P trading framework allowing the flexible trading of energy and ancillary service among DERs is offered. From the network operation perspective, the possibility of utilizing V2G to mitigate voltage issues is discovered, and a cryptographic approach to maintaining the information confidentiality during the information transmission and processing is given. In the following, the summary of research contributions in terms of different aspects and the further research directions to make the current work more comprehensive are given.

6.1 Research Contributions

1. Cost-Effective Communication Network Planning Considering Performance of Pinning-Based Secondary Control in Microgrids

The cost-effective communication topology is designed considering the dynamic control constraints. The impact of the communication topology on the pinning-based secondary voltage and frequency control is examined analytically. The proposed topology designing model can be applied to the MG under construction at the planning stage. The main contributions are summarized as follows.

1) The convergence of PSC protocols for the secondary voltage and frequency control is investigated for the first time from the perspective of spectral properties of the communication graph; 2) The lower bound of the algebraic connectivity of the communication graph to guarantee the minimum convergence requirement is derived analytically, which can be used as one of the critical constraints to design the communication network; 3) In view of the graph-theoretic criteria of the proposed PSC protocols, the communication network planning problem is formulated as MISDP based on the reformulations and relaxations, which facilitates the solution process and can be solved efficiently.

2. A Multi-market Nanogrid P2P Energy and Ancillary Service Trading Paradigm: Mechanisms and Implementations

A multi-market paradigm is designed to realize the trading of both energy and ancillary service among NGs in the islanded MG, including three consecutive markets in different time phases: bilateral energy market, balancing market and ancillary service market. Through the sequential implementations, the maximal profit of producer NGs can be ensured by the proposed optimal offering strategies. Moreover, a fully distributed real-time operation is enabled to provide the frequency regulation service economically. The main contributions are summarized as follows.

1) The proposed market paradigm enables producer NGs to provide flexible balancing and frequency service in the real-time operation, in which they can pursue financial benefits, and meanwhile the system security could be ensured; 2) The tradeoff of capacity allocation between the bilateral energy market and the balancing market, as well as between the balancing market and the ancillary service market are identified. Based on that, optimal offering strategies for producers to allocate their available capacity to different markets are designed to maximize their profits; 3) By applying a hierarchical control structure comprising primary droop control and pinning-based secondary control on the NG, a fully distributed frequency regulation service based on P2P information sharing among NGs can be provided in real-time, which is compatible with the nature of P2P energy trading.

3. Distributed *P* and *Q* Provision Based Voltage Regulation Scheme by Incentivized EV Fleet Charging

Through *P* and *Q* support from EVFs, the voltage can be collectively regulated with flexibility in a fully distributed and economical manner. By involving the participation of EVF, the proposed scheme aims to provide a cost-effective option for voltage regulation without a need for further investment in the distribution network. Moreover, the proposed scheme is robust to the scenarios of communication failure and inadequate EV resources as the local energy storage system is considered backup support. The main contributions are summarized as follows.

1) Compared with the voltage regulation schemes solely based on reactive power support (like [6], [7]), both real power (*P*) and reactive power (*Q*) from EVFs are coordinately utilized to provide effective voltage support in a resistive distribution

network. Consequently, more regulation options are allowed to accommodate different *R/X* ratio scenarios and facilitate the EV penetration in the distribution network; 2) Instead of using Jacobian matrix-based analysis for the voltage sensitivity calculation, which requires the global information on the network (like [11], [12]), an adaptive coefficient is derived to describe the time-varying voltage sensitivity based on the local bus information only. Hence, the entire regulation can be network configuration-free when using such sensitivity to estimate required power for the voltage recovery; 3) A parallel-consensus sharing strategy is designed for the information sharing among EVFs and buses so that the power dispatch decision can be made locally by each EVF for the voltage regulation. Instead of appointing a leader bus for consensus-based control in [10], the communication graph is leader-free in this strategy. Thus, the voltage violation rising at an arbitrary bus in the network can be accommodated by initiating the sharing strategy.

4. Privacy-preserving Distributed Energy Management System

A well-designed EMS is a prerequisite for effective DG deployment. Under a high penetration level of DGs, multiple DGs can be organized as a VPP to provide flexible power generation and to respond fast to meet customers' demand as suppliers. In the first level of the EMS, the economic coordination among VPPs and load customers can be ensured, whereas a unified power utilization ratio for all DGs can be achieved in the second level. The privacy-preserving operation of the EMS is supported by the proposed secure exchange protocols, which protect agent privacy against eavesdropping attacks. The main contributions are summarized as follows.

1) In order to address the pressing demand for privacy preservation in a distributed EMS, privacy concerns and risks subject to eavesdropping attacks are comprehensively considered and analyzed, which are critical but still under insufficient attention; 2) In order to prevent the leakage of private information (price information, power usage data, and power utilization ratio) of each agent during the distributed operation, secure exchange protocols are developed based on the homomorphic cryptosystem techniques. As a result, the operation of secure protocols is fully distributed without the supervision of a third party, which is cost-effective and efficient to be implemented; 3) Compared with the differential privacy approach to preventing privacy breach, the proposed EMS based on homomorphic cryptosystem can accomplish two advantageous properties at the same time: privacy-preservation and correctness, guaranteeing the effectiveness of the EMS.

6.2 Recommendations for Future Work

1. Investigate interaction mechanism between communication and physical system of the low-voltage network. In Chapter 2, how the communication network influences the control system of the physical network has been investigated. As a CPS, more and more intelligent agents communicate with each other in the low-voltage network. Therefore, how the operation of the physical network influences communications among agents is worthy of examining. A mathematical model should be developed to describe the interaction between the physical and cyber networks.

2. Develop a more comprehensive P2P market trading framework applied to both islanded and grid-connected MG scenarios. In Chapter 3, the multi-market framework is designed specifically for the islanded MG and only allows the trading

among internal prosumers in the MG. The future work should extend the study and research scope so that DER prosumers can sell or buy energy and ancillary service to the main grid, which will be more practical and applicable. A more comprehensive market trading mechanism can be designed to involve the dynamics of the main grid and the interaction between the main grid and NGs.

3. Investigation of coordinated frequency and voltage regulation in the low-voltage network with high *R/X*. In Chapter 4, only voltage is regulated by utilizing *P* and *Q* in a resistive distribution network. However, due to the strong coupling between the bus voltage and system frequency in the low-voltage network with high *R/X*, it is worth systematically exploring how the voltage and frequency can be coordinately regulated by appropriately utilizing *P* and *Q*.

4. Development of distributed control strategy with the aim of mitigations for cyber-attacks. In Chapter 5, the eavesdropping attacks are the targets and secure data exchange protocols are developed based on cryptographic techniques to protect information privacy. This work more lies on the data protection during the information exchanging and processing. In future work, the distributed control strategy can be developed to detect and mitigate the consequences of cyber-attacks for the secure and stable operation of the low-voltage network.

References

[1] D. Megan and G. Isabelle, “Which countries have a net zero carbon goal?,” 2019. [Online]. Available: https://www.climatechangenews.com/2019/06/14/countries-net-zero-climate-goal/. [Accessed: 22-May-2021].

[2] S. Mallapaty, “How China could be carbon neutral by mid-century,” *Nature*, vol. 586, no. 7830. NLM (Medline), pp. 482–483, 01-Oct-2020.

[3] “EU raises renewable energy targets to 32% by 2030 | Energy industry | The Guardian.” [Online]. Available: https://www.theguardian.com/business/2018/jun/14/eu-raises-renewable-energy-targets-to-32-by-2030. [Accessed: 22-May-2021].

[4] “China Sets New Renewables Target of 35 Percent by 2030 | Renewable Energy World.” [Online]. Available: https://www.renewableenergyworld.com/baseload/china-sets-new-renewables-target-of-35-percent-by-2030/. [Accessed: 22-May-2021].

[5] J. Driesen and F. Katiraei, “Design for distributed energy resources,” *IEEE Power Energy Mag.*, vol. 6, no. 3, pp. 30–39, May 2008.

[6] M. Yazdanian and A. Mehrizi-Sani, “Distributed Control Techniques in Microgrids,” *IEEE Trans. Smart Grid*, vol. 5, no. 6, pp. 2901–2909, Nov. 2014.

[7] M. Ilic’Spong, J. Christensen, and K. L. Eichorn, “Secondary voltage control using pilot point information,” *IEEE Trans. Power Syst.*, vol. 3, no. 2, pp. 660–668, 1988.

[8] D. E. Olivares *et al.*, “Trends in microgrid control,” *IEEE Trans. Smart Grid*, vol. 5, no. 4, pp. 1905–1919, 2014.

[9] “Final report on the August 14, 2003 blackout in the United States and Canada : causes and recommendations (Miscellaneous) | ETDEWEB.” [Online]. Available: https://www.osti.gov/etdeweb/biblio/20461178. [Accessed: 04-Jun-2021].

[10] A. Vasilakis, I. Zafeiratou, D. T. Lagos, and N. D. Hatziargyriou, “The Evolution of Research in Microgrids Control,” *IEEE Open Access J. Power Energy*, vol. 7, pp. 331–343, Oct. 2020.

[11] B. A. Robbins, C. N. Hadjicostis, and A. D. Domínguez-García, “A two-stage distributed architecture for voltage control in power distribution systems,” *IEEE Trans. Power Syst.*, vol. 28, no. 2, pp. 1470–1482, 2013.

[12] Y. Xiang, J. Liu, and Y. Liu, “Optimal active distribution system management considering aggregated plug-in electric vehicles,” *Electr. Power Syst. Res.*, vol.

131, no. February, pp. 105–115, 2016.

[13] M. Shafie-khah, P. Siano, J. Aghaei, M. A. S. Masoum, F. F. Li, and J. P. S. Catalao, “Comprehensive Review of the Recent Advances in Industrial and Commercial DR,” *IEEE Trans. Ind. Informatics*, vol. 15, no. 7, pp. 1–1, 2019.

[14] T. Lv and Q. Ai, “Interactive energy management of networked microgrids-based active distribution system considering large-scale integration of renewable energy resources,” *Appl. Energy*, vol. 163, pp. 408–422, 2016.

[15] J. M. Guerrero, J. C. Vasquez, J. Matas, L. G. De Vicuña, and M. Castilla, “Hierarchical control of droop-controlled AC and DC microgrids - A general approach toward standardization,” *IEEE Trans. Ind. Electron.*, vol. 58, no. 1, pp. 158–172, 2011.

[16] A. Bidram and A. Davoudi, “Hierarchical structure of microgrids control system,” *IEEE Trans. Smart Grid*, vol. 3, no. 4, pp. 1963–1976, 2012.

[17] A. Mehrizi-Sani and R. Iravani, “Potential-function based control of a microgrid in islanded and grid-connected modes,” *IEEE Trans. Power Syst.*, vol. 25, no. 4, pp. 1883–1891, 2010.

[18] F. Guo, C. Wen, J. Mao, and Y. D. Song, “Distributed Secondary Voltage and Frequency Restoration Control of Droop-Controlled Inverter-Based Microgrids,” *IEEE Trans. Ind. Electron.*, vol. 62, no. 7, pp. 4355–4364, 2015.

[19] Q. Hu and S. Bu, “Economic frequency regulation based on nanogrid partition and cost-driven droop function: Enable a scattered microgrid,” in *Proceedings - 2020 International Conference on Smart Grids and Energy Systems, SGES 2020*, 2020, pp. 320–325.

[20] J. Hu and P. Bhowmick, “A consensus-based robust secondary voltage and frequency control scheme for islanded microgrids,” *Int. J. Electr. Power Energy Syst.*, 2020.

[21] G. Chen, “Pinning control and synchronization on complex dynamical networks,” *Int. J. Control. Autom. Syst.*, vol. 12, no. 2, pp. 221–230, 2014.

[22] Q. Zhou, M. Shahidehpour, Z. Li, L. Che, A. Alabdulwahab, and A. Abusorrah, “Compartmentalization Strategy for the Optimal Economic Operation of a Hybrid AC/DC Microgrid,” *IEEE Trans. Power Syst.*, vol. 35, no. 2, pp. 1294–1304, 2020.

[23] A. Bidram, A. Davoudi, F. L. Lewis, and J. M. Guerrero, “Distributed cooperative secondary control of microgrids using feedback linearization,” *IEEE Trans. Power Syst.*, vol. 28, no. 3, pp. 3462–3470, 2013.

[24] X. Wu, Y. Xu, J. He, X. Wang, J. Vasquez, and J. M. Guerrero, “Pinning-based Hierarchical and Distributed Cooperative Control for AC Microgrid Clusters,” *IEEE Trans. Power Electron.*, vol. 8993, no. c, pp. 1–1, 2020.

[25] W. Yao, Y. Wang, Y. Xu, T. L. Nguyen, and X. Feng, “Distributed Multi-

Functional Finite-Time Secondary Control in Cyber-Physical Microgrid," *IEEE Power Energy Soc. Gen. Meet.*, vol. 2019-Augus, pp. 0–4, 2019.

[26] N. Gaeini, A. Moradi Amani, M. Jalili, and X. Yu, "Cooperative secondary frequency control of distributed generation: The role of data communication network topology," *Int. J. Electr. Power Energy Syst.*, vol. 92, pp. 221–229, 2017.

[27] G. Lou, W. Gu, J. Wang, W. Sheng, and L. Sun, "Optimal Design for Distributed Secondary Voltage Control in Islanded Microgrids: Communication Topology and Controller," *IEEE Trans. Power Syst.*, vol. 34, no. 2, pp. 968–981, 2019.

[28] J. Lai, X. Lu, A. Monti, and G. P. Liu, "Stochastic Distributed Pinning Control for Co-Multi-Inverter Networks with A Virtual Leader," *IEEE Trans. Circuits Syst. II Express Briefs*, 2019.

[29] W. Liu, W. Gu, W. Sheng, X. Meng, S. Xue, and M. Chen, "Pinning-Based Distributed Cooperative Control for Autonomous Microgrids under Uncertain Communication Topologies," *IEEE Trans. Power Syst.*, vol. 31, no. 2, pp. 1320–1329, 2016.

[30] R. Dai and M. Mesbahi, "Optimal topology design for dynamic networks," *Proc. IEEE Conf. Decis. Control*, pp. 1280–1285, 2011.

[31] H. Shakeri, N. Albin, F. Darabi Sahneh, P. Poggi-Corradini, and C. Scoglio, "Maximizing algebraic connectivity in interconnected networks," *Phys. Rev. E*, vol. 93, no. 3, pp. 1–6, 2016.

[32] H. Liu, X. Xu, J. A. Lu, G. Chen, and Z. Zeng, "Optimizing Pinning Control of Complex Dynamical Networks Based on Spectral Properties of Grounded Laplacian Matrices," *IEEE Trans. Syst. Man, Cybern. Syst.*, vol. PP, pp. 1–11, 2018.

[33] S. Manaffam, M. Talebi, A. K. Jain, and A. Behal, "Intelligent Pinning Based Cooperative Secondary Control of Distributed Generators for Microgrid in Islanding Operation Mode," *IEEE Trans. Power Syst.*, vol. 33, no. 2, pp. 1364–1373, 2018.

[34] N. F. Avila and C. C. Chu, "Distributed Pinning Droop Control in Isolated AC Microgrids," *IEEE Trans. Ind. Appl.*, vol. 53, no. 4, pp. 3237–3249, 2017.

[35] A. A. Anderson, S. Suryanarayanan, and S. Member, "Review of Energy Management and Planning of Islanded Microgrids," *CSEE J. Power Energy Syst.*, vol. 6, no. 2, pp. 329–343, 2020.

[36] T. Morstyn, N. Farrell, S. J. Darby, and M. D. McCulloch, "Using peer-to-peer energy-trading platforms to incentivize prosumers to form federated power plants," *Nat. Energy*, vol. 3, no. 2, pp. 94–101, 2018.

[37] A. Monacchi and W. Elmenreich, "Assisted energy management in smart microgrids," *J. Ambient Intell. Humaniz. Comput.*, vol. 7, no. 6, pp. 901–913,

Dec. 2016.

[38] E. Mengelkamp, J. Gärttner, K. Rock, S. Kessler, L. Orsini, and C. Weinhardt, "Designing microgrid energy markets: A case study: The Brooklyn Microgrid," *Appl. Energy*, vol. 210, pp. 870–880, 2018.

[39] W. Tushar, T. K. Saha, C. Yuen, D. Smith, and H. V. Poor, "Peer-to-Peer Trading in Electricity Networks: An Overview," *IEEE Trans. Smart Grid*, vol. 11, no. 4, pp. 3185–3200, 2020.

[40] W. Tushar *et al.*, "A motivational game-theoretic approach for peer-to-peer energy trading in the smart grid," *Appl. Energy*, vol. 243, no. March, pp. 10–20, 2019.

[41] W. Tushar *et al.*, "Peer-to-peer energy systems for connected communities: A review of recent advances and emerging challenges," *Appl. Energy*, vol. 282, no. PA, p. 116131, 2021.

[42] J. An, M. Lee, S. Yeom, and T. Hong, "Determining the Peer-to-Peer electricity trading price and strategy for energy prosumers and consumers within a microgrid," *Appl. Energy*, vol. 261, p. 114335, Mar. 2020.

[43] C. Zhang, J. Wu, Y. Zhou, M. Cheng, and C. Long, "Peer-to-Peer energy trading in a Microgrid," *Appl. Energy*, vol. 220, no. March, pp. 1–12, 2018.

[44] K. Anoh, S. Maharjan, A. Ikpehai, Y. Zhang, and B. Adebisi, "Energy Peer-to-Peer Trading in Virtual Microgrids in Smart Grids: A Game-Theoretic Approach," *IEEE Trans. Smart Grid*, vol. 11, no. 2, pp. 1264–1275, 2020.

[45] W. Tushar *et al.*, "Energy Storage Sharing in Smart Grid: A Modified Auction-Based Approach," *IEEE Trans. Smart Grid*, vol. 7, no. 3, pp. 1462–1475, 2016.

[46] C. Long, J. Wu, Y. Zhou, and N. Jenkins, "Peer-to-peer energy sharing through a two-stage aggregated battery control in a community Microgrid," *Appl. Energy*, vol. 226, no. April, pp. 261–276, 2018.

[47] A. Paudel, K. Chaudhari, C. Long, and H. B. Gooi, "Peer-to-peer energy trading in a prosumer-based community microgrid: A game-theoretic model," *IEEE Trans. Ind. Electron.*, vol. 66, no. 8, pp. 6087–6097, 2019.

[48] J. Guerrero, A. C. Chapman, and G. Verbic, "Decentralized P2P Energy Trading under Network Constraints in a Low-Voltage Network," *IEEE Trans. Smart Grid*, 2018.

[49] C. Essayeh, M. R. El Fenni, and H. Dahmouni, "Optimization of energy exchange in microgrid networks: a coalition formation approach," *Prot. Control Mod. Power Syst.*, vol. 4, no. 1, pp. 1–10, Dec. 2019.

[50] J. Kang, R. Yu, X. Huang, S. Maharjan, Y. Zhang, and E. Hossain, "Enabling Localized Peer-to-Peer Electricity Trading among Plug-in Hybrid Electric Vehicles Using Consortium Blockchains," *IEEE Trans. Ind. Informatics*, vol. 13, no. 6, pp. 3154–3164, Dec. 2017.

[51] J. Lin, M. Pipattanasomporn, and S. Rahman, “Comparative analysis of auction mechanisms and bidding strategies for P2P solar transactive energy markets,” *Appl. Energy*, vol. 255, p. 113687, Dec. 2019.

[52] M. R. Alam, M. St-Hilaire, and T. Kunz, “Peer-to-peer energy trading among smart homes,” *Appl. Energy*, vol. 238, pp. 1434–1443, Mar. 2019.

[53] C. Stevanoni, Z. De Grève, F. Vallée, and O. Deblecker, “Long-Term Planning of Connected Industrial Microgrids: A Game Theoretical Approach Including Daily Peer-to-Microgrid Exchanges,” *IEEE Trans. Smart Grid*, vol. 10, no. 2, pp. 2245–2256, Mar. 2019.

[54] N. Liu, X. Yu, C. Wang, C. Li, L. Ma, and J. Lei, “Energy-Sharing Model with Price-Based Demand Response for Microgrids of Peer-to-Peer Prosumers,” *IEEE Trans. Power Syst.*, vol. 32, no. 5, pp. 3569–3583, Sep. 2017.

[55] S. Nguyen, W. Peng, P. Sokolowski, D. Alahakoon, and X. Yu, “Optimizing rooftop photovoltaic distributed generation with battery storage for peer-to-peer energy trading,” *Appl. Energy*, vol. 228, pp. 2567–2580, Oct. 2018.

[56] Y. Wu, J. Shi, G. Lim, L. Fan, and A. Molavi, “Optimal Management of Transactive Distribution Electricity Markets with Co-optimized Bidirectional Energy and Ancillary Service Exchanges,” *IEEE Trans. Smart Grid*, vol. 3053, no. c, pp. 1–1, 2020.

[57] N. Grid, “GC022 - Frequency Response Workgroup Report,” 2013. [Online]. Available: https://www.nationalgrid.com/sites/default/files/documents/16927-Workgroup Report.pdf.

[58] “A MILP optimization model for assessing the participation of distributed residential PV-battery systems in the ancillary services market,” *CSEE J. Power Energy Syst.*, 2020.

[59] T. K. Chau, S. S. Yu, T. Fernando, and H. H. C. Iu, “Demand-Side Regulation Provision From Industrial Loads Integrated With Solar PV Panels and Energy Storage System for Ancillary Services,” *IEEE Trans. Ind. Informatics*, vol. 14, no. 11, pp. 5038–5049, 2018.

[60] Y. Du and F. Li, “A Hierarchical Real-Time Balancing Market Considering Multi-Microgrids with Distributed Sustainable Resources,” *IEEE Trans. Sustain. Energy*, vol. 11, no. 1, pp. 72–83, 2020.

[61] Y. Zhou, Z. Wei, G. Sun, K. W. Cheung, H. Zang, and S. Chen, “A robust optimization approach for integrated community energy system in energy and ancillary service markets,” *Energy*, vol. 148, pp. 1–15, 2018.

[62] M. Rayati, A. Sheikhi, and A. M. Ranjbar, “Optimal contract design for purchasing from frequency regulation service providers with private information,” *IEEE Trans. Power Syst.*, vol. 34, no. 3, pp. 2445–2448, 2019.

[63] A. G. Madureira and J. A. Peças Lopes, “Ancillary services market framework for voltage control in distribution networks with microgrids,” *Electr. Power*

Syst. Res., vol. 86, pp. 1–7, May 2012.

[64] T. Yang, "ICT technologies standards and protocols for active distribution network," in *Smart Power Distribution Systems*, Elsevier, 2019, pp. 205–230.

[65] A. Keane, L. F. Ochoa, E. Vittal, C. J. Dent, and G. P. Harrison, "Enhanced utilization of voltage control resources with distributed generation," *IEEE Trans. Power Syst.*, vol. 26, no. 1, pp. 252–260, 2011.

[66] N. K. Trehan, "Ancillary services-reactive and voltage control," in *2001 IEEE Power Engineering Society Winter Meeting. Conference Proceedings (Cat. No.01CH37194)*, vol. 3, pp. 1341–1346.

[67] M. Farhadi-Kangarlu, E. Babaei, and F. Blaabjerg, "A comprehensive review of dynamic voltage restorers," *International Journal of Electrical Power and Energy Systems*, vol. 92. Elsevier Ltd, pp. 136–155, 01-Nov-2017.

[68] K. Zhang, D. Recalde, T. Massier, and T. Hamacher, "Fast Online Distributed Voltage Support in Distribution Grids using Consensus Algorithm," *Int. Conf. Innov. Smart Grid Technol. ISGT Asia 2018*, pp. 350–355, 2018.

[69] M. Brenna *et al.*, "Automatic distributed voltage control algorithm in smart grids applications," *IEEE Trans. Smart Grid*, vol. 4, no. 2, pp. 877–885, 2013.

[70] D. Wang, K. Meng, X. Gao, J. Qiu, L. L. Lai, and Z. Dong, "Coordinated Dispatch of Virtual Energy Storage Systems in LV Grids for Voltage Regulation," *IEEE Trans. Ind. Informatics*, vol. 3203, no. c, 2017.

[71] Q. Shafiee, V. Nasirian, J. C. Vasquez, J. M. Guerrero, and A. Davoudi, "A Multi-Functional Fully Distributed Control Framework for AC Microgrids," *IEEE Trans. Smart Grid*, vol. 9, no. 4, pp. 3247–3258, 2018.

[72] L. Zhang, Y. Chen, C. Shen, W. Tang, and J. Liang, "Coordinated voltage regulation of hybrid AC/DC medium voltage distribution networks," *J. Mod. Power Syst. Clean Energy*, vol. 6, no. 3, pp. 463–472, 2018.

[73] Q. Hu, S. Bu, S. Xia, and H. Cai, "A Novel Voltage Regulation Strategy for Secure Operation of High Renewable Penetrated Distribution Networks with Different R/X and Topologies," in *2019 IEEE PES Innovative Smart Grid Technologies Asia, ISGT 2019*, 2019, pp. 3424–3429.

[74] Y. Wang, T. Zhao, C. Ju, Y. Xu, and P. Wang, "Two-Level Distributed Volt/Var Control Using Aggregated PV Inverters in Distribution Networks," *IEEE Trans. Power Deliv.*, vol. 35, no. 4, pp. 1844–1855, 2020.

[75] A. R. Malekpour, A. M. Annaswamy, and J. Shah, "Hierarchical Hybrid Architecture for Volt/Var Control of Power Distribution Grids," *IEEE Trans. Power Syst.*, vol. 35, no. 2, pp. 854–863, 2020.

[76] K. Alzaareer, M. Saad, H. Mehrjerdi, D. Asber, and S. Lefebvre, "Development of New Identification Method for Global Group of Controls for Online Coordinated Voltage Control in Active Distribution Networks," *IEEE Trans.*

Smart Grid, vol. 11, no. 5, pp. 3921–3931, 2020.

[77] M. N. Kabir, Y. Mishra, G. Ledwich, Z. Y. Dong, and K. P. Wong, "Coordinated control of grid-connected photovoltaic reactive power and battery energy storage systems to improve the voltage profile of a residential distribution feeder," *IEEE Trans. Ind. Informatics*, vol. 10, no. 2, pp. 967–977, 2014.

[78] M. Brenna *et al.*, "Automatic Distributed Voltage Control Algorithm in Smart Grids Applications," *IEEE Trans. Smart Grid*, vol. 4, no. 2, pp. 877–885, 2013.

[79] D. Vincent, P. S. Huynh, N. A. Azeez, L. Patnaik, and S. S. Williamson, "Evolution of Hybrid Inductive and Capacitive AC Links for Wireless EV Charging - A Comparative Overview," *IEEE Trans. Transp. Electrif.*, vol. 5, no. 4, pp. 1060–1077, 2019.

[80] N. B. G. Brinkel *et al.*, "Impact of rapid PV fluctuations on power quality in the low-voltage grid and mitigation strategies using electric vehicles," *Int. J. Electr. Power Energy Syst.*, vol. 118, Jun. 2020.

[81] S. Xia, S. Q. Bu, X. Luo, K. W. Chan, and X. Lu, "An autonomous real time charging strategy for plug-in electric vehicles to regulate frequency of distribution system with fluctuating wind generation," *IEEE Trans. Sustain. Energy*, vol. 3029, no. 3174057, 2017.

[82] W. Wang, L. Liu, J. Liu, and Z. Chen, "Energy management and optimization of vehicle-to-grid systems for wind power integration," *CSEE J. Power Energy Syst.*, vol. 7, no. 1, pp. 172–180, Jan. 2021.

[83] Z. Huang, B. Fang, and J. Deng, "Multi-objective optimization strategy for distribution network considering V2G-enabled electric vehicles in building integrated energy system," *Prot. Control Mod. Power Syst.*, vol. 5, no. 1, pp. 1–8, Dec. 2020.

[84] Z. Moghaddam, I. Ahmad, D. Habibi, and Q. V. Phung, "Smart Charging Strategy for Electric Vehicle Charging Stations," *IEEE Trans. Transp. Electrif.*, vol. 4, no. 1, pp. 76–88, 2017.

[85] Q. Hu, H. Li, and S. Bu, "The Prediction of Electric Vehicles Load Profiles Considering Stochastic Charging and Discharging Behavior and Their Impact Assessment on a Real UK Distribution Network," *Energy Procedia*, vol. 158, pp. 6458–6465, Feb. 2019.

[86] J. G. Pinto, V. Monteiro, H. Gonçalves, and J. L. Afonso, "Onboard reconfigurable battery charger for electric vehicles with traction-to-auxiliary mode," *IEEE Trans. Veh. Technol.*, vol. 63, no. 3, pp. 1104–1116, 2014.

[87] M. C. Kisacikoglu, M. Kesler, and L. M. Tolbert, "Single-phase on-board bidirectional PEV charger for V2G reactive power operation," *IEEE Trans. Smart Grid*, vol. 6, no. 2, pp. 767–775, 2015.

[88] Y. Mo *et al.*, "Cyber-physical security of a smart grid infrastructure," *Proc.*

IEEE, vol. 100, no. 1, pp. 195–209, 2012.

[89] D. Kundur, X. Feng, S. Liu, T. Zourntos, and K. L. Butler-Purry, “Towards a Framework for Cyber Attack Impact Analysis of the Electric Smart Grid,” 2010, pp. 244–249.

[90] W. Chen, D. Ding, H. Dong, and G. Wei, “Distributed Resilient Filtering for Power Systems Subject to Denial-of-Service Attacks,” *IEEE Trans. Syst. Man, Cybern. Syst.*, vol. 49, no. 8, pp. 1688–1697, 2019.

[91] J. Liu, Y. Du, S. il Yim, X. Lu, B. Chen, and F. Qiu, “Steady-State Analysis of Microgrid Distributed Control under Denial of Service Attacks,” *IEEE J. Emerg. Sel. Top. Power Electron.*, vol. 6777, no. c, pp. 1–15, 2020.

[92] L. Ding, Q. L. Han, B. Ning, and D. Yue, “Distributed Resilient Finite-Time Secondary Control for Heterogeneous Battery Energy Storage Systems under Denial-of-Service Attacks,” *IEEE Trans. Ind. Informatics*, vol. 16, no. 7, pp. 4909–4919, 2020.

[93] S. Liu, Z. Hu, X. Wang, and L. Wu, “Stochastic Stability Analysis and Control of Secondary Frequency Regulation for Islanded Microgrids Under Random Denial of Service Attacks,” *IEEE Trans. Ind. Informatics*, vol. 15, no. 7, pp. 4066–4075, 2019.

[94] J. Duan and M. Y. Chow, “A Resilient Consensus-Based Distributed Energy Management Algorithm against Data Integrity Attacks,” *IEEE Trans. Smart Grid*, vol. 10, no. 5, pp. 4729–4740, 2018.

[95] A. Mustafa, B. Poudel, A. Bidram, and H. Modares, “Detection and Mitigation of Data Manipulation Attacks in AC Microgrids,” *IEEE Trans. Smart Grid*, vol. 11, no. 3, pp. 2588–2603, 2020.

[96] Q. Zhou, M. Shahidehpour, A. Alabdulwahab, and A. Abusorrah, “A Cyber-Attack Resilient Distributed Control Strategy in Islanded Microgrids,” *IEEE Trans. Smart Grid*, vol. 11, no. 5, pp. 3690–3701, 2020.

[97] S. Zuo, O. A. Beg, F. L. Lewis, and A. Davoudi, “Resilient Networked AC Microgrids under Unbounded Cyber Attacks,” *IEEE Trans. Smart Grid*, vol. 11, no. 5, pp. 3785–3794, 2020.

[98] Y. Lu and M. Zhu, “Privacy preserving distributed optimization using homomorphic encryption,” *Automatica*, vol. 96, pp. 314–325, 2018.

[99] Y. Lu, J. Lian, and M. Zhu, “Privacy-Preserving Transactive Energy System,” *Proc. Am. Control Conf.*, vol. 2020-July, pp. 3005–3010, 2020.

[100] L. Yan, X. Chen, J. Zhou, M. Shi, Q. Yang, and J. Wen, “Privacy-preserving economic dispatch for microgrids with a distributed event-triggered communication scheme,” *IEEE Power Energy Soc. Gen. Meet.*, vol. 2020-Augus, no. 51607075, pp. 0–4, 2020.

[101] C. Zhao, J. Chen, J. He, and P. Cheng, “Privacy-preserving consensus-based

energy management in smart grids," *IEEE Trans. Signal Process.*, vol. 66, no. 23, pp. 6162–6176, 2018.

[102] F. Ye, Z. Cheng, X. Cao, and M. Y. Chow, "A Random-Weighted Privacy-Preserving Distributed Algorithm for Energy Management in Microgrid with Energy Storage Devices," *Proc. - 2020 2nd IEEE Int. Conf. Ind. Electron. Sustain. Energy Syst. IESES 2020*, pp. 249–254, 2020.

[103] T. W. K. Mak, F. Fioretto, L. Shi, and P. Van Hentenryck, "Privacy-Preserving Power System Obfuscation: A Bilevel Optimization Approach," *IEEE Trans. Power Syst.*, vol. 35, no. 2, pp. 1627–1637, 2020.

[104] Y. Xiong, J. Xu, K. You, J. Liu, and L. Wu, "Privacy-Preserving Distributed Online Optimization over Unbalanced Digraphs via Subgradient Rescaling," *IEEE Trans. Control Netw. Syst.*, vol. 7, no. 3, pp. 1366–1378, 2020.

[105] X. Yi, R. Paulet, and E. Bertino, *Homomorphic Encryption and Applications*. Cham: Springer International Publishing, 2014.

[106] T. Yin, Y. Lv, and W. Yu, "Accurate Privacy Preserving Average Consensus," *IEEE Trans. Circuits Syst. II Express Briefs*, vol. 67, no. 4, pp. 690–694, 2020.

[107] M. Ruan, H. Gao, and Y. Wang, "Secure and Privacy-Preserving Consensus," *IEEE Trans. Automat. Contr.*, vol. 64, no. 10, pp. 4035–4049, 2019.

[108] C. N. Hadjicostis and A. D. Dominguez-Garcia, "Privacy-Preserving Distributed Averaging via Homomorphically Encrypted Ratio Consensus," *IEEE Trans. Automat. Contr.*, vol. 65, no. 9, pp. 3887–3894, 2020.

[109] T. Yang *et al.*, "Distributed Energy Resource Coordination Over Time-Varying Directed Communication Networks," *IEEE Trans. Control Netw. Syst.*, vol. 6, no. 3, pp. 1124–1134, 2019.

[110] D. Yang, S. Member, S. Zhang, and B. Zhou, "Consensus-Based Decentralized Optimization for Distributed Generators Power Allocation Over Time-Varying Digraphs in Microgrids," *IEEE Syst. J.*, pp. 1–12, 2020.

[111] W. Zhang, Y. Xu, W. Liu, and S. Member, "Distributed Online Optimal Energy Management for Smart Grids," *IEEE Trans. Ind. Informatics*, vol. 11, no. 3, pp. 717–727, 2015.

[112] M. H. Ullah, B. Babaiahgari, A. Alseyat, and J. Do Park, "A Computationally Efficient Consensus-Based Multiagent Distributed EMS for DC Microgrids," *IEEE Trans. Ind. Electron.*, vol. 68, no. 6, pp. 5425–5435, Jun. 2021.

[113] Y. Khayat *et al.*, "On the Secondary Control Architectures of AC Microgrids: An Overview," *IEEE Trans. Power Electron.*, vol. 35, no. 6, pp. 6482–6500, 2020.

[114] Q. Xu, Y. Xu, S. Member, C. Zhang, S. Member, and P. Wang, "A Robust Droop-based Autonomous Controller for Decentralized Power Sharing in DC Microgrid," *IEEE Trans. Ind. Informatics*, vol. 3203, no. c, pp. 1–11, 2019.

[115] X. Yu, C. Cecati, T. Dillon, and M. G. Simes, "The new frontier of smart grids," *IEEE Ind. Electron. Mag.*, vol. 5, no. 3, pp. 49–63, 2011.

[116] U. Miekkala, "Graph properties for splitting with grounded Laplacian matrices," *BIT*, vol. 33, no. 3, pp. 485–495, 1993.

[117] Q. Zhou, M. Shahidehpour, Z. Li, L. Che, A. Alabdulwahab, and A. Abusorrah, "Compartmentalization Strategy for the Optimal Economic Operation of a Hybrid AC/DC Microgrid," *IEEE Trans. Power Syst.*, vol. 35, no. 2, pp. 1–1, 2019.

[118] Q. Song and J. Cao, "On pinning synchronization of directed and undirected complex dynamical networks," *IEEE Trans. Circuits Syst. I Regul. Pap.*, vol. 57, no. 3, pp. 672–680, 2010.

[119] A. Di Meglio, P. De Lellis, and M. Di Bernardo, "Decentralized gain adaptation for optimal pinning controllability of complex networks," *IEEE Control Syst. Lett.*, vol. 4, no. 1, pp. 253–258, 2020.

[120] R. B. Bapat, *Graphs and Matrices*. Springer London, 2010.

[121] G. Lou, W. Gu, J. Wang, W. Sheng, and L. Sun, "Optimal Design for Distributed Secondary Voltage Control in Islanded Microgrids: Communication Topology and Controller," *IEEE Trans. Power Syst.*, vol. 34, no. 2, pp. 968–981, 2019.

[122] M. Rafiee and A. M. Bayen, "Optimal network topology design in multi-agent systems for efficient average consensus," *Proc. IEEE Conf. Decis. Control*, vol. 94720, pp. 3877–3883, 2010.

[123] C. Godsil and G. Royle, *Algebraic Graph Theory*, vol. 207. New York, NY: Springer New York, 2001.

[124] S. Boyd and L. Vandenberghe, *Convex Optimization*. Cambridge University Press, 2004.

[125] E. Galvan, P. Mandal, and Y. Sang, "Networked microgrids with roof-top solar PV and battery energy storage to improve distribution grids resilience to natural disasters," *Int. J. Electr. Power Energy Syst.*, vol. 123, 2020.

[126] Y. Wang, A. O. Rousis, and G. Strbac, "On microgrids and resilience: A comprehensive review on modeling and operational strategies," *Renewable and Sustainable Energy Reviews*, vol. 134. Elsevier Ltd, 01-Dec-2020.

[127] H. Bevrani, T. Ise, and Y. Miura, "Virtual synchronous generators: A survey and new perspectives," *Int. J. Electr. Power Energy Syst.*, vol. 54, pp. 244–254, 2014.

[128] Z. Zhou, T. Levin, and G. Conzelmann, "Survey of U.S. Ancillary Services Markets," p. 59, 2016.

[129] J. Hu, M. R. Sarker, J. Wang, F. Wen, and W. Liu, "Provision of flexible

ramping product by battery energy storage in day-ahead energy and reserve markets," *IET Gener. Transm. Distrib.*, vol. 12, no. 10, pp. 2256–2264, 2018.

[130] California ISO, "Flexible Ramping Products: Revised Draft Final Proposal," 2015. [Online]. Available: http://www.caiso.com/documents/draftfinalproposal-flexiblerampingproduct.pdf.

[131] K. Oureilidis *et al.*, "Ancillary services market design in distribution networks: Review and identification of barriers," *Energies*, vol. 13, no. 4, 2020.

[132] R. Aghatehrani and R. Kavasseri, "Sensitivity-analysis-based sliding mode control for voltage regulation in microgrids," *IEEE Trans. Sustain. Energy*, vol. 4, no. 1, pp. 50–57, 2013.

[133] M. N. Mojdehi and P. Ghosh, "Modeling and revenue estimation of EV as reactive power service provider," *IEEE Power Energy Soc. Gen. Meet.*, vol. 2014-Octob, no. October, pp. 1–5, 2014.

[134] P. Belotti, C. Kirches, S. Leyffer, J. Linderoth, J. Luedtke, and A. Mahajan, "Mixed-integer nonlinear optimization," *Acta Numerica*, vol. 22, no. 10. Cambridge University Press, pp. 1–131, May-2013.

[135] M. Kuzlu, M. Pipattanasomporn, and S. Rahman, "Communication network requirements for major smart grid applications in HAN, NAN and WAN," *Comput. Networks*, vol. 67, pp. 74–88, 2014.

[136] I. Serban, S. Cespedes, C. Marinescu, C. A. Azurdia-Meza, J. S. Gomez, and D. S. Hueichapan, "Communication requirements in microgrids: A practical survey," *IEEE Access*, vol. 8, pp. 47694–47712, 2020.

[137] M. Garau, M. Anedda, C. Desogus, E. Ghiani, M. Murroni, and G. Celli, "A 5G cellular technology for distributed monitoring and control in smart grid," in *IEEE International Symposium on Broadband Multimedia Systems and Broadcasting, BMSB*, 2017.

[138] G. Bag, L. Thrybom, and P. Hovila, "Challenges and opportunities of 5G in power grids," *CIRED - Open Access Proc. J.*, vol. 2017, no. 1, pp. 2145–2148, 2017.

[139] Allen J. Wood and Bruce F. Wollenberg, *Power Generation, Operation and Control*. Wiley, 2012.

[140] S. Yang, S. Tan, and J. X. Xu, "Consensus based approach for economic dispatch problem in a smart grid," *IEEE Trans. Power Syst.*, vol. 28, no. 4, pp. 4416–4426, 2013.

[141] Y. Liu, H. Xin, Z. Qu, and D. Gan, "An Attack-Resilient Cooperative Control Strategy of Multiple Distributed Generators in Distribution Networks," *IEEE Trans. Smart Grid*, vol. 7, no. 6, pp. 2923–2932, 2016.

[142] P. Paillier, "Public-Key Cryptosystems Based on Composite Degree

Residuosity Classes," in *Advances in Cryptology --- EUROCRYPT '99*, 1999, pp. 223–238.

[143] Y. Yan, Z. Chen, V. Varadharajan, J. Hossain, and G. Town, "Distributed Consensus-Based Economic Dispatch in Power Grids Using the Paillier Cryptosystem," *IEEE Trans. Smart Grid*, vol. 3053, no. c, pp. 1–10, 2021.

[144] J. Wang, D. Shi, J. Chen, and C.-C. Liu, "Privacy-Preserving Hierarchical State Estimation in Untrustworthy Cloud Environments," *IEEE Trans. Smart Grid*, vol. 12, no. 2, pp. 1–1, 2020.